

Characterizing antipsychotic drug behavioral and neurophysiological responses to
psychotomimetic challenge

by

Gwenaëlle E. Thomas

Department of Neurobiology
Duke University

Date: _____

Approved:

Kafui Dzirasa, Supervisor

Anne E. West,

R. Alison Adcock

Hiro Matsunami

Dissertation submitted in partial fulfillment of
the requirements for the degree of Doctor
of Philosophy in the Department of
Neurobiology in the Graduate School
of Duke University

2022

ABSTRACT

Characterizing antipsychotic drug behavioral and neurophysiological responses to
psychotomimetic challenge

by

Gwenaëlle E. Thomas

Department of Neurobiology
Duke University

Date: _____

Approved:

Kafui Dzirasa, Supervisor

Anne E. West,

R. Alison Adcock

Hiro Matsunami

Dissertation submitted in partial fulfillment of
the requirements for the degree of Doctor
of Philosophy in the Department of
Neurobiology in the Graduate School
of Duke University

2022

Copyright by
Gwenaëlle E. Thomas
2022

Abstract

Schizophrenia is marked by significant disruptions to dopaminergic signaling across the mesolimbic and mesocortical circuits. Antipsychotic drugs have been largely unsuccessful treating cognitive symptoms that debilitate the schizophrenia patient population. Dopamine 2 Receptor (D₂R)- β arrestin 2 (β arr2) biased signaling, independent of the canonical G protein signaling, has emerged as a potential mechanism for antipsychotic drugs to restore dopaminergic signaling and improve treatment resistant cognitive symptoms. In the following experiments, I described gene editing tools to systematically investigate D₂R signaling in a region or cell specific manner. Next, I evaluated the behavioral effects of two functionally selective D₂-like β arr2 biased ligands against psychotomimetic challenge from phencyclidine or amphetamine. Then I employed chemogenetics to perform synthetic pharmacology experiments e.g. studying the signaling cascade of a drug without using the drug, to discover how D₂- R β arr2 signaling produces antipsychotic effects in the prefrontal cortex. Lastly, I characterized the neurophysiological changes induced by phencyclidine and a D₂R β arr2 biased ligand within relevant brain regions in the meso -limbic and -cortical circuits. Our results determined antipsychotic like activity is 1) regulated by excitation-inhibitory balance maintained by cortical GABA interneurons 2) dependent on β arr2.

Dedication

To my late PhD adviser Marc, who guided me in his final years in this earthly realm. It was my deepest privilege to be your and my highest honor to carry on your scientific legacy.

Contents

Abstract	iv
Acknowledgements	xii
1. Introduction	1
1.1 Schizophrenia.....	1
1.1.1 Dopamine Hypothesis	2
1.1.2 Glutamate and GABA Hypotheses.....	3
1.2 Antipsychotic therapies for schizophrenia	5
1.3 Dopamine 2 Receptor Signaling.....	7
1.3.1 Isoforms	7
1.3.2 D ₂ R signaling and downstream effects	8
2.Validation of a CRISPR/Cas9 approach to manipulate D ₂ R signaling in corticostriatal regions	11
2.1 CRISPR mediated gene editing of dopamine 2 receptor expression.....	12
2.2 CRISPR/Cas9 D ₂ R Plasmid.....	13
2.3 in vitro validation of CRISPR mediated D ₂ R knockdown.....	14
2.4 In vivo validation of CRISPR mediated D ₂ R knockdown.....	16
2.5 Future Directions.....	20
3 Elucidating the effect of functionally selective β arr2 dopaminergic signaling on behavioral outcomes.....	22
3.1 Dopamine 4 Receptor's distinction within the Dopamine 2 Receptor Family	22

3.2 Functionally selective β arr2-D2-like receptor ligands	24
3.3 Cortical and Striatal β arr2-D2R signaling produces antipsychotic like activity to PCP challenge	27
3.4 Cortical β arr2-D4R and Striatal β arr2-D2R signaling produces antipsychotic like activity to AMPH challenge	32
4. Characterization of antipsychotic potential of cortical β -arrestin2 D2R-mediated signaling in vivo.....	39
4.1 Therapeutic potential of biased β -arrestin 2 signaling.....	39
4.2 Validation of the Barr2 DREADD	41
4.2.1 Confirmation of GRK2 and β arr2 expression within the cortex	41
4.2.2. Synthetic pharmacology using DREADDs	43
4.2.3. In Vitro Assessment of the β Arrestin biased DREADD	44
4.3 Determining the role of cortical β arr2 biased signaling in antipsychotic like activity.....	49
5. Characterizing psychotogenic induced corticostriatal network dynamics	58
5.1 Transitioning from neuropsychiatric nosology to data driven diagnostics.....	59
5.2 Integrating machine learning and neural circuit studies preclinically	62
5.2.1 Limitations of neural circuit studies in rodents	62
5.2.2 Discriminative Cross-Spectral Factor Analysis maintains relevant neurophysiological features.....	63
5.3 Profiling neurophysiological effect of PCP.....	66
5.3.1 Experimental Design.....	66
5.3.2 PCP induces robust neurophysiological changes	68

5.4 dCSFA Model Validation	70
5.5 Prelimbic cortex gamma oscillations underlie antipsychotic effect in PCP inhibition.....	74
5.5.1 The prelimbic cortex's role within the corticostriatal circuit.....	74
5.5.2 Potential antipsychotic cellular interactions within the prefrontal cortex	76
5.5.3 The analogous region of the prelimbic cortex in the human brain	77
5.6 Biological interpretation of 94A drug effect electome factors	78
5.6.1 94A normalizes PCP disruptions to neural circuit in time-frequency analysis	79
5.6.2 94A significantly increases gamma power in cortical regions.....	81
5.6.3 94A rescues PCP induced circuit disruptions	82
5.7 Integrating dopaminergic dynamics into a PCP drug effect model.....	85
6. Conclusions.....	90
Appendix A : Methods and Materials.....	93
A.1 Materials and methods for chapter 2.....	95
A.2 Materials and methods for chapter 3.....	96
A.3 Materials and methods for chapter 4.....	96
A.4 Materials and methods for chapter 5.....	100
References	108
Biography	129

List of Figures

Figure 1 Schizophrenia deficits in the prefrontal cortex	5
Figure 2 Schematic of dopamine D2 receptor function and expression in corticostriatal regions.	8
Figure 3 Schematic of sensor to monitor cell surface expression of GPCRs.....	15
Figure 4 Infrared imaging monitoring of FAP D2R membrane expression.	16
Figure 5 Validation of in vivo CRISPR/Cas9-mediated gene KO in brain.....	17
Figure 6 Distinct cortical and striatal behavioral responses to D2R knockdown in psychotogenic induced locomotion.....	19
Figure 7 Dopamine receptor subtype densities in corticostriatal regions.	24
Figure 8 Pharmacological Models of Schizophrenia.....	26
Figure 10 Cortical D2R- β arr2 biased antipsychotic like activity in response to PCP is dependent on GRK2.	28
Figure 11 Cortical D2R- β arr2 signaling has antipsychotic like activity with PCP.	29
Figure 12 Striatal D2R- β arr2 signaling has antipsychotic like activity with PCP.....	31
Figure 13 Cortical D4R- β arr2 biased antipsychotic like activity in response to AMPH is dependent on GRK2.	33
Figure 14 Cortical D2R- β arr2 signaling loses its antipsychotic like activity while D4R- β arr2 signaling inhibits the AMPH responses.....	34
Figure 15 Striatal D2R- β arr2 signaling regains its antipsychotic like activity with AMPH.	36
Figure 16 Functionally selective β -arrestin2 -D ₂ R ligand has more antipsychotic potential than β -arrestin2 -D ₄ R ligand.....	38
Figure 17 Cortical and striatal expression of GRK2 and β arr2:.....	42

Figure 18 Cartoon of Designer Receptors Exclusively Activated by Designer Drugs (DREADDs) signaling properties.	44
Figure 19 Schematic of bioluminescence resonance energy transfer (BRET) assay to monitor protein-protein interactions.	45
Figure 20 BRET Receptor Arrestin Recruitment Assay.	46
Figure 21 TGF α Shedding Assay Schematic.	47
Figure 22 Evaluation of DREADD agonist (Cpd21) activity in the TGF α shedding assay.	48
Figure 23 Excitatory DREADD expression in cortical interneurons.	51
Figure 24 Activating cortical interneurons inhibits PCP, but not AMPH responses.	53
Figure 25 : Exciting cortical interneurons with biased β arr2 signaling produces antipsychotic like responses to PCP.	54
Figure 26 Cortical interneuron excitability requires β arr2 biased signaling to inhibit the PCP response.	55
Figure 27 Clinical clustering using machine learning schematic.	60
Figure 28: Electome Model Overview.	65
Figure 29: Experimental design for studying corticostriatal neurophysiological and behavioral changes induced by PCP.	67
Figure 30 PCP induced neurophysiological changes at the single unit and LFP level.	69
Figure 31 Power spectrogram shows neurophysiological changes that mirror PCP induced behavior and pharmacokinetics.	70
Figure 32 dSCFA model can reliability predict PCP or 94a + PCP conditions.	72
Figure 33 dCSFA generated electome factor identifying PCP condition:	73
Figure 34 Mouse prelimbic cortex laminar layers and projections.	75

Figure 35: 94A stabilizes PCP's neurophysiological effects over time.	80
Figure 36: 94A reduces PCP induced regional circuit disruptions to power.	81
Figure 37 94A normalizes PCP disruptions to power in all corticostriatal regions.....	82
Figure 38 Antipsychotic effect on cortical-midbrain synchrony.	83
Figure 39 94A exhibits the key-locke theory to PCP challenge.	85
Figure 40 Measuring PCP effects on dopamine with a dopaminergic biosensor.	88
Figure 41 Prelimbic cortex identified as an antipsychotic drug relevant brain region	92

Acknowledgements

Thank you to everyone who has supported not just this work, but me. I am grateful for my NSF GRFP and NIH R21 funding that enabled data collection and analysis.

First, I would like to thank my PhD advisor Dr. Kafui Dzirasa for our long-standing relationship since 2015. You saw something to me when I didn't see it in myself- you identified my scientific potential and put my work ethic to the test. I am grateful for the lab you cultivated and the support I received from my mentors and peers. None of the neural analysis would be possible without Jack Goffinet and Dr. David Carlson. My mentor dream team: Dr. Mai-Anh Vu, Dr. Rainbo Hultman, Dr. Kathryn Walder, and Dr. Stephen Mague – your unwavering belief in me and academic, mental, and emotional support catapulted me to the end when I had nothing left to give. To my scientific better half, Dalton Hughes: I don't know how I would've done this without you being my parallel, confidant, and data analysis partner. My beloved LBs – Elise Adamson, Ashleigh Rawls, Karim Abdelaal, Cameron Blount, Nkemdilim Ndubuizu, and Rachel Fisher-Foye your intellectual contributions are always appreciated, but the moral support mattered most to me. Thank you to all my former

undergraduate trainees who trusted me as a mentor and made science worth doing, especially Alexandra Fink who was integral to data collection.

To the Caron lab, especially Dr. Rahul Chandrasekhar, Dr. Lauren Slosky, and Dr. Tom Pack, thank you your contribution to data collection and most importantly teaching me fundamental cell biology techniques, theories, and analysis tools necessary to complete this body of work. Marc's sudden death rocked all our worlds. I was moved that even amidst mourning, Caron lab past and current members showed me such care and consideration to ensure I could continue my defense and put together my manuscripts. Marc's legacy lives on in all of us.

My Neurobiology besties, Dr. Thuy Hua and Dr. Urann Chan -without your friendship, counsel, and academic support, I would have never lasted in this program. To Dr. Sherilynn Black, thank you for paving the way for me to come through as the second Black female PhD trainee in our department. Your mentorship and guidance means the world to me. Your expertise and experiences created the BioCore community that was integral to my professional development and scientific camaraderie at Duke. I am grateful for the opportunity to be a co-founder of BlackInNeuro and finding a community of so many like-minded scientists and friends. Thank you to my team at Cientifico Latino for believing in me from day 1 and emphasizing care for diversity,

culture, mentorship, and outreach. Thank you to the Meyerhoff scholarship for providing me a strong network of Black scientists and meticulous training in research. Thank you to all my friends from UMBC who have cheered me on along the way - especially squad2nasty. My home chapter of Delta Sigma Theta Sorority, Inc. -Lambda Kappa: thank you for teaching me such valuable lessons on seeing it through and showing me sisterhood when I needed it most.

To my family, thank you for your unparalleled sacrifices to help me get where I am. My mother showed me unconditional love even when she didn't quite understand what I was going through. My father pushed me and if/when he couldn't build me up after I was broken down, he found people who could. My grandmas for raising me and teaching me the true value of character- how to be kind, empathetic, honest, vulnerable, and resilient. I believe these are the traits that carried me where I am. Kevin for always making sure I stayed on the right path and reminding me I could be more than I imagined. Lastly, to all the friends and family I lost along the way, thank you for being a guardian angel to me and shining your light when I felt I was alone on my darkest days.

1. Introduction

1.1 *Schizophrenia*

Schizophrenia, a highly heterogeneous lifelong psychiatric illness, affects roughly 1% of the global population(1). Schizophrenia is classified by 3 core symptoms: 1) positive symptoms (abnormally present) - hallucinations and delusions 2) negative symptoms (abnormally absent) – anhedonia, emotional flattening, social withdrawal 3) cognitive symptoms: deficits in learning, memory, attention, and organization(2). Schizophrenia was first characterized by the positive symptoms associated with psychosis related to hyperdopaminergia - increased dopamine release - in the dorsal striatum. Many therapeutic treatments, specifically antipsychotic drugs, can clinically manage positive symptoms by pharmacologically normalizing striatal hyperdopaminergia. Although positive symptoms were the first schizophrenia diagnostic markers; cognitive symptoms are now classified as core symptoms of schizophrenia and affect up to 80% of people living with schizophrenia. Cognitive symptoms cause severe functional impairments that complicate personal, professional, and social outcomes; consequently, the most debilitating schizophrenia symptoms measured by quality of life are cognitive symptoms(3). Currently there are no antipsychotic therapies that successfully ameliorate cognitive symptoms. The research described in this body of work aims to address this gap in knowledge and investigates

cellular and neurophysiological mechanisms that may ultimately shed light on how to improve treatment for cognitive symptoms.

1.1.1 Dopamine Hypothesis

Dopamine is a monoamine neurotransmitter that contributes cognition, reward, motivation, emotional affect, and movement(4,5). Dysregulation of dopamine is correlated with many psychiatric illnesses and has been posited to be a core hypothesis describing the pathophysiology of schizophrenia. The dopamine hypothesis emerged about 70 years ago after the serendipitous discovery that the intended antihistamine chlorpromazine actually functioned as a neuroleptic drug therapeutic efficacy treating irritability and psychosis in patients(6). In 1966 van Rossum challenged the pharmacodynamics of chlorpromazine being attributed to antiadrenergic action and hypothesized it was an “amphetamine antagonist” i.e. dopamine antagonist that blocked the dopamine receptor(7). Dopamine’s role in schizophrenia pathophysiology was solidified after observing several dopamine mimetic drugs such as amphetamine (increase extracellular dopamine by reducing dopamine transporter reuptake) and Disulfiram (increases extracellular dopamine by inhibiting dopamine metabolism to norepinephrine) led to drug induced psychosis that resembled the clinically observed hallucinations and delusions in schizophrenia(8,9). The dopamine hypothesis was updated to include cortical hypodopaminergia in addition to the established striatal hyperdopaminergia(10–13). Cortical hypodopaminergia has been correlated with the

onset of cognitive symptoms specifically deficits in working memory and attention(13–16).

1.1.2 Glutamate and GABA Hypotheses

Additional studies have contributed alternative hypothesis of neurobiological disruptions that may underlie schizophrenia however I will focus on two – glutamate and gamma-aminobutyric acid (GABA). Glutamate, the most abundant neurotransmitter in the brain, is an excitatory neurotransmitter mediated by N-methyl-d-aspartate receptors (NMDARs)(17,18). Decreased cortical mRNA expression of NMDAR subunits and postsynaptic density protein PSD95 have been linked to NMDA hypofunctioning e.g. decrease in long term potentiation and depression observed in schizophrenia(19). Dopaminergic neurons in the prefrontal cortex are regulated by glutamatergic projections to the midbrain dopamine nuclei thus disruptions in dopamine transmissions could arise altered glutamatergic function. Dopamine in the prefrontal cortex modulates NMDAR- and AMPAR-mediated currents via D₂Rs(17,20). D₂R can form heteroreceptor complexes with NMDARs. These D₂-NMDA heteroreceptors at the synapse reduce Ca²⁺/calmodulin dependent phosphorylation of NMDAR subunits and decrease NMDA receptor signaling (21) NMDAR antagonists PCP and ketamine disrupt this heteroreceptor complex by increasing dopamine synthesis ultimately decreasing glutamate transmission observed in schizophrenia(22–24).

GABA is the major inhibitory neurotransmitter in the central nervous system. GABAergic interneurons generate high frequency synchronized brain rhythms, gamma oscillations, that aid in cognition, memory, attention and perception(25,26). Abnormal gamma oscillations and cognitive deficits are observed in schizophrenia as well as decreased expression and excitation of GABAergic interneurons, specifically parvalbumin positive fast spiking interneurons, in the prefrontal cortex(24,27) **(Figure 1)**. Neurons in the cerebral cortex consist of a majority of excitatory (glutamatergic) pyramidal neurons (75%–80%) making synaptic contacts both locally (local network) and over long distances (across distinct cortical areas) and of inhibitory (GABAergic) interneurons (25%–20%) making extensive local connection(28–31). Glutamate and GABA work closely together to maintain stable global circuit activity called excitatory-inhibitory (EI) balance(25,32). NMDAR antagonists, phencyclidine or ketamine, induce cortical disinhibition disrupting the EI balance and cause cognitive deficits observed in schizophrenia(23,33,34).

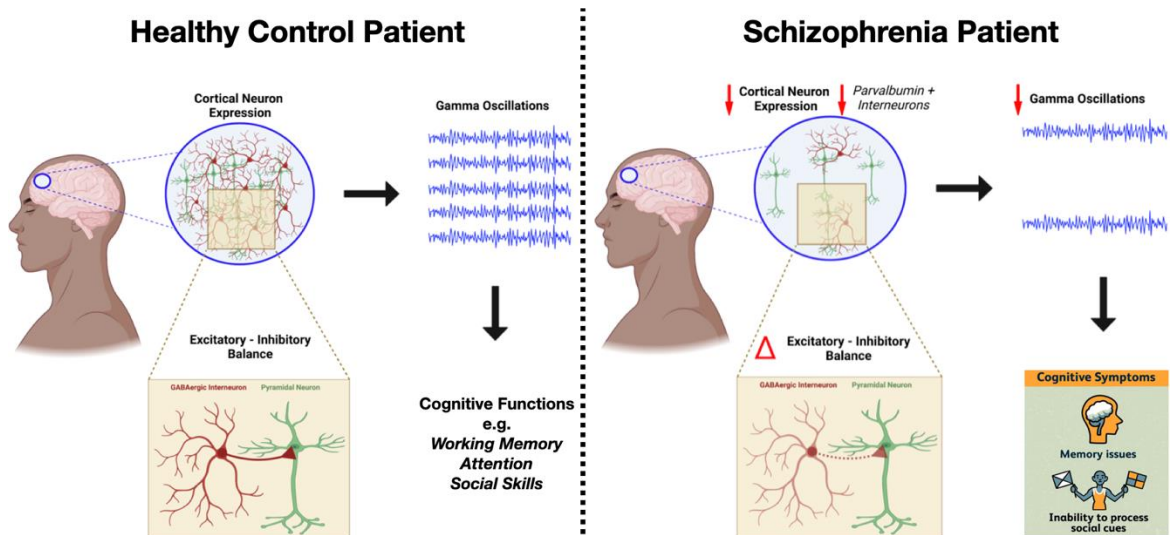


Figure 1 Schizophrenia deficits in the prefrontal cortex

(Left) Healthy patients without schizophrenia have an excitatory-inhibitory (EI) balance maintained by GABAergic interneurons inhibiting excitatory glutamatergic pyramidal neurons. These neurons help regulate gamma oscillations observed in cognitive tasks in clinical neural imaging recording studies. (Right) Schizophrenia patients are observed to have significant reductions in expression and function of GABAergic interneurons, specifically parvalbumin positive interneurons. Consequently, less functional GABAergic interneurons result in a disruption in the EI balance (increased excitatory activity) and is observed to lead to fewer gamma oscillations and poorer cognitive abilities

1.2 Antipsychotic therapies for schizophrenia

Antipsychotic drugs mainly target dopaminergic receptors to restore dysfunctional dopaminergic signaling. Dopamine receptors are G protein-coupled receptors (GPCRs) divided into two classes that are grouped by their coupled G protein and downstream effect on intracellular signaling. The D1 class (D₁ and D₅) couple G_{αs} and activate intracellular signaling cascade while the D2 class (D₂₋₄) couples G_{αi} and has inhibitor signaling. The majority of antipsychotic drugs preferentially bind to D₂ class of

receptors. Pharmacokinetics and receptor binding affinity was further used to mechanistically classify antipsychotic drugs into 3 generations. First generation antipsychotic drugs or typical antipsychotic drugs had high affinity for D₂R and primarily functioned as D₂R antagonist. The prolonged D₂R binding in typical antipsychotics led to several motor and muscle deficits characterized within extrapyramidal effects. Second generation antipsychotic drugs still function as D₂R antagonists but display higher affinity for the serotonin 5-HT_{2A} receptor. Additionally, atypical antipsychotic terms have faster dissociation rates from the dopamine receptor and produce less extrapyramidal side effects. First and second-generation antipsychotics do not treat cortical hypodopaminergia, rather they exacerbate cognitive and negative symptoms. This led to the third generation of antipsychotic D₂R partial agonist designed to simultaneously target cortical hypodopaminergia and striatal hyperdopaminergia. However, third generation antipsychotic drugs also sub optimally treat cognitive and negative symptoms. Recent discoveries in GPCR signaling revealed D₂Rs can signal independently of G proteins and mediate distinct cellular and physiological outcomes through beta arrestin scaffold signaling. This discovery has set the foundation for functional selective ligands – pharmacological compounds that are biased towards a specific signaling cascade. This body of work will characterize functionally selective dopamine- beta arrestin biased ligands and their antipsychotic like activity in the prefrontal cortex and striatum.

1.3 Dopamine 2 Receptor Signaling

1.3.1 Isoforms

Drd2, the gene that encodes D₂Rs, is the only dopamine receptor gene that has been identified as a risk factor for schizophrenia through genome wide association studies(35,36). Pre mRNA alternative splicing of exon 6 generates 2 D₂R isoforms, D₂R short (D_{2s}R) and D₂R long (D_{2L}R)(37). Both isoforms inhibit intracellular cAMP through G protein inhibitory signaling and function at pre- and post-synaptic sites(38). While only separate by 29 amino acids, these D₂R isoforms have distinct physiological functions and drastically different receptor densities throughout the brain(37). D_{2s}Rs are mainly presynaptic autoreceptors (receptors that respond to its own ligand e.g., the neurotransmitter released by their own neuron terminals) predominantly expressed on dopaminergic cell bodies, dendrites, and projection axons from midbrain structures e.g. substantia nigra and ventral tegmental area(39). Contrarily, the majority of D₂Rs are postsynaptic heteroreceptors (receptors that respond to other ligands e.g., neurotransmitters released by other neurons) like D_{2L}Rs (**Figure 2A**). D_{2L}Rs are densely expressed in striatum e.g. caudate nucleus and putamen and have more sparse expression in other brain structures receiving dopaminergic inputs such as the prefrontal cortex(40)(**Figure 2B**).

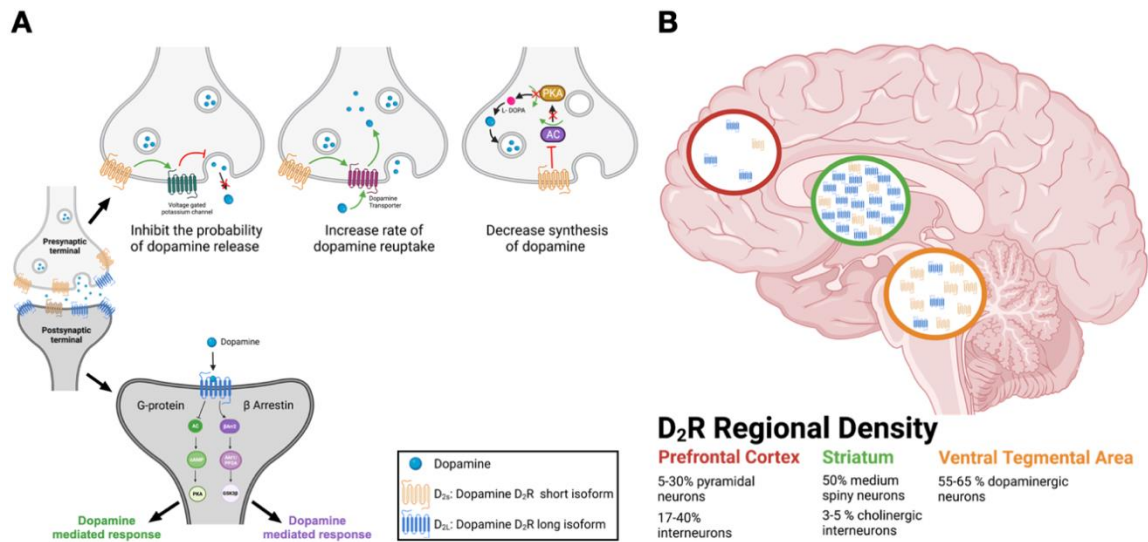


Figure 2 Schematic of dopamine D2 receptor function and expression in corticostriatal regions.

(A) Dopamine 2 Receptors are expressed as two isoforms : D₂R Short (D_{2s}R) primarily located on presynaptic terminals and function as autoreceptors ; D₂R long (D_{2l}R) primarily located on postsynaptic neurons and function as heteroreceptors. D_{2s}R regulate dopamine release and synthesis on dopaminergic neurons. D_{2l}R signal through G-protein inhibitory cascades or via G-protein independent mechanisms such as Beta-Arrestin signaling to produce dopamine mediated responses. (B) A visual approximation of D₂R density in the prefrontal cortex, striatum, and midbrain – specifically the ventral tegmental area. D_{2s}R largely are located on dopaminergic neurons in the midbrain while D_{2l}R densely populated the striatum and are sparser in cortical regions.

1.3.2 D₂R signaling and downstream effects

After a ligand binds to D₂R, heterotrimeric G proteins facilitate downstream extracellular signals. The mechanistic action of heterotrimeric G proteins is described by the distinct functions of G α and G $\beta\gamma$ subunits(41,42). In its inactivate state, the catalytic G α subunit binds GDP which results in the G $\beta\gamma$ subunit sterically blocking its effector

domain. When the D₂R is bound by a ligand, G α subunit is active and binds GTP(41,42). The activated G α i subunits inhibit adenylyl cyclase and decreases cAMP production(41,43). Protein kinase A relies on cAMP to phosphorylate the dopamine- and cAMP-regulated neuronal phosphoprotein (DARPP-32). Increased DARPP-32 phosphorylation is correlated with increased dopamine expression and observed in many dopamine mediated behaviors like locomotion(16,44).After agonist stimulation, G protein-coupled receptor kinases (GRKs) are recruited to the D₂R. GRKs phosphorylate serine and threonine residues on the third intracellular and recruit β -arrestin to the ligand bound D₂R(45,46). β -arrestin facilitates uncoupling G proteins from the D₂R, internalizes the D₂R through clathrin-mediated endocytosis, and transduce G protein-independent signaling(47,48).

Though classically associated with terminating GPCR signaling cascades, β -arrestin can facilitate signaling independently of G protein mediation. Protein interaction studies and single molecule imaging revealed that receptor agonism leading to GRK phosphorylation and receptor C-tail release determine β -arrestin biased signaling(49). β -arrestin forms a multimeric protein scaffold with protein phosphatase 2A(PP2A) and leads to an Akt/glycogen synthase kinase 3 α/β (GSK α/β) signaling. Stimulating D₂ class receptors leads to specific dephosphorylation of Akt's regulatory serine/threonine activates Akt's substrate GSK3 α/β (50,51). Our lab has shown pharmacologically activating AKT or inhibiting GSK 3 α/β results in loss of DA

mediated behaviors like locomotion, even when responding to amphetamine challenges(51). Importantly, inhibiting cAMP/PKA signaling did not affect Akt/GSK 3 activity, showing these signaling cascades are acting independently(52–54).

2.Validation of a CRISPR/Cas9 approach to manipulate D₂R signaling in corticostriatal regions

Dopamine receptors influence activity in many brain regions related to reward, cognition motivation, and locomotion(55). Consequently, dopamine receptors are pharmacological targets for treatment of a variety of psychiatric diseases and all current antipsychotic drugs treating schizophrenia target the dopamine D₂ receptor (D₂R). These antipsychotics are effective in managing manifestations of psychosis through antagonism of D₂R striatal hyper-functioning but are ineffective in regulating the cognitive and social deficits of the illness correlated with cortical D₂R hypo-functioning. Schizophrenia's paradoxical dopaminergic disruptions within the basal ganglia circuit as well as a lack of understanding of receptors and downstream signaling mechanisms has greatly limited beneficial therapeutic outcomes(56). We set out to determine D₂R functions in vivo by combining pharmacological models of schizophrenia and gene editing using an intersectional CRISPR/Cas9 approach.

Genomic studies report 95-99 % shared homology between human and rodent D₂ mRNA (57). Previous computational modeling and molecular dynamics research have completed high resolution crystal structure of D₂Rs, in addition to establishing gene structure and the map of the eight exons of *Drd2*(58,59). Many D₂ transgenic mouse lines have been generated by modifying the amino terminus of the mouse D₂R using standard cloning techniques, specifically using vectors targeting *Drd2* exon 2(60). Altogether,

Drd2's widely studied structure and genomic sequence makes it an ideal candidate for CRISPR/Cas9 with minimal potential off-target sites(61,62).

2.1 CRISPR mediated gene editing of dopamine 2 receptor expression

Genome editing technology has revolutionized the way disease processes and pathophysiology is interrogated. Clustered regularly interspaced short palindromic repeats (CRISPRs) are classes of repeated DNA sequences that use RNA-guided Cas9 nucleases to edit targeted DNA sequences(63). After being guided by an artificial short guide RNA (gRNA), the enzyme Cas9 induces double strand breaks in DNA that leads to a cascade of frameshift mutations and termination of translation of proteins of interest(64). The CRISPR/Cas9 system is commonly used to generate mice with gain or loss of function mutations in genes of interest to study developmental deficits and disease(65).

The CRISPR/Cas9 system takes advantage of adaptive immunity. CRISPR/Cas9 integrates short spaced-out sequences of the targeted viral DNA, protospacers, into the CRISPR locus(64). As protospacers are usually added to one end of the CRISPR and create a chronological order of previously encountered viruses, they serve as recognition elements and facilitates cells to quickly send Cas9 nucleases to identify and destroy the invasive viral DNA(66). Polymerase III gene promoters, such as U6, drive gRNA expression and determine Cas9 cleaving specificity. However, the mechanism U6 and related promoters transcribe gRNA from nucleotides is highly specific and restrains the

potential placement of protospacers within the targeted DNA sequence(66,67). As a result, CRISPR/Cas9 system using gRNAs has been reported to have many off target effects and greatly limit biological and clinical interpretations of genetic modification. A strategy to improve gRNA expression using polycistronic endogenous transfer RNAs (tRNA) has been demonstrated to improve CRISPR Cas9 targeting(67). tRNAs are highly conserved in living organisms and have been demonstrated to be effective in genetically modified mice. Using an artificial polycistronic tRNA processing system, multiple gRNAs can be expressed simultaneously to improve precision for genome editing(67,68).

2.2 CRISPR/Cas9 D₂R Plasmid

The purpose of the CRISPR/Cas9 approach was to partially knockdown D₂R in vivo within the prefrontal cortex and the striatum to investigate the role of dopaminergic signaling in psychotomimetic induced behaviors. Four multiplexed gRNAs targeting exon 2 of D₂R were encoded within a single polycistronic tandemly linked by a tRNA precursor. The gRNA scaffold in *Drd2* cloning site containing 4 BsmBI sites was inserted downstream of the U6 promoter. The construct also encoded a spectrally resolvable, nuclear-localized fluorescent tags that can be visualized to quantify neurons expressing gRNAs, where D₂R is deleted. Large indels in exon 2 of the *Drd2* gene were confirmed by deep sequencing (MGH, DNA Core) (not shown).

2.3 *in vitro* validation of CRISPR mediated D₂R knockdown

Fluorogen activating proteins (FAPs), small and selective genetically encoded single chain antibody tags, can be used to monitor cell surface expression of GPCRs(69,70). FAPs take advantage of noncovalent steric strains and nonradiative excitation states with specific fluorogenic dye; consequently, these dyes are nonfluorescent until bound to their respective FAP(71) (**Figure 3**). We utilized a MarsCy1-FAP with a far red fluorogen, SC1. FAP offers a high signal to noise ratio as previous studies reported a 20,000 fold increase in fluorescence after Sci1 bound to MarsCy1-FAP(72). Sci1 is a membrane impermeant variant of SC1 which enables monitoring of cell surface expression of the FAP-GPCR. We will use this approach to validate our *Drd2* gRNA vector efficiently reduce D₂R expression at the cell membrane.

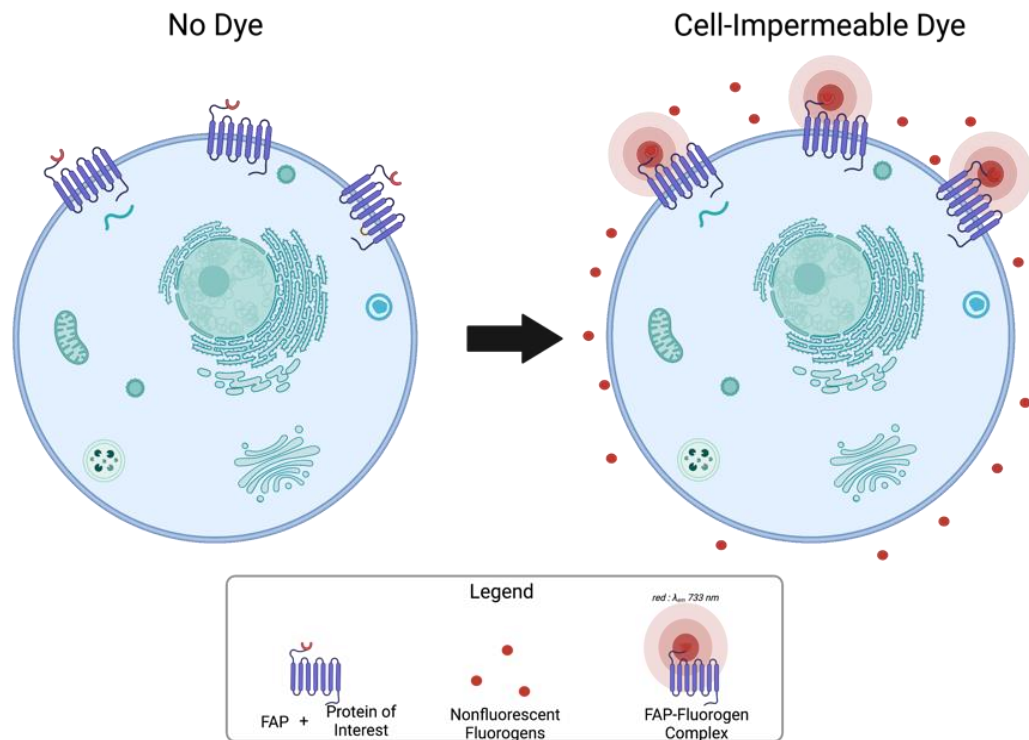


Figure 3 Schematic of sensor to monitor cell surface expression of GPCRs.

Dopamine 2 Receptors were tagged with a transmembrane fused protein MarsCy1-CD80. Cells expressing MarsCy1 were pulsed with the far-red membrane impermeant fluorogen Sci1. Sci1 will not fluorescence unless bound to MarsCy1. Cells expressing MarsCy1-Sci1 were imaged using a LiCOR-Odyssey IR imaging system and quantified.

The MarsCy1-FAP was cloned onto the N-terminus of the mus musculus D2R previously tagged with eYFP on the C-terminus. We transfected stable USO2 cells with EF1 α -mKO1-polycistronic *Drd2* gRNAs or EF1 α -mKO1-polycistronic *Drd2* gRNAs and Cas9-2A-eYFP. Following U2O2 cells incubation with Sci1, infrared plate imaging with FAP-tagged D2R pulse was performed. We imaged and quantified the cells using the FAP tag via the near-infrared Licor scanner(72). The control cells (without Cas9) robustly expressed on the cell surface. Co-transfection of *Drd2*-gRNAs and Cas9

significantly reduced D₂R at the cell membrane (**Figure 4**). This experiment provided preliminary proof our engineered CRISPR gRNA *Drd2* vector successfully targeted D₂Rs.

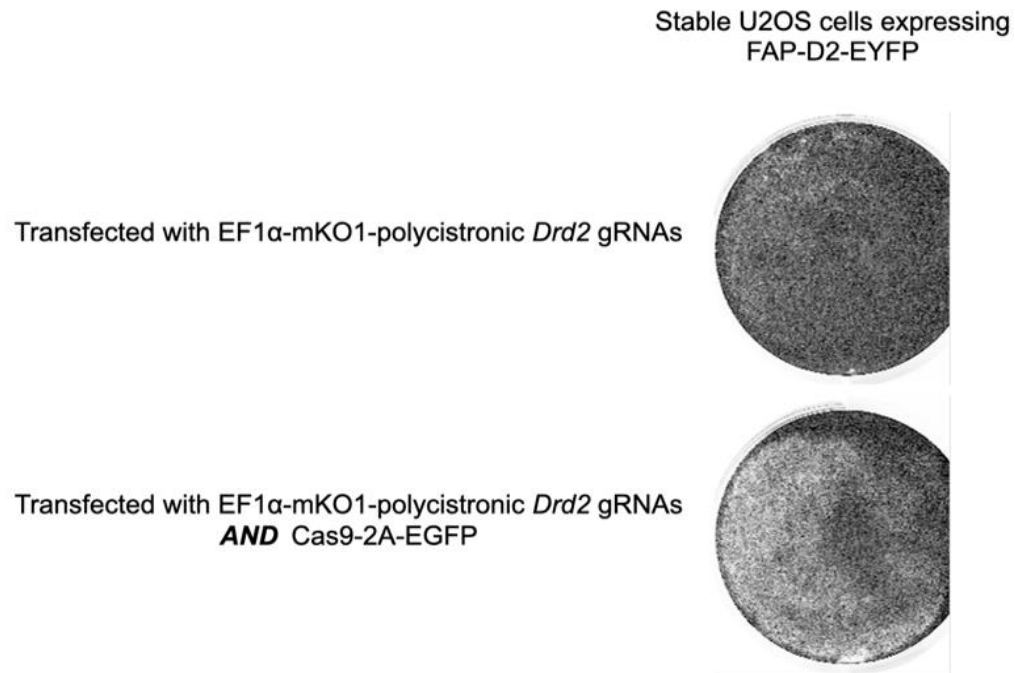


Figure 4 Infrared imaging monitoring of FAP D₂R membrane expression.

After stable USOS were permeabilized in a 12 well plate, they were transfected with the fluorogen activating protein MarsCy1 designed to target D₂Rs on the cell membrane. Control cells were transfected with only the CRISPR vector containing gRNAs against exon 2 of the *Drd2* gene. Experimental cells were transfected with *Drd2* gRNAs and a Cas9 to systematically decrease D₂Rs expression at the cell membrane. FAP-tagged D₂R cell were pulsed with the far red fluorogen SCi1 and a primary HA-epitope antibody then imaged. D₂R cell surface expression was visually quantified between control and Cas9 transfected cells.

2.4 In vivo validation of CRISPR mediated D₂R knockdown

To validate the CRISPR construct in vivo, we stereotaxically co-injected 2 AAV constructs encoding a Cre recombinase and gRNAs targeting *Drd2*, both under the

control of an EF1 α promoter to drive high neuronal expression, into the striatum of Cre inducible LSL-Cas9 mice (73). Coronal vibratome sections were taken from fixed brains of Cas9 mice injected with virus and images were taken using a Zeiss Axiozoom microscope (Figure 5).

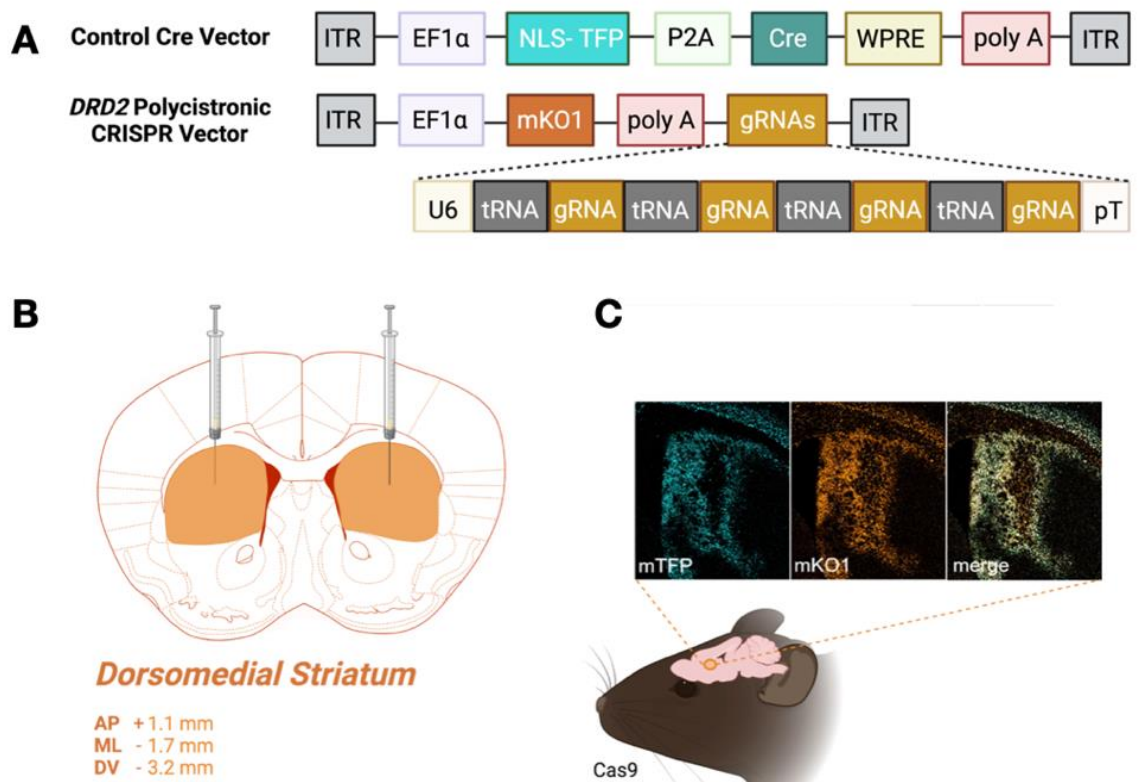


Figure 5 Validation of in vivo CRISPR/Cas9-mediated gene KO in brain.

(A) AAV constructs encoding Cre recombinase and a *Drd2* polycistronic CRISPR vector. Both vectors use Ef1 α to enhance viral expression in neurons. 4 tandemly arranged unique gRNAs against exon 2 of *Drd2*. 4 tRNAs sequences were inserted to optimize gRNA mediated deletion of *Drd2* with minimal off target effects. B) Stereotaxic coordinates to bilaterally deliver viral constructs to dorsomedial striatum (C) Representative images of neurons co-expressing spectrally-resolvable nuclear localized fluorescent proteins of TFP-Cre (left, blue), mKO1-gRNAs (middle, orange), and merge (right))

As behavioral proof-of-concept, we used an open field assay to measure psychostimulant induced hyperlocomotion. Amphetamine causes presynaptic dopamine release and inhibits dopamine reuptake(74,75). Importantly, dopamine in the striatum is highly correlated with movement(76). We expected the psychostimulant-induced hyperlocomotion would be reduced in Cas9 mice with striatal D₂R KD as compared to WT C57 mice. Animals were virally injected with EF1 α -NLS-mkO1-polycistronic *Drd2* gRNAs unilaterally into the dorsal medial striatum to partially knockdown D₂R. After 2 weeks of recovery, C57 WT and Cas9 mice were systemically injected with AMPH (3 mg/kg, i.p.). For AMPH-induced locomotion, we observed a significant genotype difference for Cas9 mice as compared to wildtype controls. Cas9 with decreased striatal D₂R expression significantly reduced the AMPH induced hyperlocomotion as compared to WT controls, **p = 0.0022 (**Figure 6B**). These results show CRISPR targeted deletion of D₂Rs in the striatum were consistent with the antipsychotic contribution of striatal D₂R antagonism and its inhibition on amphetamine-mediated responses(21).

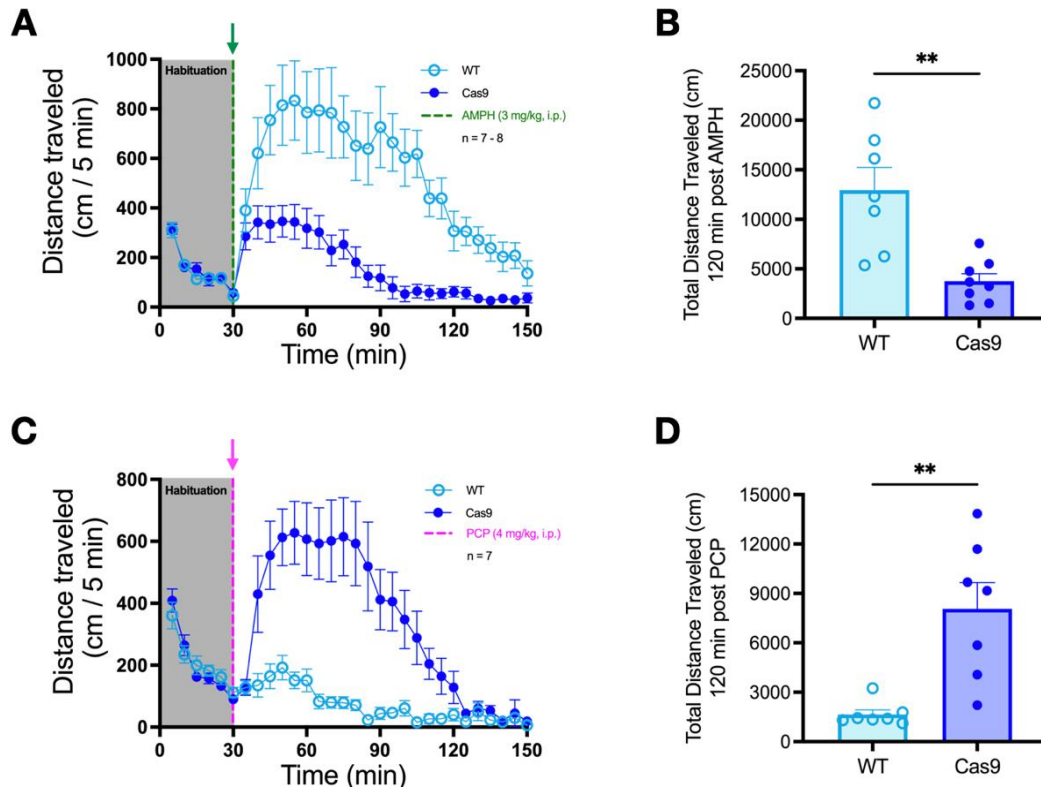


Figure 6 Distinct cortical and striatal behavioral responses to D2R knockdown in psychotogenic induced locomotion.

WT and Cas9 mice received a systemic injection of (A) AMPH (3 mg/kg, i.p.) [green arrow, 30 min] or (C) PCP (4 mg/kg, i.p.) [pink arrow, 30 min]. Distance traveled was calculated for 120 min after 30 min of habituation. Data were analyzed using a two-way ANOVA test with post hoc Bonferroni corrections. When stimulated with AMPH, a main effect of genotype $F(1,13) = 16.54$, $p < 0.0001$ and an interaction of genotype and time $F(29, 377) = 6.698$, $p < 0.0001$ were detected. controls. In mice stimulated with PCP, we report a main effect of genotype $F(1, 360) = 191.5$, $p < 0.0001$ and an interaction between genotype and time $F(29, 360) = 6.423$, $p < 0.0001$. Total cumulative distance after systemic administration of psychotogenic drugs was calculated for Cas9 mice and WT controls. Data were analyzed using an unpaired, non-parametric t-test-Mann-Whitney rank sums (B) Cas9 mice with reduced striatal D₂R expression inhibited the AMPH response, $**p = 0.0022$, compared with WT mice; $n = 7- 8$. (D) Cas9 mice with reduced cortical D₂R expression potentiated the PCP response and significantly increased locomotion, $**p = 0.0012$, compared with WT mice ; $n = 7$. Data shown are the mean \pm SEM

Next, we applied our validated CRISPR D₂R construct to partially knockdown D₂R in the medial prefrontal cortex. We repeated open field assay to measure psychomimetic induced hyperlocomotion using phencyclidine (PCP) was the pharmacological agent. PCP, an NMDAR antagonist, induces psychotic behavioral deficits through cortical disinhibition(77,78). Cortical D₂Rs help regular excitation-inhibition balance through inhibitory signaling on pyramidal neurons and decreasing Ca²⁺ release via dopamine-NMDA heteroreceptor complexes(20,21). Total cumulative distance after systemic injection of 4 mg/kg PCP was calculated for Cas9 mice and WT controls. Cas9 mice with cortical D₂R KD exhibited significantly higher PCP induced hyperlocomotion as compared to WT controls, **p = 0.0012. (**Figure 6D**).

The results of these CRISPR target D₂R deletion in the prefrontal cortex and striatum recapitulates the distinct and opposite behavioral effects mediated by regional dopaminergic signaling. While these meso-cortical and -striatal dopaminergic deficits have been observed for several decades, we still do not understand how these disruptions to D₂R transmission arise or the best approach to design therapeutic interventions in psychiatric illness.

2.5 Future Directions

Our objective is to combine pharmacological and genetic approaches to investigate the pathophysiology contributing to psychosis and cognitive deficits by manipulating D₂R signaling in PFC neuronal subtypes. To accomplish this, we will

apply CRISPR/Cas9 to systematically delete D₂Rs in PFC pyramidal neurons and interneurons. These findings targeting cortical D₂R signaling can offer insight as to how schizophrenia symptomology manifests and cellular mechanisms of antipsychotic drugs.

3 Elucidating the effect of functionally selective β arr2 dopaminergic signaling on behavioral outcomes

3.1 Dopamine 4 Receptor's distinction within the Dopamine 2 Receptor Family

Though the dopamine hypothesis originally focused on D₂Rs, recent studies have shown the relevance of other dopaminergic receptors in schizophrenia treatment, specifically the D₄R. The first generation of antipsychotic drugs (typical antipsychotic or neuroleptics) led to the onset of extrapyramidal side effecting motor and muscle control that was attributed to their suboptimal pharmacodynamics and -kinetics, specifically the high D₂R occupancy (> 80%) and slow dissociation rate (79–81). The second generation of antipsychotics, such as clozapine, did not produce significant extrapyramidal side effects largely due to their low occupancy (<70%) and rapid dissociation at D₂R(82). Interestingly, clozapine acts as an antagonist and preferentially binds D₄Rs with a binding affinity one magnitude higher than D₂Rs (83). Post-mortem studies reported six-fold increase in D₄R density in schizophrenia(84,85). Presently, more studies are focused on investigating D₄Rs contribution to dopamine regulation and schizophrenia.

Like D₂Rs, D₄Rs belong to the D₂ family receptors and couple Gi/o subunits to inhibit AC activity(86). Quantitative autoradiography studies, biochemical assay to determine spatial distribution and pharmacokinetics of biological ligands, report D₄R constitute 17 to 40 % of the total D₂ family receptor population(87). Genomic sequencing

of human D₄Rs report high homology to D₂Rs, namely the presence of seven transmembrane domains, conservation of catecholaminergic receptors binding sites, the short carboxy tail terminating D₂ family receptors, and protein kinase C and protein kinase A phosphorylation sites in the third cytoplasmic in G_i couples receptors (83). Conversely, D₄Rs have a unique polymorphic 16 amino acid repeat in their third intracellular loop that can express in a range of two to ten repeats and increased D₄R repeat hypervariability in humans has been correlated with psychiatric disorders such as schizophrenia, attention deficit hyperactivity disorders, and substance abuse disorders (84,88,89). D₄Rs have distinct mRNA distribution localized mainly to cortical brain regions rather than D₂R's striatal and midbrain distribution (87,90,91). Compared to D₂Rs which have low cortical receptor densities (~25%), D₄R expression is enriched in cortical regions with reported receptor densities of 77-90% (92-94) (**Figure 7**). Within the prefrontal cortex, D₄Rs are predominately expressed in GABAergic interneurons, the major cell contributor to gamma oscillations – a rhythmic neurophysiological circuit coordination highly correlated with attention and cognition (32,89,95). Abnormalities in GABAergic interneurons and reductions in gamma oscillations are displayed in schizophrenia and mice deficient in *Dlx5/6*, the gene that regulates GABAergic interneuron development(25,32,96). D₄R deficient mice have been reported to display abnormal cortical hyperexcitability and experience seizures while D₄R agonists have been shown to enhance gamma oscillations in cortical regions(89,90,97). Altogether,

D₄R's binding affinity with atypical antipsychotics, robust density in the prefrontal cortex, and physiological influence on GABAergic interneurons identifies this receptor as potential target for pharmacological treatment of cognitive deficits in schizophrenia.

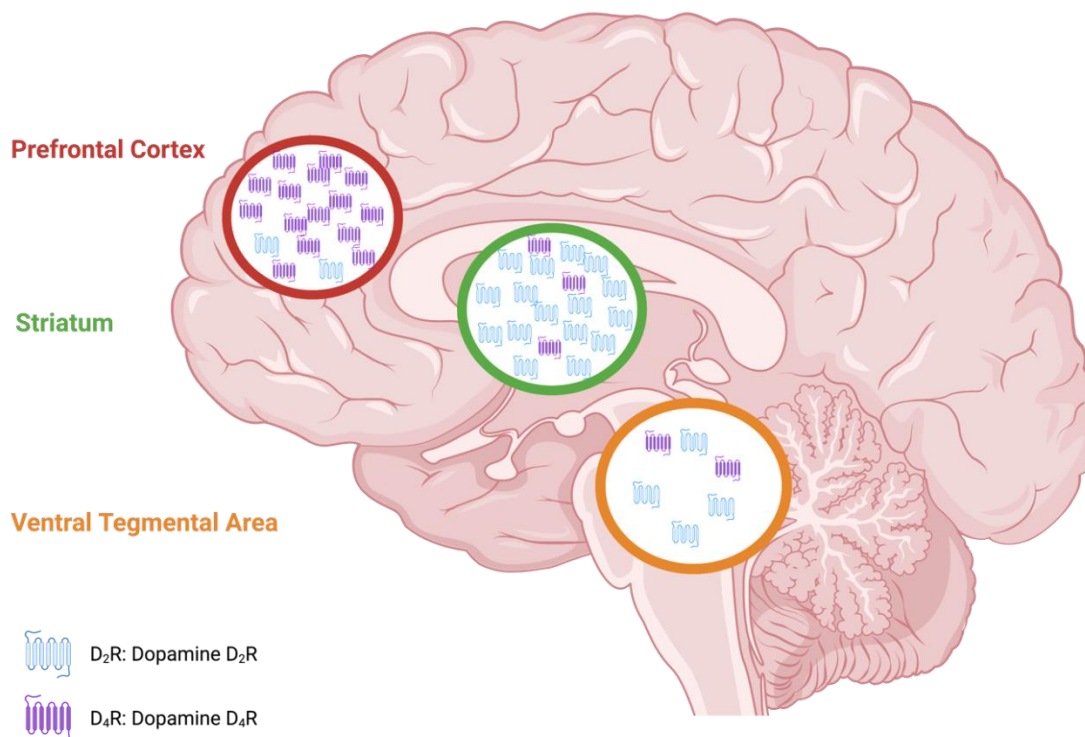


Figure 7 Dopamine receptor subtype densities in corticostriatal regions.

Dopamine receptors Dopamine receptor 2 and 4 (D₂R and D₄R, respectively) are D₂-like family of Gi- coupled GPCRs. D₂Rs (blue) are heavily expressed in the striatum and less in the prefrontal cortex and ventral tegmental area. Conversely, D₄R (purple) are highly expressed in the prefrontal cortex and sparse in the striatum and ventral tegmental area.

3.2 Functionally selective β arr2-D₂-like receptor ligands

As part of a concerted multicenter endeavor, our group recently developed and characterized a functionally selective D₂R- β arr2 biased ligand, UNC9994A (94A), that

exhibits no G protein activity but partial agonism at the β arr2 pathway. Moreover, 94A activity is entirely dependent on the expression levels of β arr2 and GRK2, such that low expression of β arr2 and GRK2 results in 94A behaving as an antagonist while high expression results in β arr2 biased agonist activity. This unique property results in 94A engaging in cortical agonism and striatal antagonism by virtue of high β arr2 and GRK2 expression in the mPFC compared to the striatum.

Recently, our collaborators Drs. Shoichet (UCSF) and Roth (UNC-Chapel Hill) used the crystal structure of the human D₄R and in silico molecular docking to design UCSF924, a D₄R- β arr2 functionally selective compound. UCSF924 exhibits no off-target effects on > 320 non-olfactory GPCRs. UCSF924 behaves as a potent partial agonist at D₄R (K_d <5 nM, 75% efficacy vs DA) and is 7- to 10-fold more biased than DA for D₄R/ β arr2 signaling in cellular assays(98).

The development of these compounds affords us a unique opportunity to study the effects of functionally selective D₂R and D₄R signaling within the corticostriatal circuit. We examined the effects of functionally selective ligands targeting cortical and striatal localized D₂R and D₄Rs. We use psychotomimetic drugs phencyclidine (PCP) and amphetamine (AMPH) induced DA disruptions and use as a pharmacological model of schizophrenia (**Figure 8**). AMPH can model positive symptoms of schizophrenia by increasing dopamine transmission via dopamine transporter inhibition(74,99,100). PCP models positive and cortical symptoms by increasing

dopamine and causing cortical disinhibition by increasing excitatory activity by reducing NMDAR activity on GABAergic cells(33,77,101). Using local administration of these functional selective ligands, we demonstrated cortical and striatal D₂R and D₄R signaling through β -arrestin pathways produce different antipsychotic like activity in the open field assay.

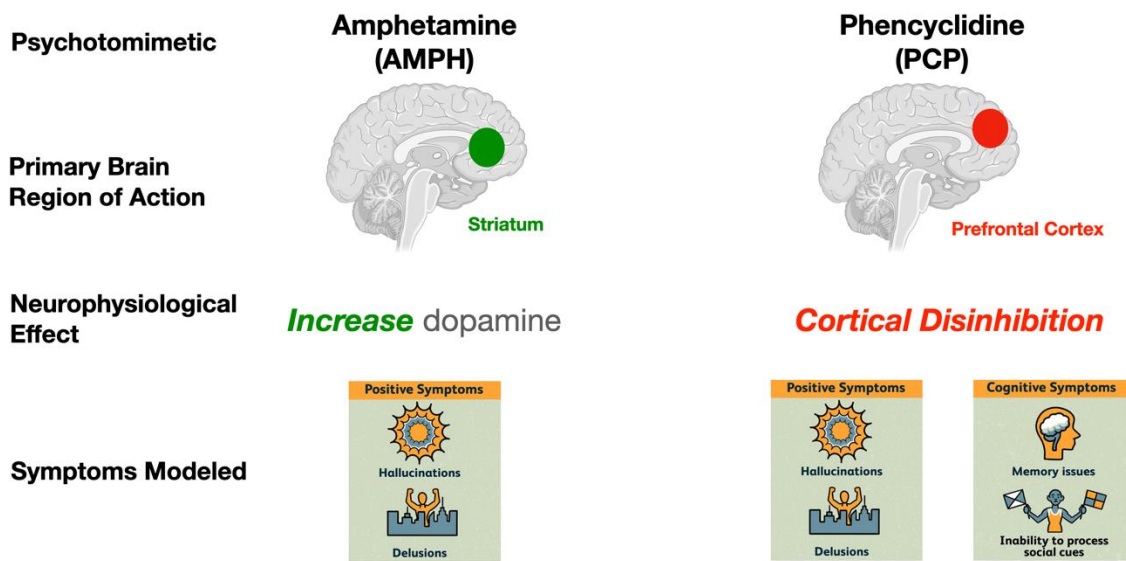


Figure 8 Pharmacological Models of Schizophrenia.

Amphetamine models striatal hyperdopaminergia and models positive symptoms of schizophrenia. Phencyclidine models positive symptoms by increasing dopamine transmission in the striatum and cognitive symptoms by causing cortical disinhibition in the prefrontal cortex. While its effects can be observed in many regions, phencyclidine's primary site of action is the prefrontal cortex

3.3 Cortical and Striatal β arr2-D2R signaling produces antipsychotic like activity to PCP challenge

To determine the effect of biased β arr2-D2 like signaling, we measured the effects of injecting 94A (β arr2- D₂R) or UCSF (β arr2-D₄R) locally into the PFC and STR of WT mice on PCP-induced locomotion.

To confirm the role of β arr2 signaling in our functioning selective ligands, we co-administered the pharmacological GRK2 inhibitor compound 101 with 94A. β arr2 recruitment to dopamine receptors is dependent on GRK2 phosphorylation; thus, inhibiting GRK2 should result in loss of β arr2 dependent behavioral outcomes. We previously reported local prefrontal cortex co-administration of 0.5 μ g compound 101 blocked the antipsychotic effect of 1 μ g 94A to PCP challenge (4 mg/kg, i.p). Consistent with previous findings, 94A lost its antipsychotic activity and failed to reduce PCP induced hyperlocomotion when co-administered with compound 101. (p =0.6480, compared with 94A) (**Figure 9**).

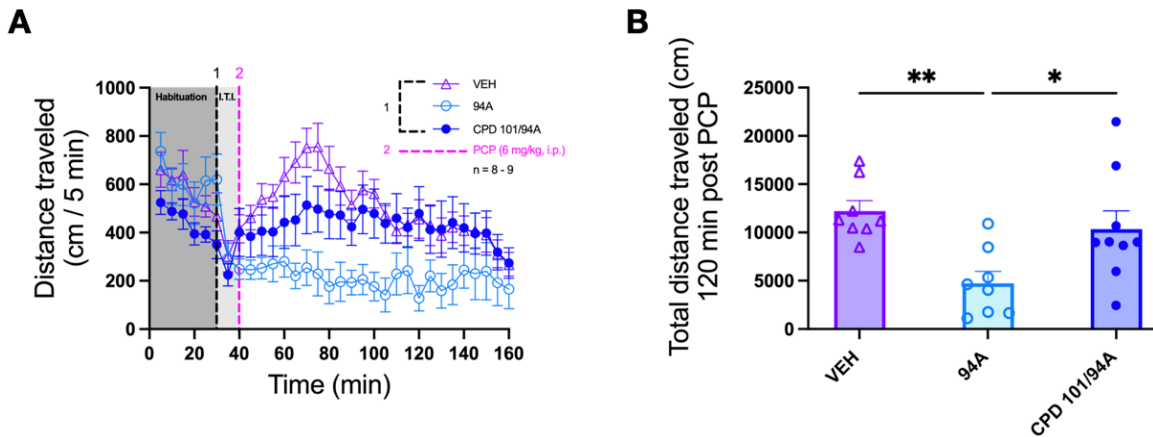


Figure 9 Cortical D2R-βarr2 biased antipsychotic like activity in response to PCP is dependent on GRK2.

(A) WT mice received a bilateral local infusion in the prefrontal cortex of 1) 1 μg per side of VEH or D₂R -βarr2 biased ligand 94A with or without 0.5 μg per side of GRK2 inhibitor CPD101 [black line, 30 min] followed by 2) a systemic PCP injection (6 mg/kg i.p.) [pink line, 40 min]. Distance traveled was calculated for 120 min after 30 min of habituation. Data were analyzed using a two-way ANOVA test with post hoc Bonferroni corrections. Main effect of treatment $F(2, 21) = 3.718$, $p = *0.0415$ and interaction between treatment and time $F(62, 651) = 2.939$, $p < 0.0001$. (B) Total cumulative distance after PCP was calculated for mice administered VEH, 94A, and CPD101/94A. Data were analyzed using a one-way ANOVA with post hoc Tukey test, $n = 8 - 9$ per group. A significant treatment and time interaction was observed: $F(2,22) = 6.609$, $**p = 0.0057$. Only 94A treatment was able to inhibit the PCP response. VEH: $*p = 0.0346$, CPD101/94a: $**p = 0.0057$, compared with 94A. Co-injection with GRK2 inhibitor prevented 94A's antipsychotic like activity. The PCP response of CPD101/94a compared with VEH was not significant, $p = 0.6480$. Data shown are the mean \pm SEM.

Next, we evaluated the effects of 94A or UCSF local administration in the prefrontal cortex on PCP's response (**Figure 10**). Our data was consistent with our previously published work showing 94A significantly decreases PCP induced locomotion ($p = 0.0111$, compared with VEH control; $n = 7$) Despite having significantly

more receptors in the prefrontal cortex, the D₄R ligand UCSF had no effect on PCP induced behaviors ($p = 0.5737$, compared with VEH control; $n = 8$).

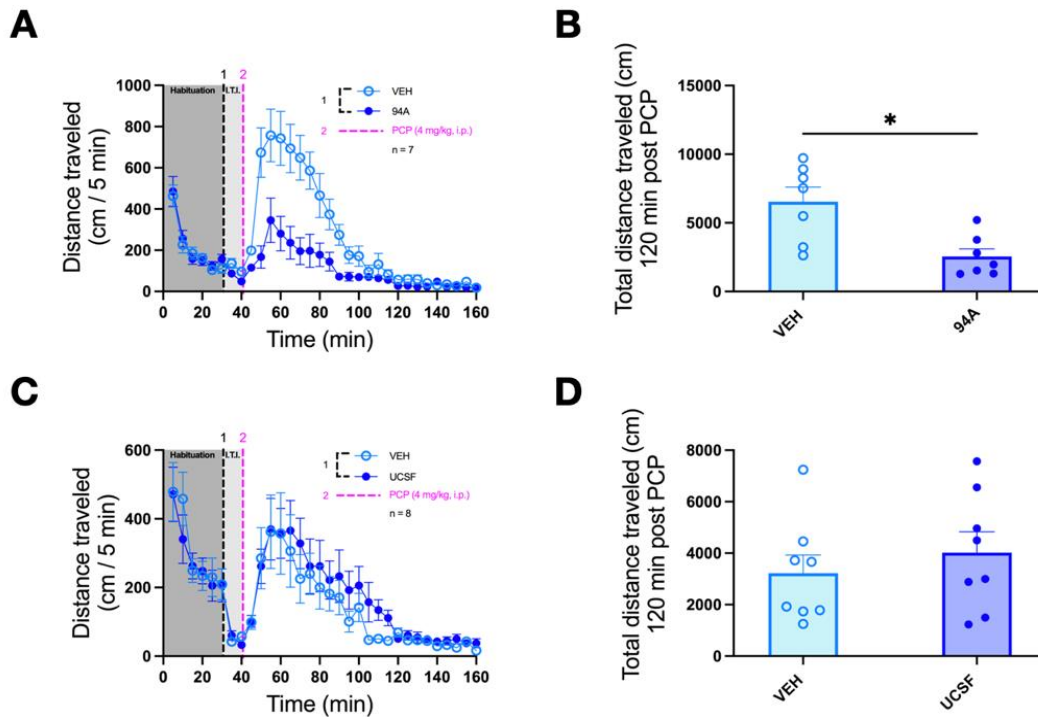


Figure 10 Cortical D2R-βarr2 signaling has antipsychotic like activity with PCP.

WT mice received a bilateral local infusion in the prefrontal cortex of 1) 1 μ g per side of VEH, (A) D2R-βarr2 biased ligand 94A, or (C) D4R-βarr2 biased ligand UCSF [black line, 30 min] followed by 2) a systemic PCP injection (6 mg/kg i.p.) [pink line, 40 min]. Distance traveled was calculated for 120 min after 30 min of habituation. Data were analyzed using a two-way ANOVA test with post hoc Bonferroni corrections. A main effect of 94A treatment $F(1,12) = 11.28$, $**p = 0.0057$ and 94A treatment \times time interaction $F(31,372) = 7.259$ $p < 0.0001$ were reported. UCSF treatment \times time interaction $F(31,434) = 0.9867$, $p < 0.0001$. Total cumulative distance after systemic injection of PCP was calculated for mice administered VEH and D2- like ligands. Data were analyzed using an unpaired, non-parametric t-test- Mann-Whitney rank sums. (B) Cortical infusion of the D2R-βarr2 biased ligand 94A was able inhibit the PCP response, $* p = 0.0111$, compared with VEH control; $n = 7$. (D) The D4R-βarr2 biased ligand UCSF had no effect

on PCP induced locomotion, $p = 0.5737$, compared with VEH control; $n = 8$. Data shown are the mean \pm SEM.

As dopaminergic activity and D2 receptor density in the striatum opposes the prefrontal cortex, we repeated this experiment with local administration in the dorsomedial striatum (**Figure 11**). Once again, 94A significantly decreases PCP induced locomotion $**p=0.0093$, compared with VEH control; $n = 7- 8$. The D₄R ligand UCSF had no effect on PCP induced behaviors in the striatum, $p = 0.9591$, compared with VEH control; $n = 8$. UCSF's lack of antipsychotic activity was expected as D₄R is sparse in the striatum and receive inputs from different inputs than the D₂R that heavily co-express on striatal medium spiny neurons.

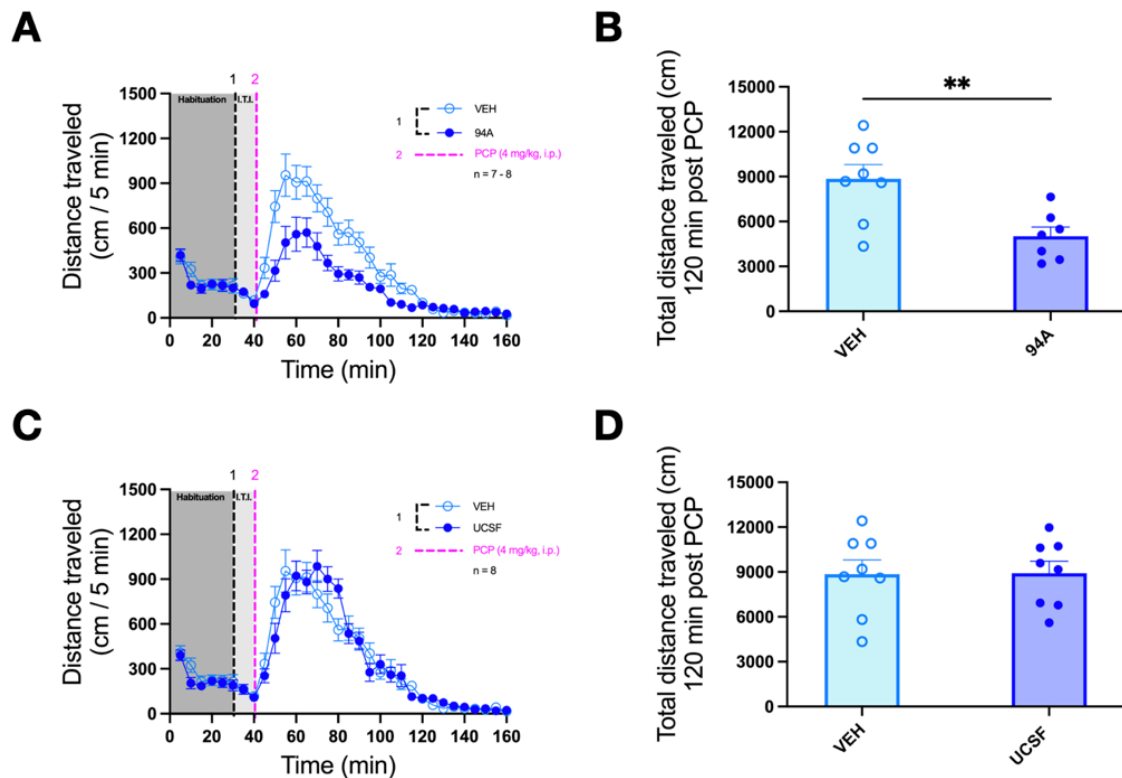


Figure 11 Striatal D2R-βarr2 signaling has antipsychotic like activity with PCP.

WT mice received a bilateral local infusion in the dorsomedial striatum of 1) 1 μ g per side of VEH, (A) D2R-βarr2 biased ligand 94A, or (C) D4R-βarr2 biased ligand UCSF [black line, 30 min] followed by 2) a systemic PCP injection (6 mg/kg i.p.) [pink line, 40 min]. Distance traveled was calculated for 120 min after 30 min of habituation. Data were analyzed using a two-way ANOVA test with post hoc Bonferroni corrections. A main effect of 94A treatment $F(1,13) = 8.820$, $*p=0.0057$ and 94A treatment \times time interaction $F(31,403) = 5.1289$, $p < 0.0001$ were reported. UCSF treatment \times time interaction $F(31,434) = 1.905$, $p < 0.0001$. Total cumulative distance after systemic injection of PCP was calculated for mice administered VEH and D2- like ligands. Data were analyzed using an unpaired, non-parametric t-test- Mann-Whitney rank sums. (B) Striatal infusion of the D2R-βarr2 biased ligand 94A was able inhibit the PCP response, $**p=0.0093$, compared with VEH control; $n = 7- 8$. (D) The D4R-βarr2 biased ligand UCSF had no effect on PCP induced locomotion, $p = 0.9591$, compared with VEH control; $n = 8$. Data shown are the mean \pm SEM.

Our behavioral data further support 94A produces antipsychotic like effects through D₂R-βarr2 agonism in the PFC and D₂R-βarr2 antagonism in the STR. We did not find any support for the D₄R-βarr2 biased ligand have cortical agonism as previously studies suggested. Furthermore, we did not see any antipsychotic like effects from UCSF responding to PCP challenge.

3.4 Cortical βarr2-D₄R and Striatal βarr2-D₂R signaling produces antipsychotic like activity to AMPH challenge

To mimic striatal hyperdopaminergia, we used AMPH as a challenge to test the effects of our biased βarr2-D₂ like ligands. We measured the effects of injecting 94A (βarr2- D₂R) or UCSF (βarr2-D₄R) locally into the PFC and STR of WT mice on AMPH-induced locomotion.

Although UCSF did not exhibit any antipsychotic like activity, we tested if the GRK2 inhibitor Compound 101 would have an effect on local UCSF response to systemic AMPH (**Figure 12**). We co-administered the pharmacological GRK2 inhibitor compound 101 with UCSF in the PFC then systemically injected AMPH (3 mg/kg, i.p). UCSF significantly reduced AMPH induced hyperlocomotion *p = 0.0147, compared with VEH control. Importantly, UCSF lost its antipsychotic like effect when co-administered with GRK2 , *p = 0.0104, compared with UCSF. This result shows UCSF uses βarr2 signaling to produce an antipsychotic like response to AMPH.

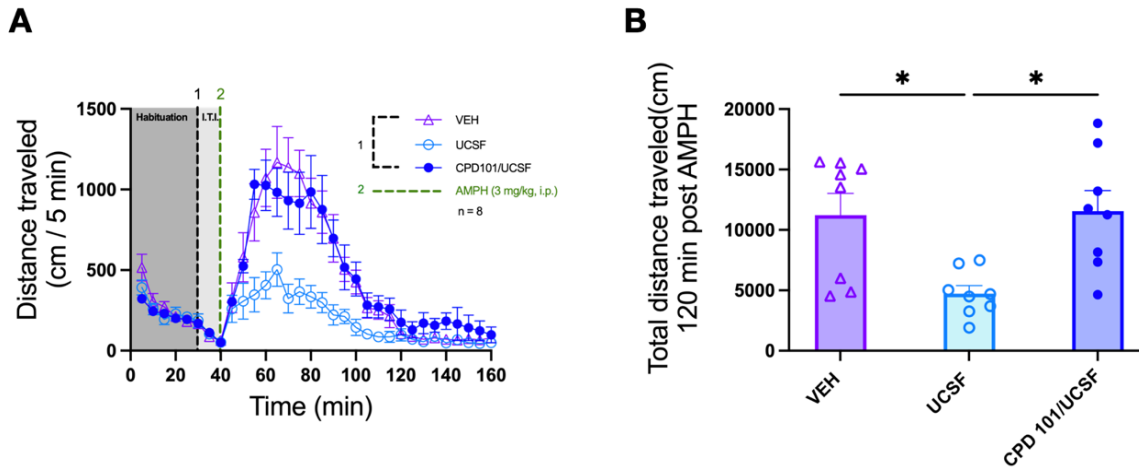


Figure 12 Cortical D4R-βarr2 biased antipsychotic like activity in response to AMPH is dependent on GRK2.

(A) WT mice received a bilateral local infusion in the prefrontal cortex of 1) 1 μg per side of VEH or D4R-βarr2 biased ligand UCSF with or without 0.5 μg per side of GRK2 inhibitor CPD101 [black line, 30 min] followed by 2) a systemic AMPH injection (3 mg/kg i.p.) [green line, 40 min]. Distance traveled was calculated for 120 min after 30 min of habituation. Data were analyzed using a two-way ANOVA test with post hoc Bonferroni corrections. Main effect of treatment $F(2, 21) = 6.216$, $*p = 0.0415$ and interaction between treatment and time $F(31, 651) = 41.53$ $p < 0.0001$. (B) Total cumulative distance after AMPH was calculated for mice administered VEH, UCSF, and CPD101/UCSF. Data were analyzed using a one-way ANOVA with post hoc Tukey test, $n = 8$ per group. A significant treatment and time interaction was observed: $F(2,21) = 6.703$, $**p = 0.0056$. Only UCSF was able to inhibit the AMPH response. VEH: $*p = 0.0147$, CPD101/94a: $*p = 0.0104$, compared with UCSF. Co-injection with GRK2 inhibitor prevented UCSF's antipsychotic like activity. The PCP response of CPD101/94a compared with VEH was not significant, $p = 0.9870$. Data shown are the mean \pm SEM.

We measured the effects of injecting 94A (βarr2- D₂R) or UCSF (βarr2-D₄R) locally into the PFC mice on AMPH-induced locomotion (Figure 13). 94A had no effect on AMPH induced hyperlocomotion ($p = 0.2593$, compared to VEH control) while UCSF significantly inhibited AMPH response and significantly decreased distance traveled ($*p = 0.0148$, compared with VEH control). These results suggest the D₄R have an inhibitory

role to AMPH either because their significantly larger cortical receptor density compared to D₂R or they modulate activity through different cellular mechanisms that act independently of GABAergic interneurons.

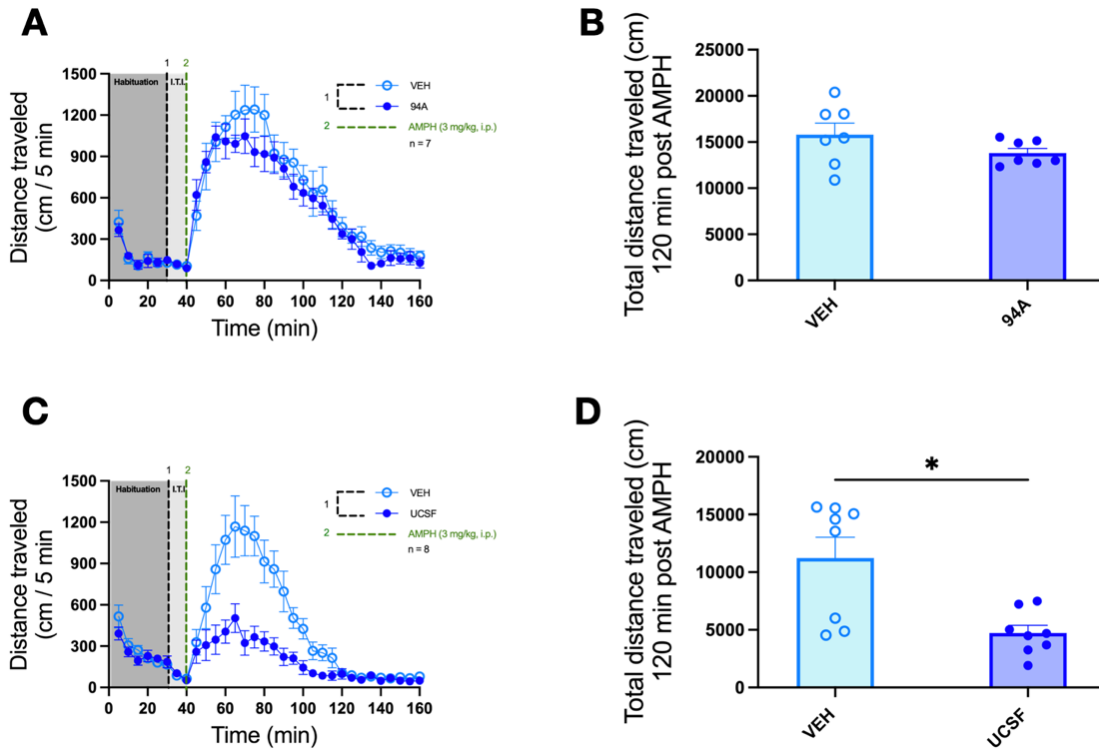


Figure 13 Cortical D₂R-βarr₂ signaling loses its antipsychotic like activity while D₄R-βarr₂ signaling inhibits the AMPH responses.

WT mice received a bilateral local infusion in the prefrontal cortex of 1) 1 μg per side of VEH, (A) D₂R-βarr₂ biased ligand 94A, or (C) D₄R-βarr₂ biased ligand UCSF [black line, 30 min] followed by 2) a systemic AMPH injection (3 mg/kg i.p.) [green line, 40 min]. Distance traveled was calculated for 120 min after 30 min of habituation. Data were analyzed using a two-way ANOVA test with post hoc Bonferroni corrections. There was no significant 94A treatment × time interaction $F(31,372) = 0.6163$, $p = 0.9488$. A main effect of UCSF treatment $F(1,14) = 11.02$, $p = 0.0051$ and UCSF treatment × time interaction $F(31,424) = 8.091$, $p < 0.0001$. Total cumulative distance after systemic injection of AMPH was calculated for mice administered VEH and D₂- like ligands. Data

were analyzed using an unpaired, non-parametric t-test- Mann-Whitney rank sums. (B) Cortical infusion of the D2R- β arr2 biased ligand 94A did not attenuate the AMPH response, $p = 0.2593$, compared with VEH control; $n = 7$. (D) The first display of antipsychotic like activity for the D4R- β arr2 biased ligand. UCSF significantly reduced AMPH induced locomotion, $*p = 0.0148$, compared with VEH control; $n = 8$. Data shown are the mean \pm SEM.

We then measured the effects of injecting 94A (β arr2- D₂R) or UCSF (β arr2-D₄R) locally into the STR mice on AMPH-induced locomotion(**Figure 14**). 94A regained its antipsychotic like activity and significantly decreased AMPH induced hyperlocomotion (** $p = 0.0093$, compared to VEH control). Although cortical β arr2-D₄R signaling resulted in antipsychotic like activity, in the striatum UCSF lost its inhibitory effect to AMPH challenge ($p = 0.4418$, compared with VEH control).

Our studies show contrasting regional activity of the β arr2- D₂R and β arr2-D₄R biased ligands- 94A (β arr2- D₂R) has antipsychotic like activity in the striatum and UCSF (β arr2-D₄R) has antipsychotic activity in the prefrontal cortex in response to AMPH challenge (**Figure 15**). Recent studies have investigated AMPH effect in the prefrontal cortex. Acute injections of AMPH induced cFOS, a marker of neuronal activity, in PV+ interneurons in the prelimbic and infralimbic cortex of rats(102,103). Additionally, electrophysiology experiments show aberrant pyramidal neurons firing patterns post AMPH(104). Dopamine can indirectly inhibit pyramidal cell activity in the mPFC through increases in GABA activity and suppressing other neuronal activity. We speculate UCSF is able to modulate AMPH effect in the cortex due D₄R's high expression on relevant GABAergic interneurons and pyramidal neurons(89,90,105). UCSF has significantly lower D₄R targets in the striatum, so the lack of antipsychotic activity was expected. Moving forward, we will continue to use the functionally selective β arr2- D₂R

ligand ,94A, to investigate antipsychotic like mechanisms in vivo.

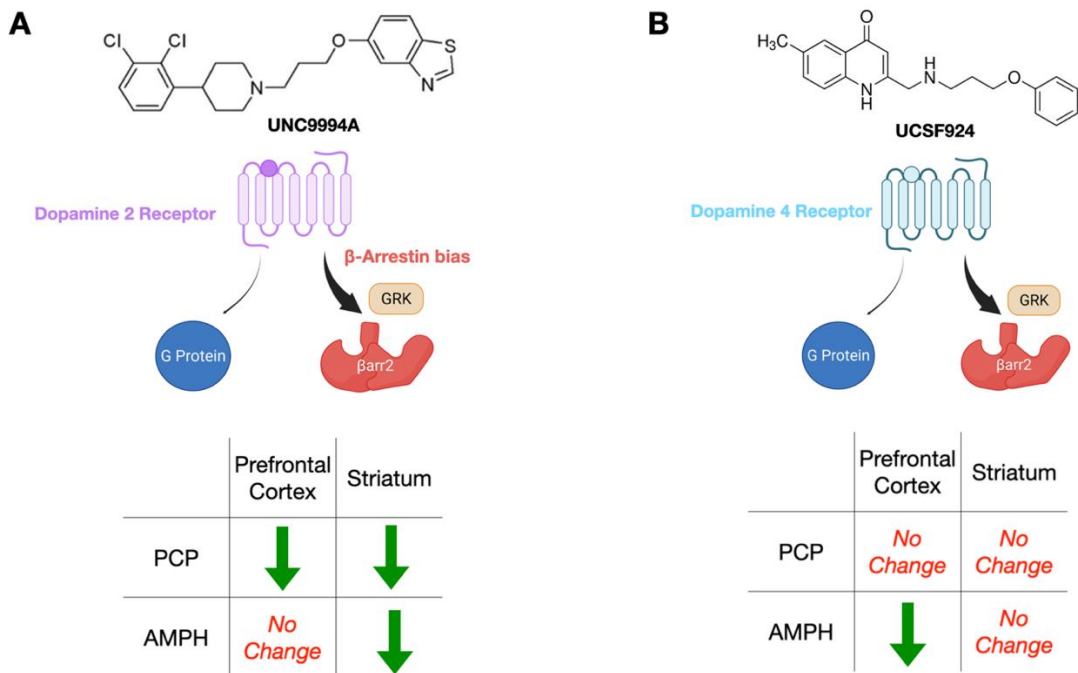


Figure 15 Functionally selective β -arrestin2 -D₂R ligand has more antipsychotic potential than β -arrestin2 -D₄R ligand.

(A) 94A – a functionally selective β -arrestin2 -D₂R ligand- resulted in antipsychotic like activity by inhibiting hyperlocomotion to local PCP challenge in the prefrontal cortex and striatum and local AMPH challenge in the striatum. (B) UCSF- a functionally selective β -arrestin2 -D₄R ligand- only produced antipsychotic like activity to local AMPH challenge in the prefrontal cortex.

4. Characterization of antipsychotic potential of cortical β -arrestin2 D₂R-mediated signaling in vivo

The prefrontal cortex receives and integrates extensive inputs from cortical and subcortical areas involved in sensorimotor and limbic activities to regulate complex cognitive and social behaviors. Executive functioning --attention, working memory, decision making, cognitive flexibility, and sociability – is influenced by cortical excitation:inhibition balance primarily coordinated by excitatory glutamatergic pyramidal neuron and inhibitory GABAergic interneurons. Dopamine helps regulate this concerted cortical E/I balance through G protein inhibitory signaling and dysregulation of cortical dopamine is correlated with many psychiatric illnesses like schizophrenia. In addition to cortical hypodopaminergia, decreased excitability and expression of parvalbumin positive (PV+) GABAergic interneurons and cortical pyramidal is observed in schizophrenia. For decades, the field of neuropharmacology has attempted to rescue cognitive impairments with antipsychotic therapies targeting cortical D₂R. Unfortunately, these extensive studies have been unsuccessful, and no FDA approved antipsychotic improves cognitive or social deficits.

4.1 Therapeutic potential of biased β -arrestin 2 signaling

Functionally selective ligands that selectively engage one signaling pathway over others may provide insight into novel drug targets and relevant signaling cascades. Like all GPCRs, activation of dopamine receptors results in G protein-dependent modulation of second messengers like cAMP which, in turn, mediates further

downstream signaling cascades. Sustained DA stimulation results in receptor phosphorylation by G-protein-coupled Receptor Kinases (GRKs) and the recruitment of β -arrestins which subsequently cause receptor desensitization, endocytosis and supposed termination of the signal.

Over the past decade, our lab has demonstrated that like other GPCRs, DARs can signal through a distinct G-protein independent pathway that is dependent on the ability of β -arrestin2 (β arr2) to scaffold intracellular signaling complexes that ultimately mediate distinct cellular and behavioral processes. Importantly, β arr2 is expressed at contrasting high and low levels in the prefrontal cortex and striatum, respectively. A major limitation of antipsychotic drugs that signal that G protein pathways is their inability to function as a partial agonist to simultaneously treat cortical *hypodopaminergia* and striatal *hyperdopaminergia*. The inverse expression of β arr2 may provide the ideal mechanism for achieving dopaminergic cortical agonism and striatal antagonism with minimum off target effects.

Our laboratory contributed to the development and characterization of a β arr2 biased D₂R ligand-UNC9994A (94A) with little to no activity at the G protein pathway. In vitro electrophysiology experiments showed 94a acted as an agonist in the cortex—increasing excitability of fast spiking interneurons—and an antagonist in the striatum – have no effect on medium spiny neuron excitability(106). Characterizing the cellular

and neurophysiological outcomes of cortical β arr2 biased D₂R signaling may provide valuable insight into treating cognitive deficits in psychiatric illness.

To understand more about the antipsychotic like activity exhibited by 94A, we attempted to recapitulate inhibition of psychotogenic induced responses and increased cortical GABAergic excitation. We utilized chemogenetics (Designer Receptors Exclusively Activated by Designer Drugs, DREADDs) to selectively increase neuronal activity in cortical interneurons and studied PCP induced effects in a β arr2 KO mouse line. To add to the significance of this work, we are the first group using the β arr2-biased DREADD to study functionally selective signaling and therapeutic potential.

4.2 Validation of the Barr2 DREADD

4.2.1 Confirmation of GRK2 and β arr2 expression within the cortex

The β arr2-biased D₂R ligand UNC9994A (94A) was designed using the scaffold of aripiprazole, a third-generation antipsychotic and partial D₂R agonists. To determine the β arr2 functional selectivity of this ligand, rigorous biochemical, protein interaction, behavioral, and electrophysiological assays were completed testing 94A against endogenous ligand dopamine and other well characterized D₂R ligand. A protein-protein interaction assay measuring β arr2 recruitment to the D₂R determined low GRK2 levels enhanced agonist activity and high GRK2 levels increase antagonist activity of 94A(45). The tested D₂R ligands that preferentially signal through G protein signaling pathways did not show changes in agonist and antagonist profiles with varying

concentration of GRK2(44,107). These results are consistent with the GPCR signaling cascade that has long established β arr2 recruitment to the GPCR is dependent on GRK phosphorylation of the G protein subunit. Our lab previously quantified GRK2 distribution in the prefrontal cortex and striatum and reported significantly higher expression in the prefrontal cortex as compared to the striatum(106). As our future experiments and working hypothesis about the therapeutic potential of β arr2-biased D₂R signaling rely heavily on this distinct cortical and striatal expression, we repeated the western blot analysis. Our regional GRK2 and β arr2 expression complemented the previously published expression pattern (Figure 16).

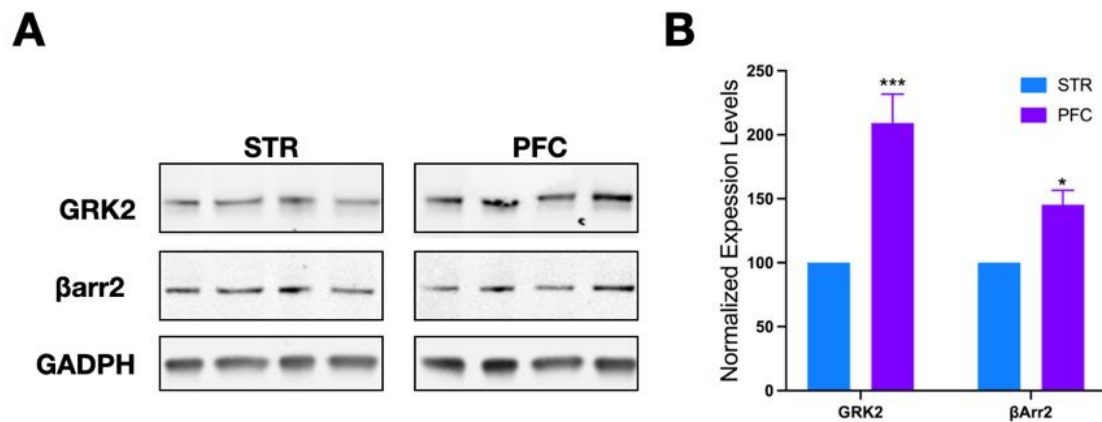


Figure 16 Cortical and striatal expression of GRK2 and β arr2:

(A) Western blot analysis in brain slices from the prefrontal cortex (PFC) and striatum (STR) from C57Bl6 mice probed with antibodies to GRK2, β arr2, and GAPDH (B) Quantification of Western blot band intensities normalized to the loading control GAPDH. STR levels were set to 100%. * $p < 0.05$, *** $p < 0.001$, comparing STR with PFC using a two-way ANOVA test with post hoc Bonferroni corrections. Error bars depict SEM of 4 independent experiments.

4.2.2. Synthetic pharmacology using DREADDs

GPCRs are the most ubiquitous membrane receptors, consequently, they are common drug targets(108). Pharmacologically characterizing GPCRs and the outcome of their mediated signaling cascades can help understand disease pathophysiology and improve drug therapy. DREADDs, chemogenetic tools that can temporally control neuronal activity with cell specificity, can uniquely contribute to learning mechanisms underlying therapeutic efficacy(109,110). DREADDs are high sensitivity engineered GPCRs that can respond to nanomolar concentrations of its designed exogenous ligand with high efficacy (109). DREADDs act on comparable timescales and hormonal signaling mechanisms ongoing in the brain. We will utilize DREADDs as ‘synthetic pharmacology’ or manipulating neuronal activity to resemble pharmacotherapeutic drug action(111).

The first engineered DREADDs introduced mutations to modify the human muscarinic receptors and change its coupling preference with G proteins(112). Presently, many DREADD variants exist with distinct G protein coupling and downstream signaling effects. Rat and human muscarinic receptor were hybridized to create a new DREADD rM3Dqarr that has a coupling preference to Arrestin 2 rather than any G protein subunits(113). We used two different excitatory DREADDs (HM3Dq and β arr2 biased rM3Dq) to study how 94A modulates neuronal activity within the prefrontal cortex (**Figure 17**).

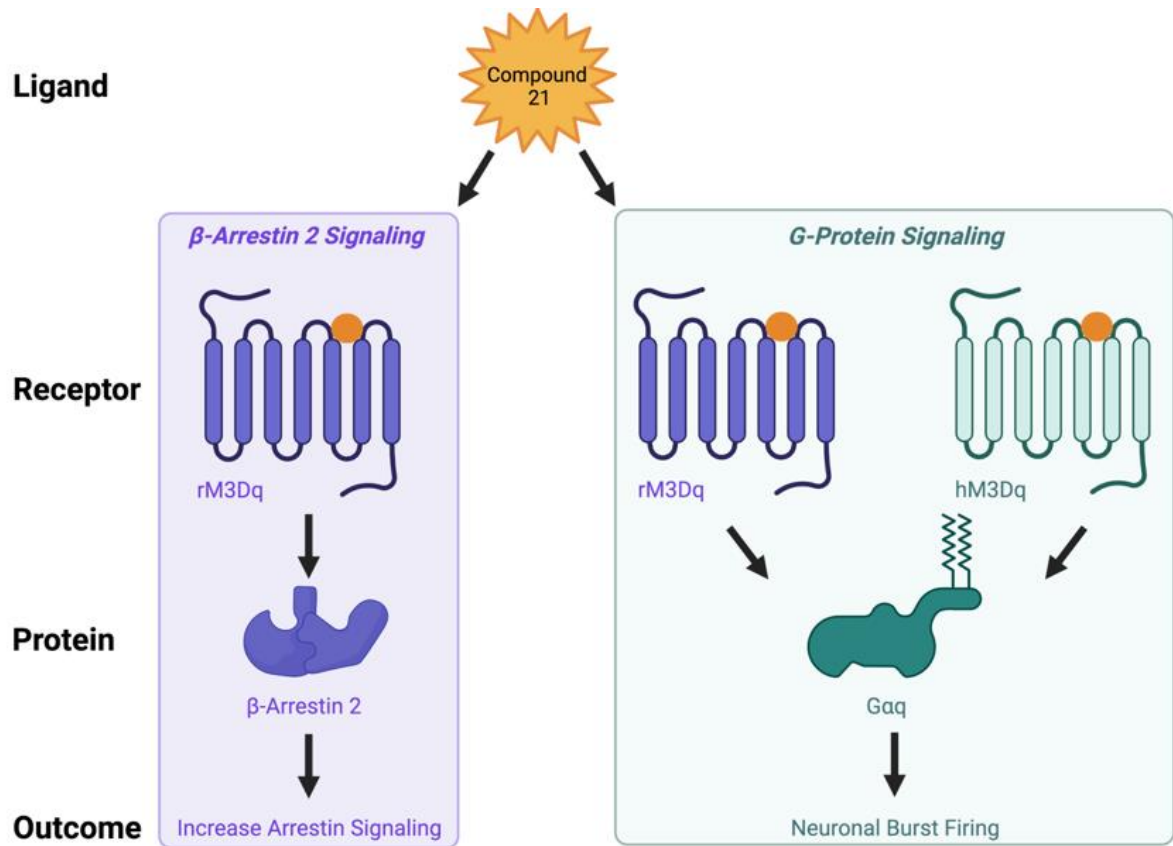


Figure 17 Cartoon of Designer Receptors Exclusively Activated by Designer Drugs (DREADDs) signaling properties.

Muscarinic receptor based DREADDs are engineered G-Protein Coupled Receptors that selectively influence cellular signaling after binding with an exogenous ligand, Compound 21. rM3Dq (left) is biased towards the effector protein β Arrestin mediated signaling. rM3Dq and hM3Dq (right) signal through the Gaq effector protein to increase Ca^{2+} and neuronal burst firing.

4.2.3. In Vitro Assessment of the β Arrestin biased DREADD

We used bioluminescent resonance energy transfer (BRET) assays to measure the interaction between β arrs and the DREADD receptors (**Figure 18**). As a negative control we included rM3Dq as it functions through the same receptor as the β arr-biased rM3Dq but preferentially couples to G proteins like HM3Dq. As described in methods, we co-

transfected HEK293T cells with DREADDs fused to RLucII and Venus tagged β arr2.

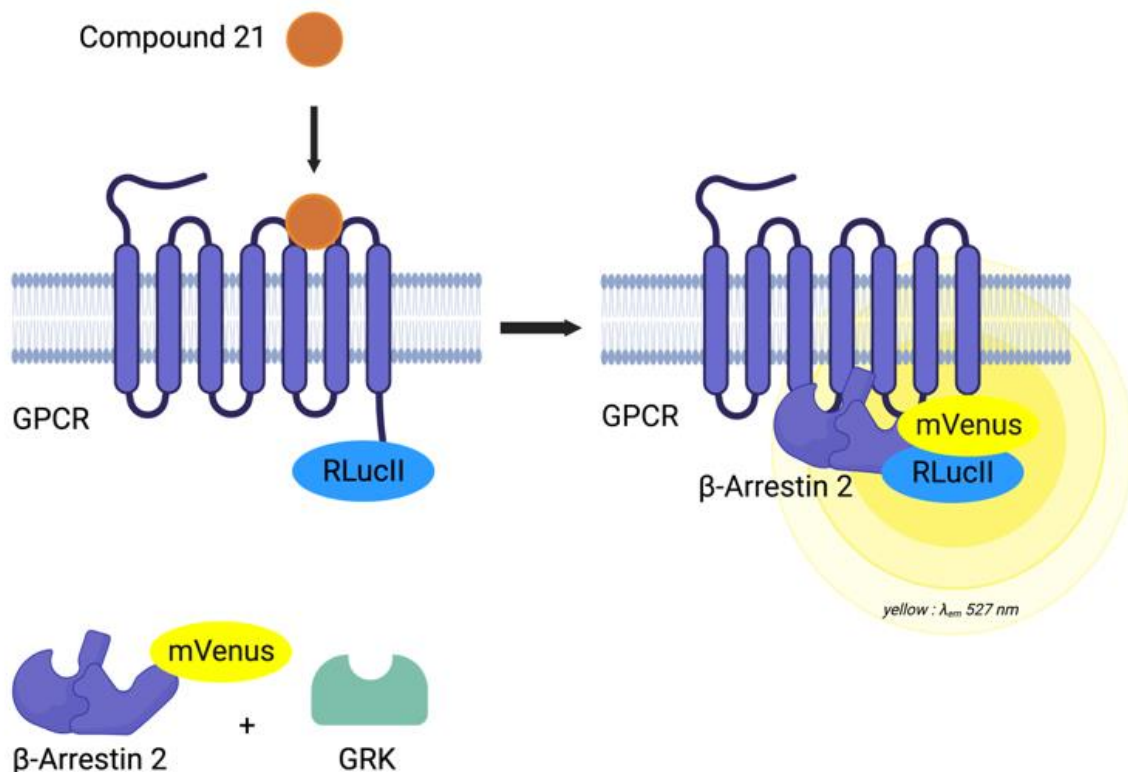


Figure 18 Schematic of bioluminescence resonance energy transfer (BRET) assay to monitor protein-protein interactions.

This biochemical assay depends on dipole-dipole energy transfer from a donor enzyme-luciferase (RLucII, blue) to an acceptor fluorophore (mVenus, yellow). When the fluorophore tagged protein, β -Arrestin 2, is within 10 nm of the luciferase fused protein, GPCR, an enzyme-mediated oxidation of the luciferase substrate will produce a quantifiable fluorescent signal.

We stimulated cells with increasing concentrations of GRK2 and DREADD agonist Compound 21 and reported NET BRET ratios (**Figure 19**) (114). hM3Dq had the highest NET BRET reflecting high β arr2 recruitment to the receptor. Importantly, CPD21 β arr2-rM3Dq had the lowest [CPD21] BRET₅₀ reflecting the effect of β arr2 bias. The

control rM3Dq had the lowest NET BRET and the highest [CPD21]BRET₅₀, otherwise low recruitment of β arr2

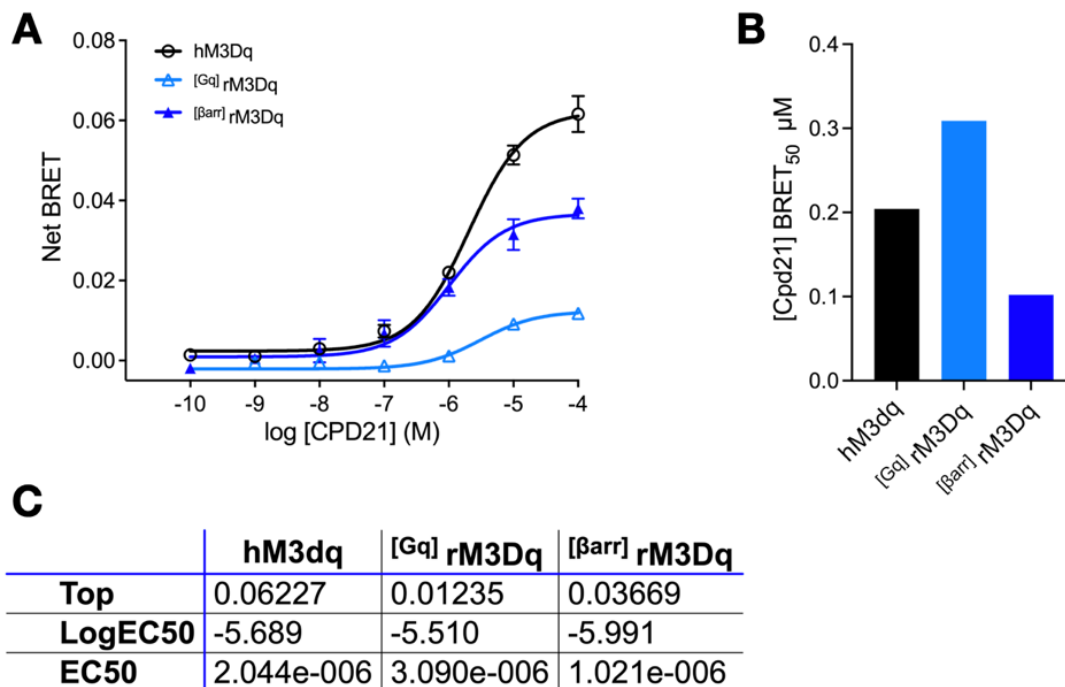


Figure 19 BRET Receptor Arrestin Recruitment Assay.

(A) HEK293T cells co-expressing BRET donor, hM3Dq-RLuc, [Gq]rM3D-RLucII or [βarr]rM3D-RLuc, and BRET acceptor β arr2-mVenus. GRK2 were incubated with increasing concentrations of CPD21. BRET measurements were performed as described under Materials and Methods. Readings were averaged per plate and the NET BRET ratio was calculated by subtracting the stimulated CPD21 Venus/RLuc ratios from the unstimulated vehicle Venus/RLuc ratio. (B values (μ M) were as follows: hM3Dq= 2.04 ± 0.07 , [Gq]rM3Dq= 3.090 ± 0.18 , and [βarr]rM3Dq= 1.021 ± 0.14 With the lowest CPD21 BRET₅₀, the CPD21 displayed the highest potency at the biased β arr2-rM3Dq (C) A table summarizing the DREADDs arrestin recruitment. The NET BRET ratio presented is a combined average from 3 experiments. Data are presented as Mean NET BRET ratio \pm SEM.

We next evaluated DREADD preferred G protein coupling using the TGF α shedding assay. A schematic describes the mechanism to quantify G protein activity

(Figure 20). Our lab modified this assay to measure fluorescence from alkaline phosphatase substrate, 4-methylumbelliferyl phosphate(45,115). G proteins are classified into four families according to their α subunit: G_s , G_i , $G_{12/13}$, and G_q (116) DREADDs are engineered to preferentially couple to a specific G protein(s). We measured the amount of $TGF\alpha$ released for each DREADD co- expressed with 3 different G protein subunits subunit: G_s , G_i , and G_q and a negative control $G_{q\Delta C\text{ term}}$: G_q protein lacking 6 C-terminal residues essential for coupled to receptors. The objective was to validate $[\beta\text{arr}]rM3D$ preferentially engaged βarr which would be interpreted as little to no $TGF\alpha$ shedding.

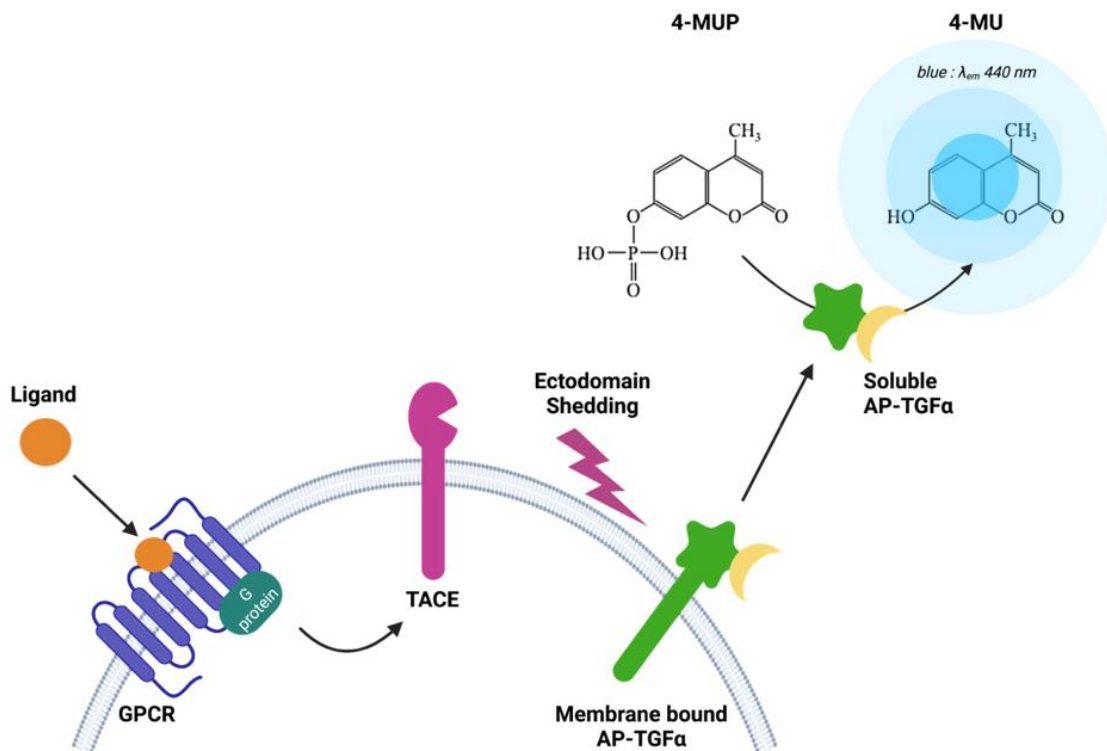


Figure 20 $TGF\alpha$ Shedding Assay Schematic.

The $TGF\alpha$ shedding assay detects basal G protein coupled receptor (GPCR) activity and assesses G-protein binding to GPCRs. Ligand binding to the GPCR releases G protein

from the receptor and induces tumor necrosis factor α converting enzyme (TACE) activation. TACE cleaves and releases alkaline phosphatase coupled-TGF α (AP-TGF α) from the cell membrane into cell media. Soluble TGF α dephosphorylates 4-MUP into 4-MU, a blue wavelength fluorescent molecule. G-protein coupling for the various DREADDs was assessed via alkaline peroxidase activity released into the media

We observe the predicted shedding with HM3Dq and rM3Dq having the highest percentage with their preferred G protein, Gq and Gs respectively (**Figure 21**)(109,111). All DREADDs showed little to no activity with the control Gq Δ C term. The β arr2 biased rM3Dq showed little to no activity with any G protein subunits. These data and the results from the BRET recruitment support β arr2-rM3Dq is biased towards β arr2 with little G protein engagement. In conclusion, we validated the functional selectivity of the β arr2 biased DREADD in vitro, then we proceeded to in vivo DREADD studies to model 94A.

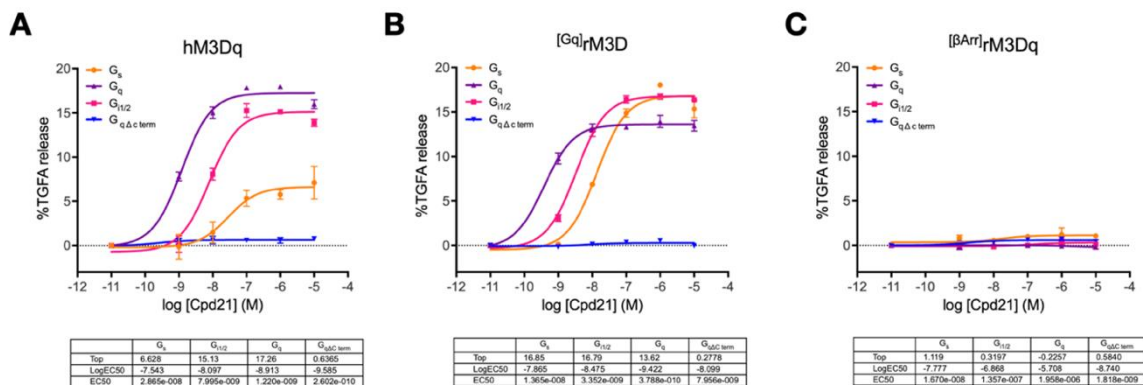


Figure 21 Evaluation of DREADD agonist (Cpd21) activity in the TGF α shedding assay.

DREADD GPCR receptors were co-expressed with chimeric G α protein subunits G_s, G_{i1/2}, G_q or a negative control G_q Δ C term. (A) When co-expressed with hM3Dq's effector G protein G_q, hM3Dq released the highest percentage of TGF α (17.26%) e.g. the most GPCR activity (B) [G_q]rM3D exhibited similar GPCR activity with all G α proteins but with a slight preference for G_s (C) [β Arr]rM3D has little to no G Protein activation in

the TGF α shedding assay confirming the intended design of the receptor. The negative control Gq Δ C term did not effectively bind with any DREADD GPCR as noted by the < 1 % TGF α release in all DREADD variants. No statistics performed.

4.3 Determining the role of cortical β arr2 biased signaling in antipsychotic like activity

Neural gamma oscillations (30- 80 Hz) have been correlated with attention, working memory, sensory processing, and other key features of cognition(117). GABAergic inhibitory interneurons, specifically parvalbumin expressing fast-spiking, work in synchrony with excitatory pyramidal neurons to generate gamma oscillations. Patients with schizophrenia experience several cognitive deficits, have abnormal reductions in gamma power as measured by electroencephalogram recordings during cognitive tasks, and have decreased expression of parvalbumin in cortical inhibitory neurons a reduction also observed in several animal models of schizophrenia(25,27). Animal models of schizophrenia utilize NMDAR antagonists such as PCP to induce cortical disinhibition. These data suggest a clear role of cortical interneurons and schizophrenia symptomology, yet the mechanisms to rescue cognitive ability and restore abnormal gamma activity remains elusive.

The D₂R antagonism that is a core pharmacodynamic feature of most antipsychotics does not improve cortical disinhibition and often worsens circuit dysfunction and behavioral abnormalities. A recent study used an NMDAR antagonist MK-801 to induce cortical disinhibition but a D₂-like partial agonist was able to stabilize gamma oscillations(118,119). Our previously whole cell, current clamping study

demonstrated 94A significantly increased GABAergic interneuron excitability(106). Additionally, a D₂R agonist quinpirole increases FSI excitability, directly contradicting its canonical inhibitory role(120). These data converge to inform our hypothesis that cortical disinhibition can be treated with G protein independent agonism targeting GABAergic interneurons. To test this hypothesis, we tested the behavioral responses after disrupting cortical circuitry with the NMDAR antagonist PCP in mice expressing excitatory hM3Dq or β arr2-rM3Dq in cortical interneurons. To examine the relationship between cortical interneuron excitability and antipsychotic actions, we evaluated locomotor response after systemic PCP injection in mice expressing excitatory DREADDs in the prefrontal cortex. Cell specific activation in the prefrontal cortex was achieved by stimulating inhibitory neurons with hM3Dq. These excitatory proteins were selectively expressed in GABAergic neurons using the DLX enhancer. Using immunohistochemistry (IHC), we confirmed cortical interneuron expression of DREADDs. We stained for GABAergic interneurons, Parvalbumin + interneurons, somatostatin interneurons, and CAMKIIa as a negative control (**Figure 22**). We quantified the total number of labeled cells and co-expression with DREADDs and respective antibody markers and confirmed we successfully targeted GABAergic

interneurons with negligible off targets of pyramidal cells (not shown).



Figure 22 Excitatory DREADD expression in cortical interneurons.

(A) AAV constructs encoding the excitatory hM3D DREADD driven by the interneuron selective Distal Less Homeobox (DLX) promoter and tagged with the fluorescent reporter mCherry. (B) This DREADD plasmid was packaged into AAV and selectively targeted to the prelimbic cortex, a region within the medial frontal cortex in C57BL6 mice aged 8- 12 weeks. Stereotaxic coordinates + 2.5 AP; \pm 0.3 ML; - 1.8 DV. AAV titers were confirmed as $> 10^{12}$ (C) DREADD expression was confirmed by visualization of the fluorescent marker mCherry. DREADD localization to cortical interneurons was confirmed through IHC, using antibodies against GAD67 (GABAergic interneuron marker; top row), PV (parvalbumin + interneuron marker; middle row), or a negative control CamKIIa (excitatory pyramidal cell marker; bottom row). Interneuron targeting was validated by quantifying DREADDs colocalization with inhibitory markers – GAD67 and PV. DREADDs were robustly co-expressed with GAD67 (merge: middle column, top row) and showed no colocalization with CAMKIIa (merge: middle column, bottom row). All antibody staining conditions had at least n= 3 mice. Scale bar 50 μ m.

We stereotaxically inject the AAV-DLX-HM3Dq construct into the prefrontal cortex of WT mice and allowed them to recover for 2 weeks. PCP-induced locomotion is a pharmacologically induced behavior commonly inhibited by APD. To assess whether cortical interneuron excitability can elicit antipsychotic-like effects, we measured the effects of systemically injecting WT mice with vehicle (saline/ DMSO) or Compound 21 (DREADD agonist) on PCP-induced locomotion. Consistent with previous findings, increased GABAergic excitability reduced PCP-induced locomotion (**Figure 23B**, ** $p = 0.0050$); This resembled our previously published PCP inhibition by 94A. In a different cohort of mice expressing hM3Dq in cortical interneurons, we measured the behavioral response when stimulated with AMPH. Cortical interneuron activation did not affect AMPH induced locomotion (**Figure 23D**, $p = 0.62000$). These results are consistent with these drugs primary mechanisms and site of action. The AMPH-induced locomotor response is dependent on striatal DA release. It is likely that animals with DREADD stimulation of cortical interneurons could exert local control to restore excitation/inhibition balance, consequently inhibiting the PCP response.

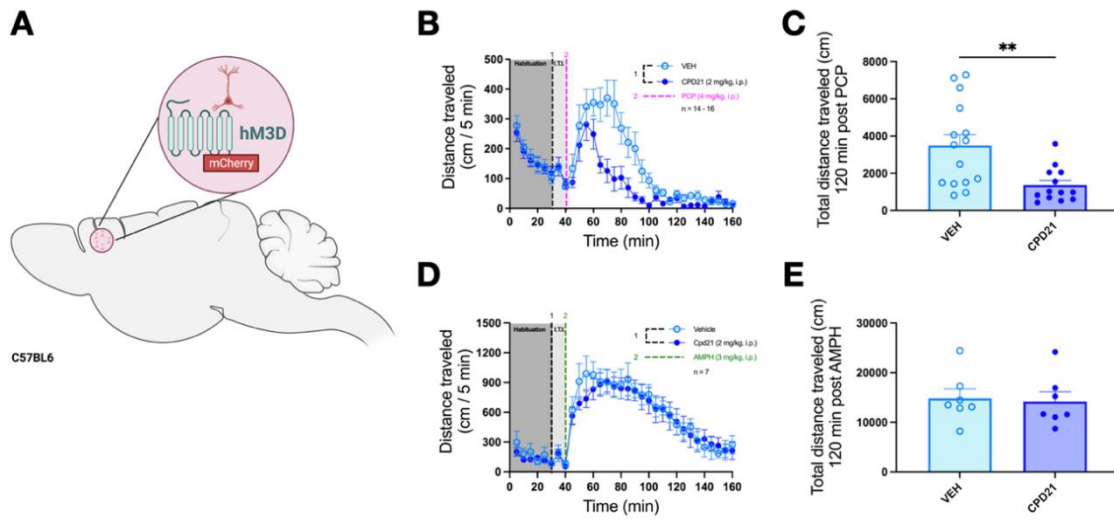


Figure 23 Activating cortical interneurons inhibits PCP, but not AMPH responses.

(A) Schematic of cortical interneurons expressing the excitatory DREADD HM3Dq in WT mice. WT mice were systemically injected with 1) VEH or DREADD agonist CPD21 2 mg/kg, i.p. [black line, 30 min] then 2) a systemic injection of psychotogenic drug (B) PCP 4 mg/kg, i.p. [pink line, 40 min] or (C) AMPH 3 mg/kg i.p [green line, 40 min]. Distance traveled was calculated for 120 min after 30 min of habituation. Data were analyzed using a two-way ANOVA test with post hoc Bonferroni corrections. With PCP responses, we report a main effect of treatment $F(1,29) = 8.442$, $**p = 0.0070$ and treatment \times time interaction $F(31,899) = 4.205$, $p < 0.0001$. There were no significant main effects or interactions observed with AMPH administration. Treatment \times time interaction $F(31,341) = 0.5475$, $p = 0.9779$. Total cumulative distance after systemic injection of (C) PCP or (E) AMPH calculated for mice administered VEH and CPD21. Data were analyzed using an unpaired, non-parametric t-test- Mann-Whitney rank sums. (C) Using DREADDs to increase cortical interneuron firing exhibited antipsychotic like behavioral effects and significantly inhibited the PCP response, $**p = 0.0050$, CPD21 compared with VEH control; $n = 14-16$. (E) Exciting cortical interneurons did not affect the AMPH response, $p = 0.6200$, CPD21 compared with VEH control; $n = 7$. Data shown are the mean \pm SEM.

Next we sought to interrogate β arr2's involvement with exciting cortical interneurons and mediating an antipsychotic response. We expressed the β arr2 biased DREADD under the control of the DLX promoter in WT mice. This enhanced β arr2

signaling in cortical interneurons. We quantified behavioral responses to PCP between VEH treated and CPD21 treated WT mice (**Figure 24**). Increased biased β arr2 signaling in cortical interneurons recapitulated the antipsychotic effect of the β arr2 biased D2R partial agonist 94A, $**p=0.0066$, compared with VEH control. We established β arr2 signaling in cortical interneurons was sufficient to inhibit PCP's response.

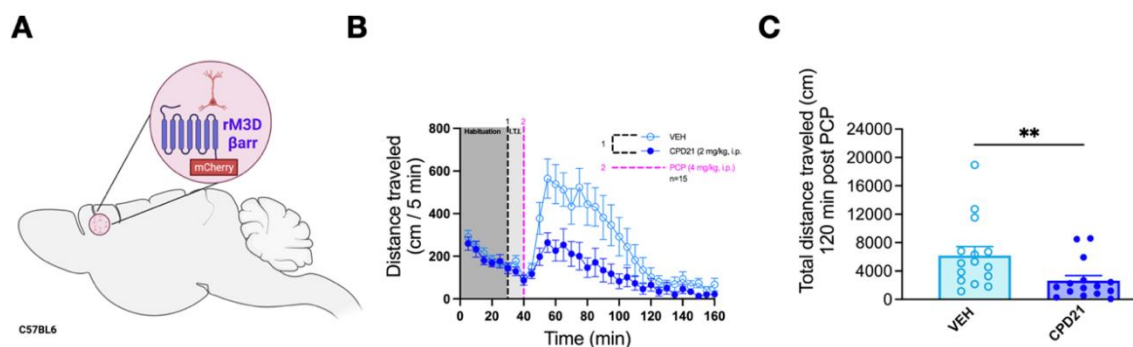


Figure 24 Exciting cortical interneurons with biased β arr2 signaling produces antipsychotic like responses to PCP

(A) Schematic of cortical interneurons expressing the excitatory β Arrestin 2 biased DREADD rM3Dq in WT mice. WT mice were systemically injected with 1) VEH or DREADD agonist CPD21 2 mg/kg, i.p. [black line, 30 min] then received 2) a systemic injection of (B) PCP 4 mg/kg, i.p. [pink line, 40 min]. Distance traveled was calculated for 120 min after 30 min of habituation. Data were analyzed using a two-way ANOVA test with post hoc Bonferroni corrections. PCP induced hyperlocomotion yielded a main effect of treatment $F(1,28) = 6.150$, $**p = 0.0194$ and a treatment \times time interaction $F(31,868) = 4.095$, $p < 0.0001$. (C) Total cumulative distance after PCP was calculated for mice administered VEH and CPD21. Data were analyzed using an unpaired, non-parametric t-test- Mann-Whitney rank sums. Increasing β Arrestin 2 signaling, and exciting cortical interneurons was sufficient to significantly inhibited the PCP response, $**p = 0.0066$, CPD21 compared with VEH control; $n = 15$. Data shown are the mean \pm SEM.

To investigate if β arr2 signaling in cortical interneurons we generated β arr2 KO mouse and measured their response in the same pharmacological behavioral assay, PCP

induced distanced travel in an open field box (**Figure 25**). β arr2 KO mice were indistinguishable from C57BL/6J mice in standard behavioral tests. β arr2 KO mice treated with CPD121 lost their antipsychotic like response to PCP (compared to VEH treated β arr2 KO mice, $p = 0.7786$). WT controls treated with CPD121 retained their antipsychotic like activity, confirming β arr2 is necessary to modulate cortical interneuron.

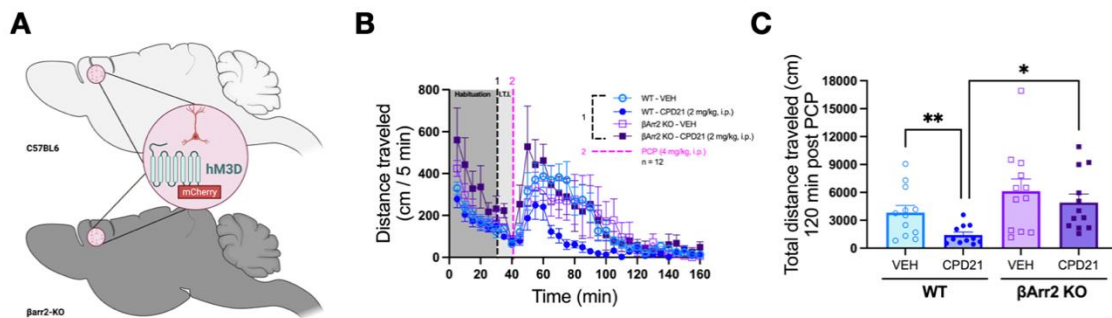


Figure 25 Cortical interneuron excitability requires β arr2 biased signaling to inhibit the PCP response.

(A) Schematic of cortical interneurons expressing the excitatory DREADD hM3Dq in WT mice or β arr2 KO (β arr2 KO) mice. (B) WT and β arr2 KO mice were systemically injected with 1) VEH or DREADD agonist CPD21 2 mg/kg, i.p. [black line, 30 min] then received 2) a systemic injection of (B) PCP 4 mg/kg, i.p. [pink line, 40 min]. Distance traveled was calculated for 120 min after 30 min of habituation. Data were analyzed using a three-way ANOVA test with post hoc Tukey corrections. After PCP administration, we observed yielded main effects of Genotype $F(1, 1376) = 122.1$ $p < 0.0001$, Treatment $F(1, 1376) = 40.28$ $p < 0.0001$ and interaction effects of Genotype \times Treatment $F(1, 1376) = 4.986$, $p = **0.0257$ (C) Total cumulative distance after PCP was calculated for mice administered VEH and CPD21. Data were analyzed using a one-way ANOVA with post hoc Tukey correction. Genotype \times Treatment \times Time $F(3,43) = 4.671$, $**p = 0.0065$. Despite being treated with CPD21 to increase cortical interneuron activity, β arr2 KO mice lost all antipsychotic-like activity and had no effect on PCP induced hyperlocomotion, $p = 0.7786$; compared with VEH treated β arr2 KO mice. WT mice treated with CPD21 inhibited the PCP response, $**p = 0.0043$, compared with VEH treated WT mice. β arr2 signaling is necessary to generate the antipsychotic like activity

to PCP from cortical interneuron excitation, CPD21 treated β Arr2 KO compared with CPD21 treated WT mice, $*p = 0.0497$. There were no significant PCP induced behavioral differences between VEH treated controls within genotypes, $p = 0.2828$, VEH treated β Arr2 KO compared with VEH treated WT mice. $n=12$ mice per group. Data shown are the mean \pm SEM.

Our synthetic pharmacology experiments shed light on 94A's antipsychotic action. We observed the same behavioral effects when induced with AMPH or PCP. Like 94A, the DREADD agonist CPD21 did not inhibit AMPH induced hyperlocomotion but significant decreases PCP effects. Our most critical finding was β Arr2 signaling in cortical interneurons is necessary to inhibit PCP's effect. This result has great therapeutic potential as GABAergic dysfunction is observed in schizophrenia. Many antipsychotic drugs do not act as D_2R agonists in the prefrontal cortex and ultimately do not rescue/improve the excitatory inhibitory balance integral to cognitive tasks. Our preliminary studies using pharmacological and transgenic mouse models of schizophrenia showed 94A can improve cognitive deficits.

Previously, we have studied the effect of 94A on memory impairments in NR1KD mice (a transgenic model of cortical disinhibition/ glutamate hypothesis of schizophrenia) and mice treated with PCP in the T-Maze behavioral assay for working memory(22,121–123). In the T Maze, mice receive sensory cues -light or sound- to indicate director of reward -left or right arm(124). Working memory - temporarily storing information for goals and decision making- is evaluated in this task as total number of correct trials after cue. Our preliminary results showed 94A significantly

improved total number of correct trials as compared to mice treated with PCP or transgenic NR1KD mice treated with the vehicle control. Additionally, we have tested our transgenic and pharmacological mouse models of schizophrenia in a social interaction assay to measure novel social behavior and social preference. Mice are prosocial animals and social interaction with other mice is encoded in the brain as rewarding or pleasurable as reported by microdialysis and neurophysiological recordings. Social deficits are another core cognitive symptom in schizophrenia(2,10,125). Mice that display social deficits have a preference for an inanimate object or a non social target or no preference for a social partner(126,127). NR1KD mice treated with vehicle spent equal time engaging with an object or social partner and displayed social deficits; however, when treated with 94A, NR1KD mice spent more time with a social partner. These preliminary data are promising and we will repeat our synthetic pharmacology experiments in WT and β Arr2 KO mice in these cognitive and social assays to uncover cellular mechanisms producing antipsychotic like behavior. We hypothesize β Arr2 dependent cortical excitation may be sufficient to rescue working memory or social behavior in PCP treated mice.

5. Characterizing psychotogenic induced corticostriatal network dynamics

Local field potentials are summations of the ongoing neural oscillatory activity and describe how neural networks produce behavioral outcomes. Cognitive dysfunction is highly prevalent in schizophrenia and is linked to morphological cortical abnormalities that can be measured using clinical brain imaging or neural recordings like functional magnetic resonance imaging (fMRI) or electroencephalograms(10,117,128,129). Recent clinical practices are using machine learning and dimensional approaches to study psychiatric disease. Rather than solely relying on diagnostic labels to create treatment plans, patients are being cluster based on their symptomology in concert with brain imaging to identify relevant biomarker that may aid in treatment.

Our lab has the unique neurophysiological and machine learning expertise to study neural circuit disruptions prevalent in disease states or induced by drugs. We use ensemble electrophysiological recordings from multiple brain areas to interrogate circuit changes(130–132). We conducted large-scale multi-array recordings across the corticostriatal circuit to neurophysiologically profile the pharmacological and behavioral effects of PCP and 94A. Our findings will be discussed in this chapter.

5.1 Transitioning from neuropsychiatric nosology to data driven diagnostics

Nosology, the medical classification of diseases, predates the current Diagnostic and Statistical Manual of Mental Disorders (DSM-5) by well over a century(133). Since the first the DSM was used in 1945, there has been a shift from solely relying on psychoanalysis or clinically presenting symptoms to considering neurobiology and psychopharmacology effects when diagnosing patients(3,133). With each iteration of the DSM there are critical evaluation of how to improve classifications. However, the vast heterogeneity and frequent co-morbidity in psychiatric disorders greatly complicates disease classification based on observable clinical symptoms. In neuro-psychiatry fields, data clustering methods are emerging quickly to aid in uncovering disease etiologies and shed light on how to improve treatment, with the overarching goal of personalized medicine in the near future. Converging neuroimaging and machine learning enable studies to non-invasively extract neurobiological information from diverse and high-

dimensional data sets in schizophrenia patient populations(134–136) (Figure 26).

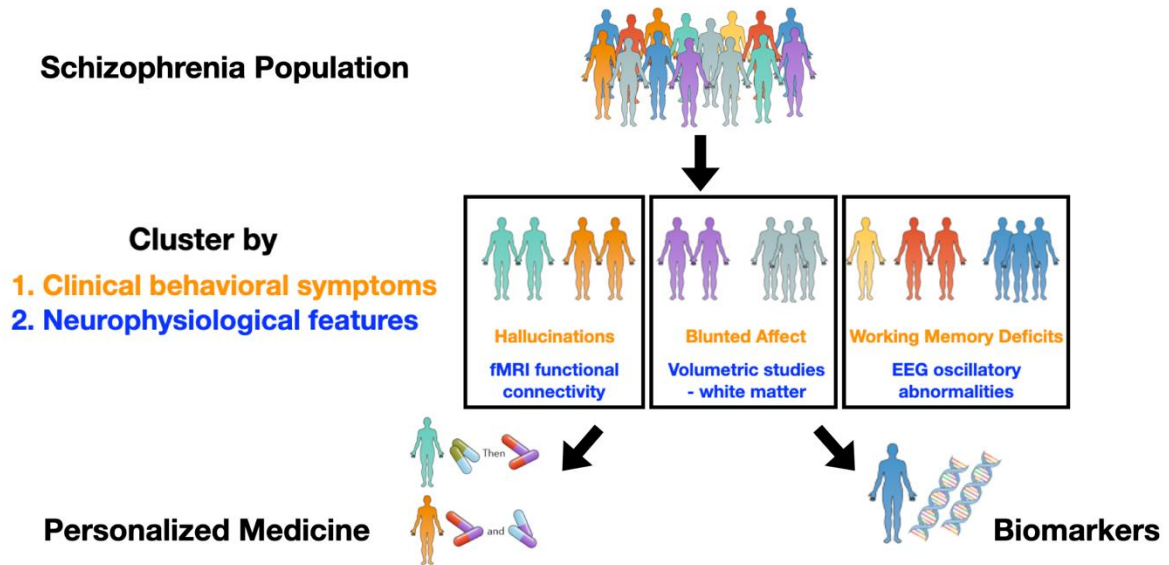


Figure 26 Clinical clustering using machine learning schematic

A schematic of the rationale for machine learning in psychiatry. Schizophrenia is a heterogenous disease and clinically presents with many symptoms which complicates treatment. Separating patients by clinical symptoms and neurophysiological features can lead to better stratification of disease and lead to personalized medicine or identification of relevant biomarkers.

Clinical studies using machine learning methods to find disease subgroups predominately use unsupervised statistical approaches e.g. find subgroups automatically based on structure within the data and algorithm heuristics (information processing technique to generate faster, more optimal solutions). The opposing methodology, supervised statistics, use labels to indicate the class to which each subject belongs (drug v placebo.) Although studies have shown high success using supervised

learning to predict diagnosis or outcome from neuroimaging data, subject diversity and disease heterogeneity complicates identifying labels.

The most common unsupervised learning in clinical cohort is clustering or using algorithms to divide data into “clusters” that have high similarity within cluster and do not share many overlapping features with other clusters. The success of this classification can be evaluated by measuring the distance between newly generated data clusters. Finite Mixture Modeling also uses unsupervised learning with the objective of represent data using a finite of parametric distributions e.g. a set number of statistical features.

Clinical studies using clustering with cohorts of patients with psychiatric disorders have not generated consistent subtypes and there are several theories how this is occurring. First, genetic polymorphisms can mimic syndromic expression of other psychiatric disorders e.g. autism and schizophrenia(137–139). Machine learning approaches cannot stratify psychiatric disorders subtypes solely using symptoms. To circumvent this issue, studies are using machine learning approaches with neuroimaging or neurophysiological recordings to converge biological phenomena and cognitive and emotional to improve disease subgroups. For example, supervised learning models using support vector machine algorithms and classifiers from MRI-derived brain morphometry features such as gray matter volume or cortical thickness have been successful in predicting schizophrenia diagnosis and differentiating

schizophrenia patients from healthy controls with accuracies of 81% and 76%, respectively(134).

Furthermore, Machine learning models combined with the high temporal resolution in EEGs are being used to establish functional markers of cognitive deficits in schizophrenia. EEG power and microstates are stable on a comparable timescale of many mental processes like working memory or identifying sensory cues. Importantly, EEG topography maps capture changes in pre-stimulus electrical activity that have been used to predict accuracy in visuo-spatial working memory tasks and identify neural connectivity abnormalities in schizophrenia (140,141).

5.2 Integrating machine learning and neural circuit studies preclinically

5.2.1 Limitations of neural circuit studies in rodents

Functional connectivity, neural network synchrony regulating sensory inputs and physiological outputs, can be used as a neurobiological map of behavioral function. Mouse neurophysiology studies using genetic modifications, cognitive, emotional, or social behavior paradigms, or acute drug administration have reported robust changes in neural activity. Much like clinical human studies, oscillatory dynamics reflect the activation state of brain circuits responsible for cognitive processes and socio-emotional states. Due to technical limitations, many studies only target a single brain region, or a microcircuit related to their physiological outcome of interest. Like clinical studies, it is unlikely changes in neural synchrony are restricted to specific brain regions. Studying

neural synchrony and brain wide activity distributed across larger networks can provide insight into many disease mechanisms and uncover how behavior is regulated. Our lab has previously demonstrated the ability to simultaneously collect neurophysiological recordings from >10 cortical and subcortical brain structures in freely behaving mice. This high spatiotemporal data collection combined with our expertise in rodent behavior and ability to generate predictive machine learning models allows us to explore brain-wide dynamics that can tease apart nuances of neural circuitry.

5.2.2 Discriminative Cross-Spectral Factor Analysis maintains relevant neurophysiological features

Similar to the lack of convergence of disease subgroups in clinical unsupervised cluster studies, machine learning can successfully classify animals into specific groups but at the expense of neurophysiological interpretability. We have recently developed a new machine learning-based model termed discriminative Cross-Spectral Factor Analysis (dCSFA) to classify animals and retain relevant and translational neural features. dCSFA discovers neural oscillations across regions that change together over seconds of time and segregates these neural synchrony patterns according to pre-specified behavioral variables. Comparable to the spatio-dynamics of neuroimaging like fMRI, our dCSFA model discovers neural dynamics that are correlated across many brain regions over seconds of time. However, dCSFA is more similar to the temporal dynamics of EEG as our model analyses neural dynamics at the millisecond timescale(142). Our model can generate several biologically relevant features from our

recorded local field potentials (LFPs)- summation of electrical potential of thousands of neurons near the micro electrode site. We observe and analyze 1) spectral power-strength of neural oscillation 2) cross power - temporal correlate of two oscillations changing together and 3) cross phase - a neural correlate of information transfer between distinct LFPs leads the other e.g. directionality. Despite occurring at different time scales, dCSFA can statistically integrate these neural features into a single framework called an electome – electrical functional connectome. As these LFP neural dynamics encompass the newly generated electome, they are referred to as “electome factors.”

(Figure 27).

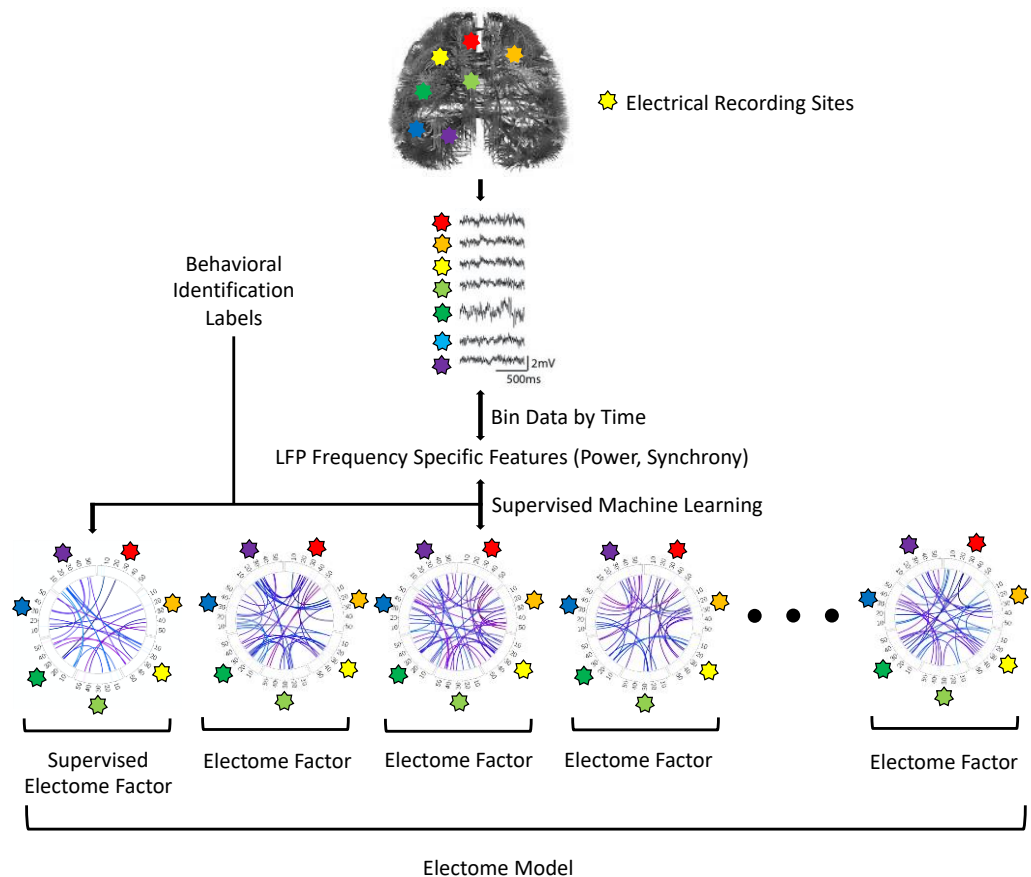


Figure 27 Electome Model Overview.

Target electrical recording sites can be observed individually during a behaviorally relevant task. Simplified LFP recordings from regions implanted are collected and separated into time windows. LFP frequency specific features are calculated for each time window. Behavioral scoring identifies behaviorally relevant windows. A supervised machine learning algorithm is applied to the data to identify supervised electome factors and unsupervised electome factors. Representative electome factors are visualized with a circle plot composed of power (outer circle) and coherence features (diagonal lines spanning inner circle).

5.3 Profiling neurophysiological effect of PCP

We used mice implanted with multi-wire electrodes to create a model that describes how cortico-striatal brain regions integrate across time and space to mediate behavioral changes related to 1) PCP and 2) antipsychotic inhibition of PCP(122,130). First, we used machine learning to discover the brain-wide spatiotemporal dynamic patterns that prelude the PCP brain state. Then, we repeated this machine learning strategy to uncover networks specific to antipsychotic activity. Together, these studies will further our understanding of the brain-wide effects of cortical disinhibition and provide insight into how antipsychotics mediate circuit deficits in schizophrenia. Importantly, as our machine learning approach yields interpretable models, we will be able to generate hypotheses for testable manipulation strategies which may provide new avenues for therapeutic intervention.

5.3.1 Experimental Design

The basal ganglia, group of neurons and subcortical structures heavily related to dopaminergic mediated behaviors i.e., movement, reward, cognition, displays impaired functional connectivity in schizophrenia and is the site of action for many antipsychotic drugs(59,143–145). We targeted key brain regions in the basal ganglia. C57 mice (age 10-14 weeks; N = 8) were implanted with microwire array bundles to target **prefrontal cortex (cingulate-, prelimbic-, and infralimbic- cortex) dorsal striatum, nucleus accumbens, ventral tegmental area, ventral hippocampus, basolateral amygdala.** The

bolded regions were chosen for their implications in schizophrenia or dopaminergic transmission. A schematic shows a simplified circuit with dopaminergic, glutamatergic, and GABAergic projections between our focal brain regions (**Figure 28A**). The placement of each electrode within region was verified by histological examination of postmortem brain slices and/or our CT-MR co-registration approach for high-throughput confirmation (**Figure 28C**).

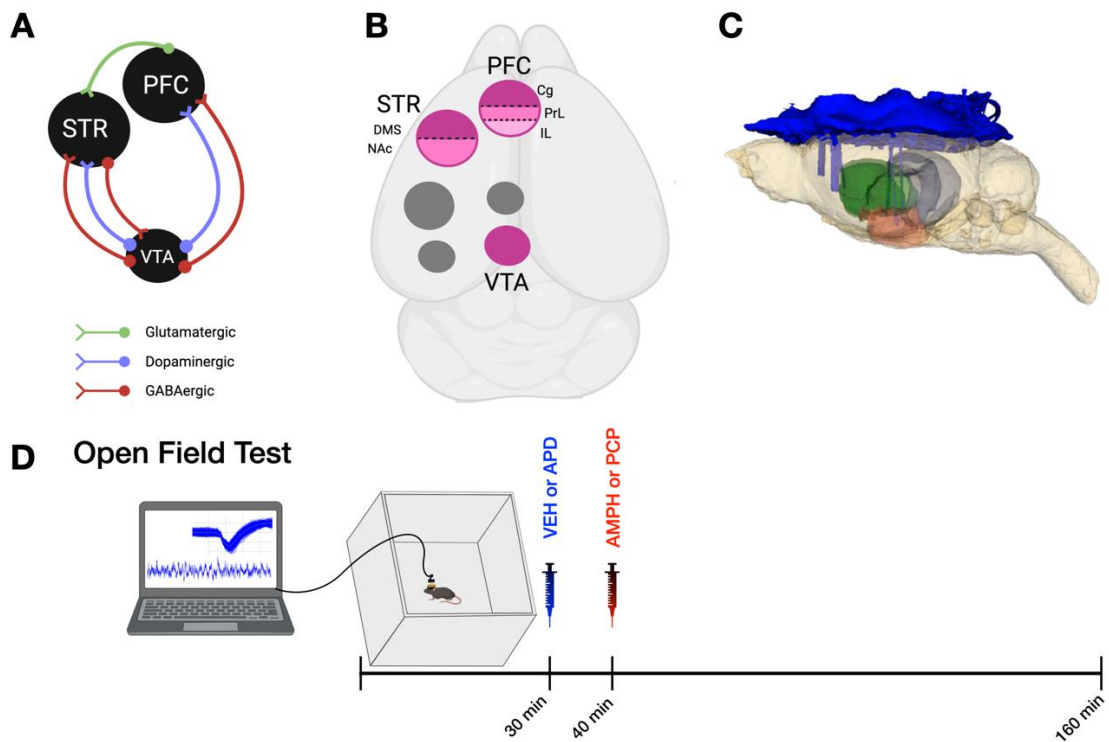


Figure 28: Experimental design for studying corticostriatal neurophysiological and behavioral changes induced by PCP.

(A) Schematic of dopaminergic, glutamatergic, and GABAergic projections between the Prefrontal Cortex (PFC), Striatum (STR), and Ventral Tegmental Area (VTA). (B) Brain regions implanted with multisite electrode. Pink regions are brain corticostriatal or dopaminergic relevant structures included in dCSFA analysis. Gray Regions were implanted but not included in the study. Circle size corresponds to number of wires per

region. PFC (8 wires) : Cingulate cortex (Cg, 4 wires), Prelimbic cortex (PrL 2 wires), Infralimbic cortex (2 wires); STR (8 Wires) : Dorsomedial striatum (DMS, 4 wires), Nucleus Accumbens (NAc, 4 wires); VTA (4 wires). (C) Sagittal view of computed tomography 3D rendering of mouse brain with multisite electrode (D) Open field behavior paradigm

Seven days following implantation surgery, mice were handled and habituated to being plugged into an amplifying neural headstage. After 5 days of habituation, mice were plugged into the amplifying system, and we systematically evaluated the integrity of neural signal while online cell sorting. The PCP induced hyperlocomotion experiment was designed to be within subject (**Figure 28D**). All mice would receive 4 treatments: 1) VEH (saline, 5% DMSO, 10% cyclodextrin) and saline 2) VEH and 94A 3) 94A and PCP 4) VEH and PCP. Mice were pseudorandomly assign mice to treatment group order (n=8). All mice received treatment 1 or 2 then were tested in the open field test for 160 minutes. After a one-week washout, mice were tested with the next treatment.

5.3.2 PCP induces robust neurophysiological changes

We simultaneously recorded single unit neurons activity and local field potentials across the corticostriatal circuit. Although we were simply preprocessing the data to use with our dCSFA model, we immediately noticed an increase in spike firing from baseline to PCP treated conditions. The raster plot shows a 10 second window of spiking the last ten minutes of baseline (pre injection) and 30 minutes after PCP administration (**Figure 29A**). Previous models have incorporated neuronal spike firing

and we also plan to investigate the neuronal dynamics that change with PCP(132,146).

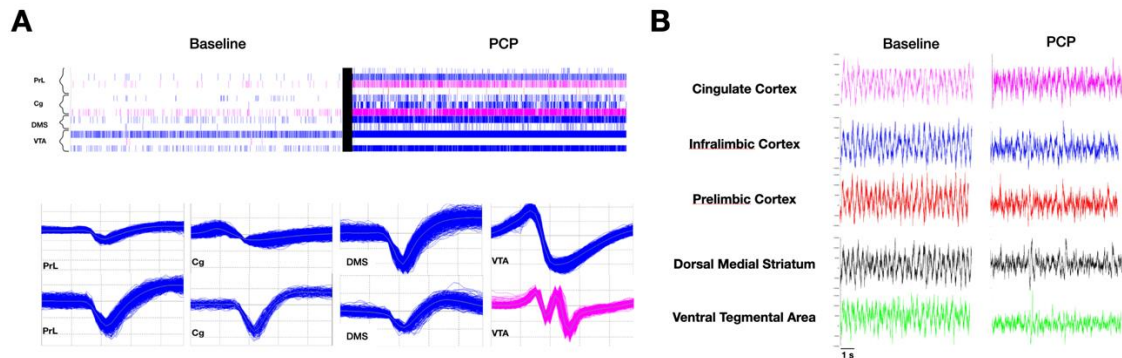


Figure 29 PCP induced neurophysiological changes at the single unit and LFP level.

(A) Top: Cortical striatal single units recorded in the same session following treatment with PCP Bottom: Representative waveforms of single units in top. (B) Local field potentials recording over 10 seconds 30 minutes after PCP was injected.

Next we generated power spectrograms of the drug treatments within subject. Our spectrograms use 1 second windows to display neurophysiological changes. We use this as a method to visually discern the integrity of the electrode as poorly electrically grounded or deficient electrodes will show aberrant activity or power that has no physiological relevance on the spectrogram. Out of curiosity, we created 5-minute time bins to match the time windows used in distance traveled plots and visualized region power by frequency. We immediately noticed neural power differences at the peak effect windows 60-80 minutes (**Figure 30B**, pink box) and the 94A and PCP power spectrogram appeared to return to baseline power while PCP did not (**Figure 30B**,

orange box). These preliminary data informed our hypothesis that 94A normalized PCP induced circuit deficits.

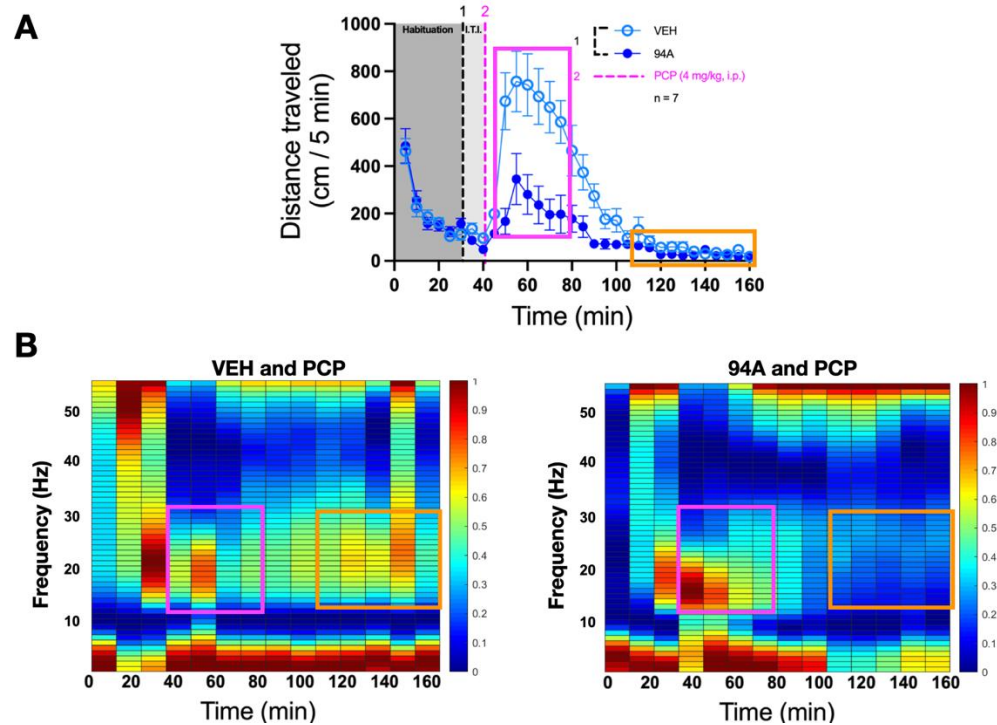


Figure 30 Power spectrogram shows neurophysiological changes that mirror PCP induced behavior and pharmacokinetics.

(A) Distance traveled in open field plot shows max PCP induced- distance traveled per 5 minute interval in box peak and loss of statistically significant behavioral differences of drug groups in orange box. (B) Power spectrogram from the prelimbic cortex in VEH and PCP (left) and 94A and PCP (right) condition, within subject 1 week apart. Pink and orange boxes on spec plots show differences in power at the same time points as the behavior in (A). Heat bar scale is normalized power spectral density.

5.4 dCSFA Model Validation

We trained out dCSFA model to learn the network features that predict drug effect by identifying behavioral sessions of VEH control and PCP or 94A and PCP. The model coefficients discovered using the initial dCSFA analysis in the baseline session

(pre drug injection) were applied to the LFP data recorded from 8 mice treated with both drug conditions, yielding network scores which quantify the expression of the original network in new animals for each condition. We tested whether the PCP brain-state was more prominent in the VEH/PCP treated mice that exhibit higher PCP induced hyperactivity. Receiver Operating Characteristic (ROC) analyses determined the performance of the model by determining the tradeoff between the true-positive rate versus the false-positive rate. Area under the ROC curve (AUC, or equivalently the concordance index) summarizes model performance - results larger than 0.5 indicates that the model has identified a network related to the classes. Thus, this analysis will determine whether the PCP brain-state was associated with behavioral deficits in animals previously untested in the model. If this analysis is successful, it will establish that the PCP-conditioned brain-state generalizes across subjects. We used a leave-one-out procedure to determine model hyperparameters and achieved an average AUC on the holdout mouse of 0.925 (range: 0.658-1.000), indicating the model was able to predict drug condition (no drug vs. PCP) well above chance levels. Then data from all 8 mice was used to train a single dCSFA model using the previously determined hyperparameters (**Figure 31**). Interestingly, plotting 1 minute time windows of our PCP or 94A+ PCP scores resembled the behavioral graphs of PCP induced locomotion with separation of treatment groups at the peak drug effect (60-80 minutes) and overlap of

groups after 100 minutes.

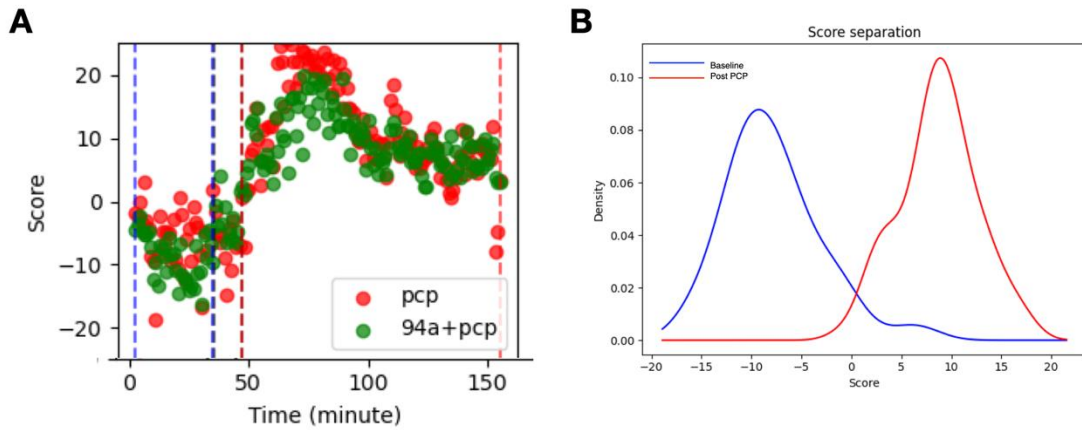


Figure 31 dCSFA model can reliably predict PCP or 94a + PCP conditions.

(A) dCSFA scores for one-minute windows in an example mouse. Time course plots shows high scores and separation of PCP and 94A + PCP at peak drug effect (60-80 min) and convergence when drug effect is diminished (100 min). (B) Score separation of dCSFA factors' Area Under the Curve (mean AUC) on the validation mice. Baseline: scores time windows between blue lines, Post PCP scores from time windows between red lines in (A). Model can accurately predict drug effect.

Mice were injected with the VEH control or 94A at 30 minutes then PCP at 40 minutes and the peak effect of PCP administered intraperitoneally at similar dosages are observed 30 minutes later(147,148). Our dCSFA model shows the highest factor scores at the peak effect of PCP, confirming we were able to capture neurophysiological changes that aligned with the PCP's pharmacokinetics. Our score separation plots demonstrate the model scores for our baseline (pre injection) factor and drug effect (post PCP injection) factor has minimal overlap.

We used the full set of neural data recorded from all of implanted brain areas of interest (PFC, STR, and VTA). dCSFA discovered the electome factor features (power,

cross power, or cross phase directionality that form the PCP brain state have the strongest predictive accuracy using gamma power in the prelimbic cortex (Figure 32).

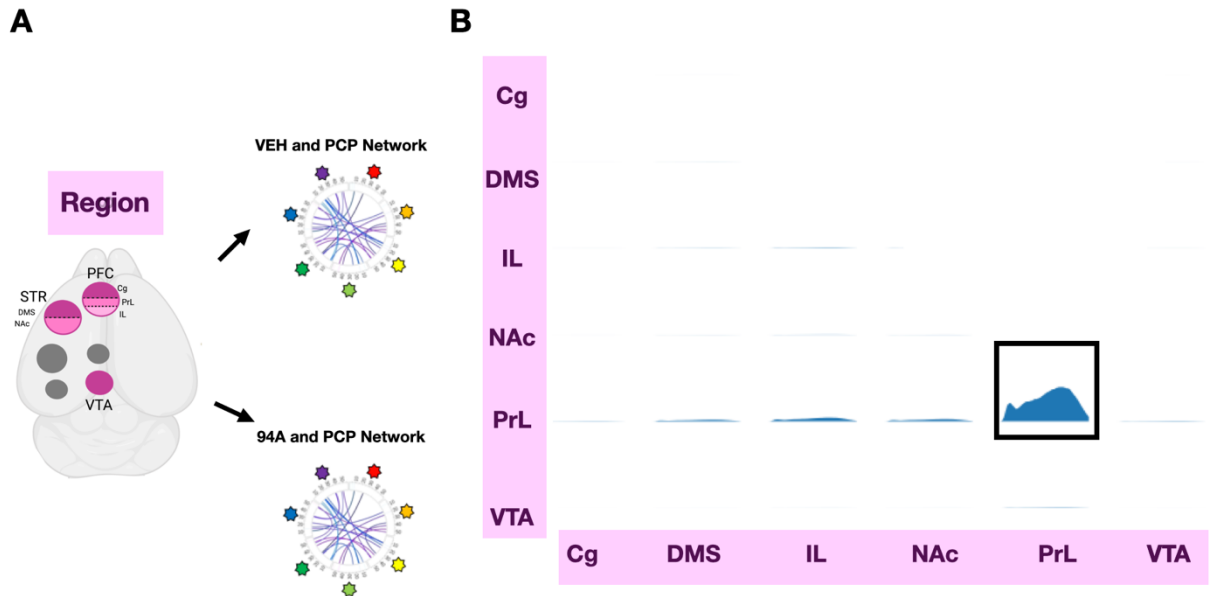


Figure 32 dCSFA generated electome factor identifying PCP condition:

(A) dCSFA used supervised autoencoders and LFP neural features (power and cross power) to train and predict the behavioral label of PCP on hold out mice. The brain regions used were cortical (cingulate cortex (Cg) , prelimbic cortex (PrL), and infralimbic (IL); striatal (dorsal mediodstriatum. (DMS) and nucleus accumbens (NAc), and midbrain (ventral tegmental area (VTA)). (B) Diagonal subplots indicate region power and off-diagonal subplots indicate cross-power, both scaled by frequency. Horizontal axes indicate frequency from 0-55Hz. The factor that predicted PCP most accurately was driven by high gamma power in the Prelimbic Cortex (PrL), shown in black box

5.5 Prelimbic cortex gamma oscillations underlie antipsychotic effect in PCP inhibition

5.5.1 The prefrontal cortex's role within the corticostriatal circuit

The prefrontal cortex is integral to regulating cognition and emotion. A sub region, the prefrontal cortex is, highly implicated with cognitive tasks involving memory, coordinating goal directed behavior, learning habits, specifically relevant for drug seeking, and regulating emotions related to fear and anxiety (149–154). The prefrontal cortex, like much of the cerebral cortex, has distinct cytoarchitecture with specific connectivity, functions, and interlaminar interactions(155,156). Layer V and VI prefrontal cortex is densely innervated by projections from limbic and autonomic regions while layers II through VI have more local cortical and limbic projections(157,158). For example, pyramidal neurons within prefrontal layer 5/6 project to infralimbic layer 5/6 and are implicated with alpha and beta oscillations (159) (**Figure 33**). When higher frequency gamma oscillations are observed, areas like the hippocampus have glutamatergic synaptic inputs on layer V prefrontal interneurons are coherent and phase locked with beta-low gamma activity(160–162). Whereas prefrontal neurons in layer 2/3 are hyperexcitable and synchronize gamma oscillations locally across the prefrontal

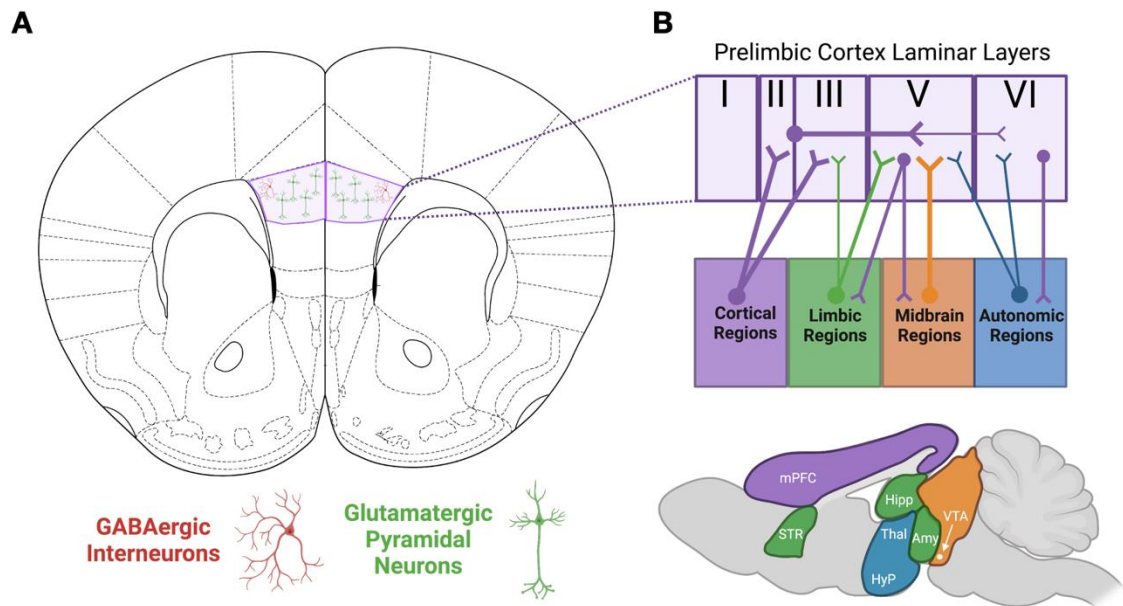


Figure 33 Mouse prelimbic cortex laminar layers and projections

(A) Schematic of mouse brain highlighting the prelimbic cortex. GABAergic interneurons and glutamatergic pyramidal neurons make up ~20 and 80% of the cell population, respectively. (B) Laminal layers in the prelimbic cortex. Width of the box represents laminar thickness e.g. Layer V is thickest and Layer II is thinnest. Each layer has distinct projects across the brain. Layer II/III sends cortical projections and receive cortical and limbic innervations. Layer V is densely innervated by the midbrain while also receiving inputs from cortical, limbic, and autonomic brain regions. Layer V/VI sends cortical projections to limbic, midbrain, and autonomic regions. These laminar specificities and projections are correlated with distinct neural oscillations frequencies.

Relevant to antipsychotics mechanism of action, dopamine inhibits pyramidal neurons of prelimbic cortex that project to subcortical targets through D₂Rs and indirectly affects GABA release from interneurons. Conditional mutant mice with D₂R deletion in PV+ interneurons led to schizophrenia like phenotypes, providing additional evidence of D₂R's role in maintaining cortical excitatory/ inhibitory balance(165,166) The

NMDAR antagonist PCP reduces gamma oscillations that is reversed in vitro with antipsychotic drugs(101). Cortical layer V has the highest density of pyramidal and GABA neurons expressing D₂Rs(167). A 2017 in situ hybridization study quantified PrL pyramidal cells with D₂Rs are 20–25% in layer V compared to 4–5% in layers II–III; PrL GABAergic cells with D₂Rs are 6-10% in layer V and 2-5% in layer II-III (31). Importantly, layer V pyramidal neurons expressing D₂Rs innervate many subcortical implicated in schizophrenia circuit dysregulation like the striatum(168). These D₂R pyramidal projections show highly sensitive to NMDAR antagonists, but these effects counteracted by antipsychotic drugs acting on D₂Rs(18,101,169,170). Our dCSFA model using prelimbic gamma power to separate PCP and 94A and PCP factors suggest 94A may be increasing excitability of GABAergic interneurons and enhancing glutamatergic transmission from the prelimbic cortex to produce antipsychotic like effects.

5.5.2 Potential antipsychotic cellular interactions within the prefrontal cortex

One of the most consistent pathological changes in schizophrenia is a decrease in gamma oscillations reflective of impaired GABAergic signaling and a decrease in PV+ interneurons density and function. Perineuronal nets, extracellular matrix, 3 dimensional lattices that cover and surround PV+ interneurons, have also been implicated in schizophrenia(171). Perineuronal nets indirectly stabilize the excitatory/inhibitory balance that is integral to cortical and subcortical circuits by protecting PV+ interneurons from oxidative stress and regulating their excitability(172). Recent

schizophrenia genetic studies identified down regulation of genes encoding perineuronal net components and speculate decreased perineuronal nets are correlated with the increased PV+ interneuron cellular degradation observed in postmortem brains(173,174).

Layer V of the prelimbic cortex is densely populated by PV+ interneurons surrounded by perineuronal nets (175) A recent study using an NMDAR antagonist, MK801, reported decrease in the density of perineuronal nets and PV + interneurons in the prelimbic cortex.(176) Decreases in perineuronal nets and abnormal gamma oscillations were also observed using a different NMDAR antagonist ketamine(177) Application of antipsychotics to tissue cultures pretreated with GABAA receptor antagonist differentially modified burst firing of PV + interneurons. Importantly, 95% of the PV+ interneurons co-expressed aggrecan, a component of perineuronal networks(178). These studies suggest cortical network connectivity disruptions could be ameliorated with antipsychotic action through the prefrontal cortex, specifically involving PV+ interneurons and likely perineuronal nets (178).

5.5.3 The analogous region of the prelimbic cortex in the human brain

The mouse prelimbic cortex corresponds to the human brain region Brodmann area 32 in the dorsal anterior cingulate cortex(179). Brodmann's area 32 has been highly investigated in schizophrenia clinical studies. Fractional anisotropy studies report many patients with schizophrenia have with decreased white matter density in Brodmann's

area 32 (180) Magnetic resonance imaging schizophrenia studies are investigating the volumetric loss in cortical regions, including Brodmann's area 32, and if antipsychotic treatment can restore cortical thickness and decrease/delay grey matter deterioration(181–183). fMRI studies on working memory, a core cognitive deficit in schizophrenia, identified Brodmann's area 32 hypoactivity as a part of the circuit dysconnectivity observed(128). Postmortem analysis of brains from schizophrenic patients report significant decrease in density of interneurons in the anterior cingulate, also including Brodmann's area 32(174,184). In conclusion, our dCSFA model identified a neural feature, prelimbic cortex gamma oscillatory power, that has high biological translation and interpretability.

5.6 Biological interpretation of 94A drug effect electome factors

Neural oscillations are being used as key clinical identifying features of the ideal psychosis or cognitive deficits. Circuit abnormalities in schizophrenia have been marked by specific changes in resting state neural oscillations in magnetoencephalography and electroencephalography studies(10,117,185,186). Combining pharmacology and neural imaging/recording is providing more insight into drug mechanisms and personalized medicine for patients. The key-locke theory postulates the ideal pharmacological treatment would induce changes that rescue – or are opposite- to neural disruptions observed in the disease state(178,187,188). We used our dCSFA model to characterize

94A's changes to PCP induced circuit deficits in regions in the prefrontal cortex, striatum, and ventral tegmental area.

5.6.1 94A normalizes PCP disruptions to neural circuit in time-frequency analysis

Time-frequency analysis, comparing the power spectra values of time-frequency, is used as a core technique to interrogate the frequency band of interest and uncover possible circuit abnormalities(189). Additionally, source localization methods determine the input location of abnormal oscillation signals(190). We targeted cortical and sub-cortical regions in vivo and confirmed their electrode placement, to determine single units and oscillations were derived from the intended region. We analyzed our PCP and 94A and PCP cross-power over time and plotted their absolute difference from baseline e.g. absolute error in decibels (dB) of the cross-power volume (channels by channels by frequencies). (**Figure 34**). The time absolute difference from baseline analysis also confirmed the pharmacokinetics of PCP and showed the PCP cross-power began deviating from baseline around 20 minutes and remained ~ 2.1 dB from baseline for the remainder of the recording session. Contrarily, 94A+ PCP dampened the effect of PCP alone and maintained a smaller deviation from baseline ~1.6 dB.

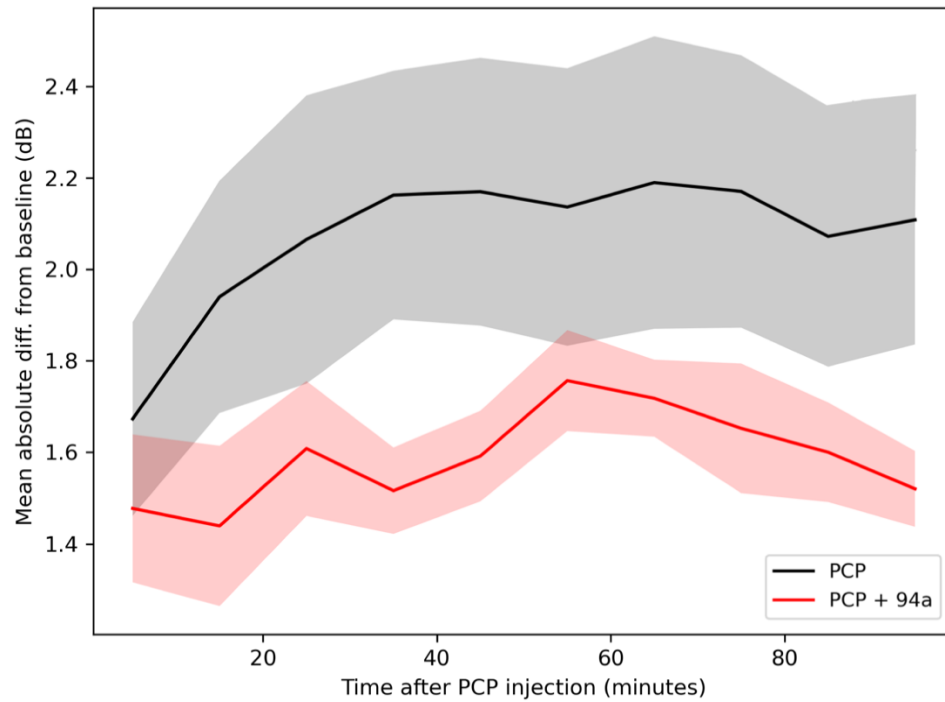


Figure 34 94A stabilizes PCP's neurophysiological effects over time.

Solid lines are averages over 8 mice. Spread indicates +/- 1 SEM.

Next we analyzed PCP and 94A and PCP absolute differences from baseline over a frequency range of 1-50 Hz. High gamma oscillations (50-80 Hz) and high frequency oscillations (100-200 Hz) have also been implicated in schizophrenia circuit disruptions, therefore further analysis will expand into including these frequencies ranges(191,192). Again, 94A and PCP decreased the circuit disinhibition caused by PCP (**Figure 29**). It is important to note that there are absolute differences and not reflective of values e.g. increase or decrease in power. Our future analyses will include power ratio analysis to

understand what PCP does to these highlighted frequencies, specifically delta (1-4 Hz) theta (5-8 Hz) and low gamma (30-50 Hz.)

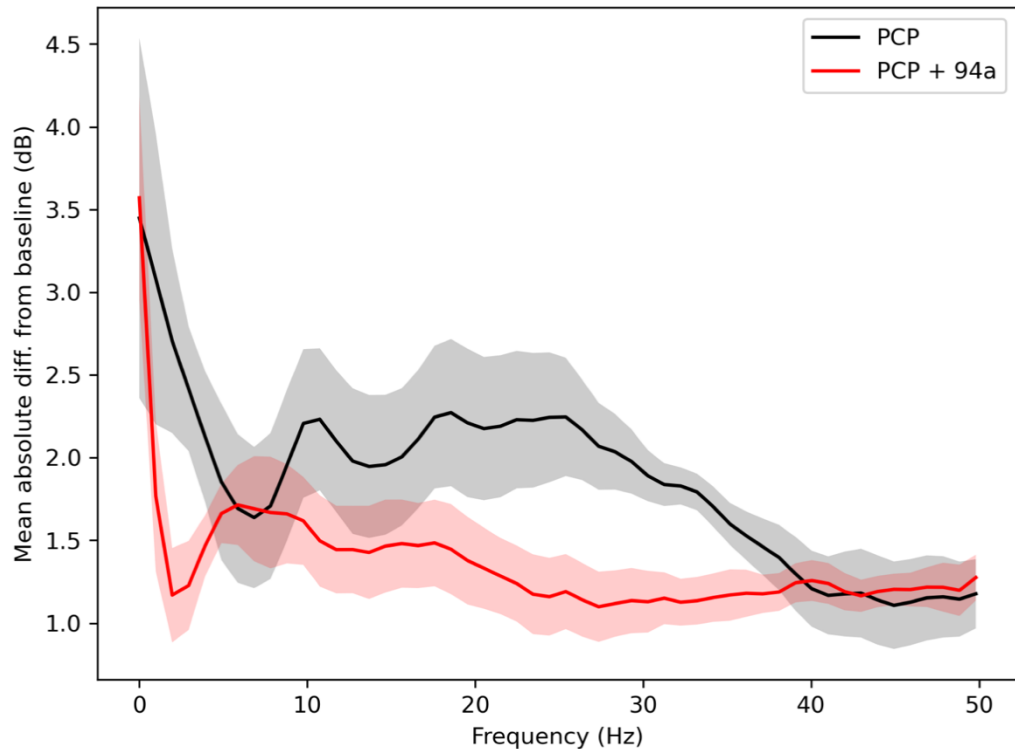


Figure 35 94A reduces PCP induced regional circuit disruptions to power.

Solid lines are averages over 8 mice. Spread indicates +/- 1 SEM.

5.6.2 94A significantly increases gamma power in cortical regions

We analyzed how PCP affects power in our implanted corticostriatal regions. Power spectral densities are plotted relative to baseline, dashed horizontal line (**Figure 36**). PCP significantly decreased power in all regions and trended towards increasing power in the delta (1-4 Hz) band in striatal regions and the ventral tegmental area. PCP has been reported to decrease gamma oscillations by decreasing the excitation of

GABAergic neurons ,specifically PV+ interneurons(25,33,101,193). Our lab's in vitro whole cell patch clamp experiment reported 94A was able to significantly increase excitation of GABAergic interneurons(106). 94A+ PCP significantly increasing gamma power in 30-50 Hz in the cingulate cortex and 40-50 Hz in the prelimbic cortex has provided in vivo support that 94A acts as an agonist in the prefrontal cortex.

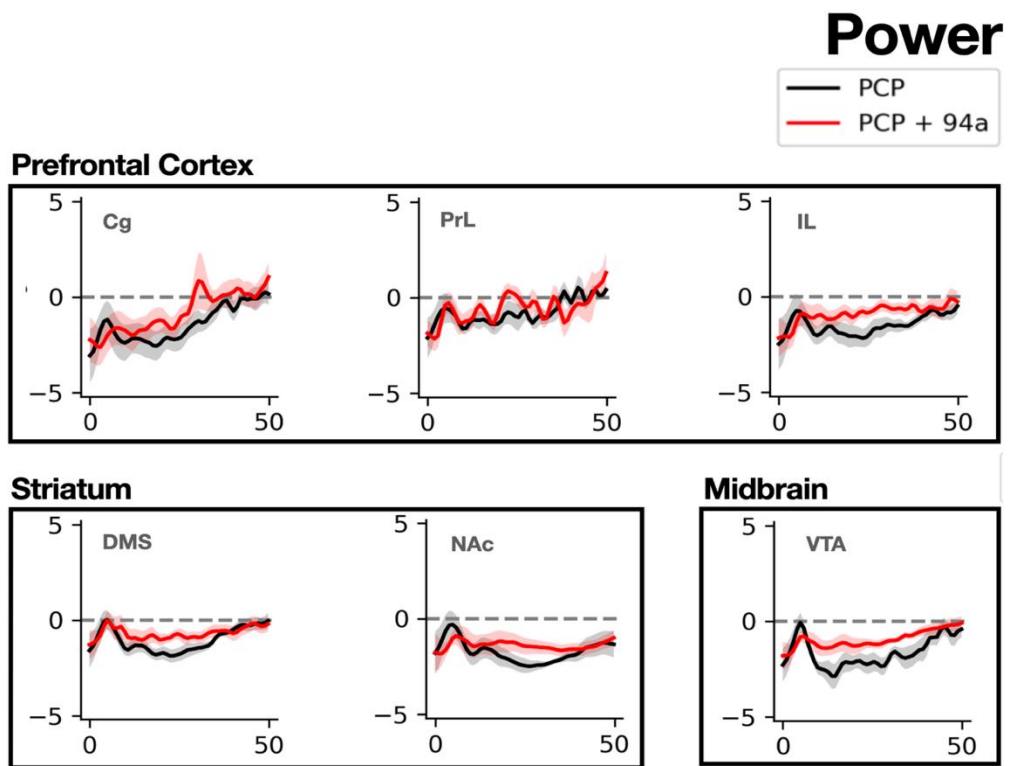


Figure 36 94A normalizes PCP disruptions to power in all corticostriatal regions.

Amplitude values (y axis) are reflecting the relative LFP spectral energy observed at each frequency (Hz, (x axis)), Dashed line is relative to baseline.

5.6.3 94A rescues PCP induced circuit disruptions

Our PCP cross power showed 94A rescues and increases cross power (region synchrony) between prelimbic cortex and cingulate cortex and prelimbic cortex and the

ventral tegmental area (**Figure 37**). The specific frequencies affected were delta (1-4 Hz) and gamma (30-50 Hz.) Gamma oscillations have been central to the discussion around abnormal functional connectivity in schizophrenia, however, delta oscillation alterations have been highly implicated as well. Delta, the oscillation band most prominent during non-rapid eye movement sleep, is integral to maintaining executive functioning(194,195). Patients with schizophrenia suffer from sleep abnormalities, have cognitive deficits, and show delta aberrations during psychosis(196,197). Cortical delta oscillations are mediated through layer V pyramidal cells. In vitro studies report pyramidal cells entering the after hyperpolarization period after synchronized with delta oscillations(198,199). Recent genome wide association studies included schizophrenia gene variants related to ion-channel and Ca²⁺ transporters and this may be correlated with abnormal delta oscillations(36,198,200). Importantly, dopaminergic terminals from VTA neurons innervate GABAergic interneurons and pyramidal cells in

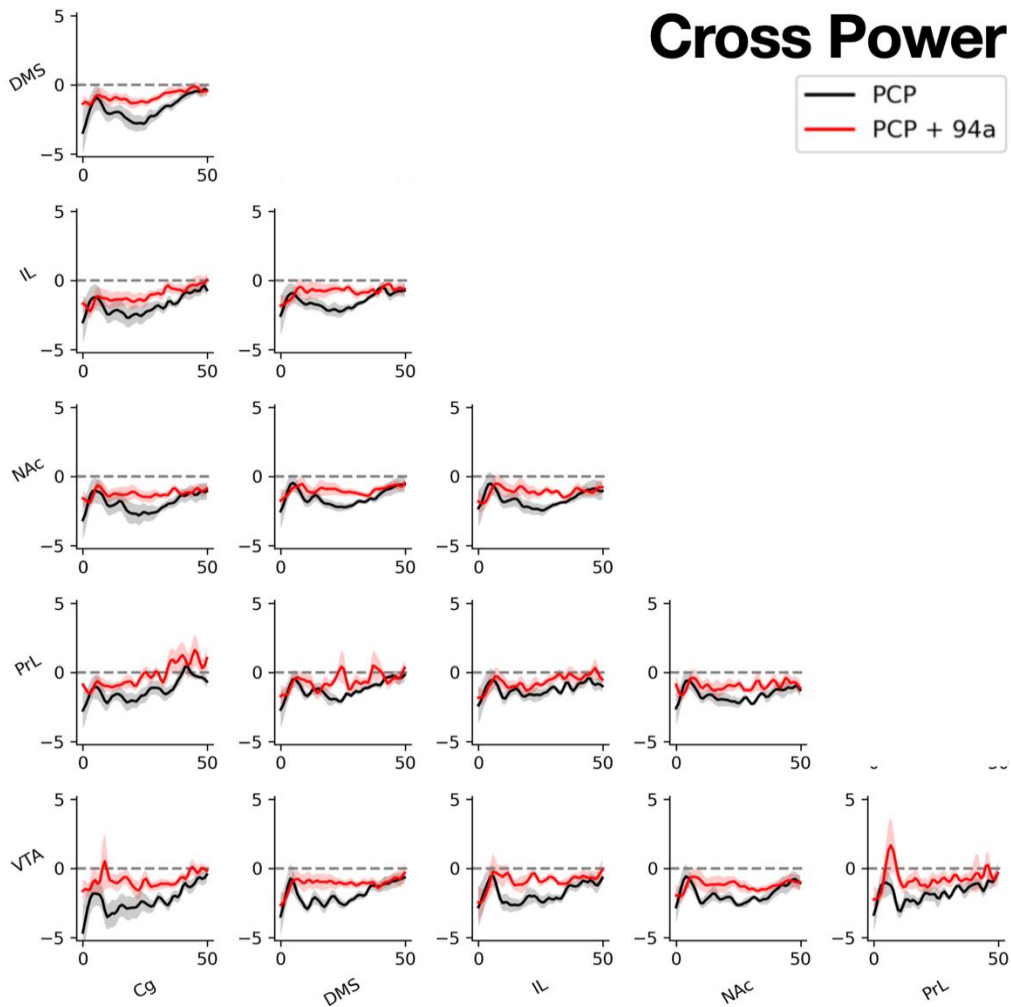


Figure 37 Antipsychotic effect on cortical-midbrain synchrony.

Power relative to baseline (dB) (y axis) are reflecting the synchrony of each paired oscillation per region at each frequency (Hz, (x axis)), Dashed line is relative to baseline

Altogether, this can explain how 94A's antipsychotic effects these regional synchronies and inhibited PCP's behavioral effect and circuit disinhibition. In conclusion, 94A exhibited the key-locke theory and may be an ideal candidate as an antipsychotic drug as it reduced PCP's increase in delta and gamma oscillations in

cortical, striatal, and midbrain regions (Figure 38).

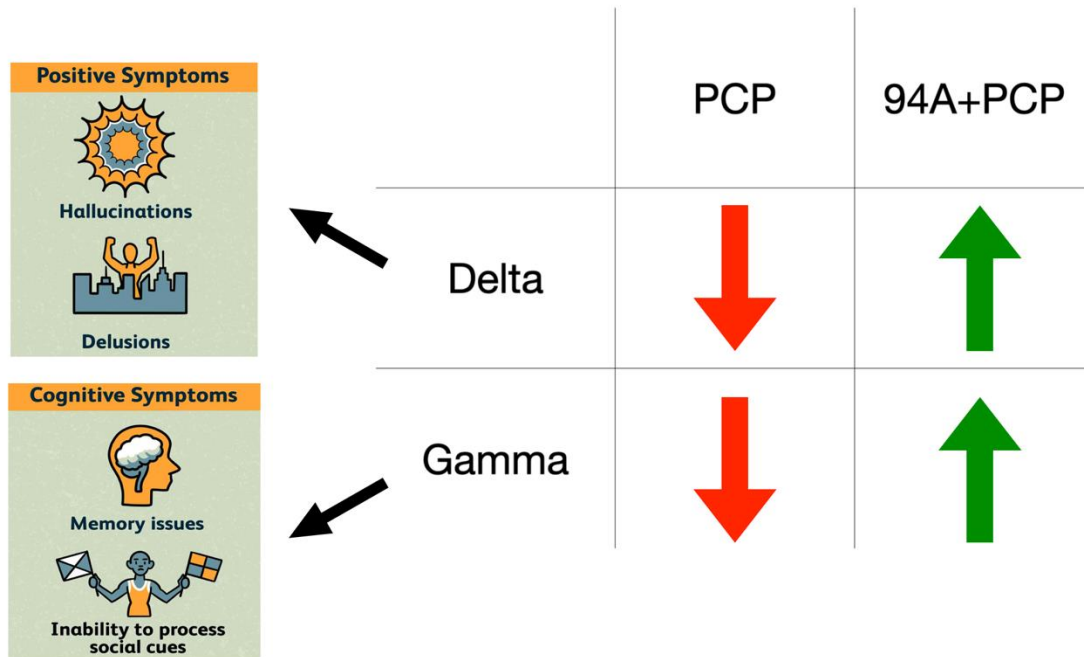


Figure 38 94A exhibits the key-locke theory to PCP challenge.

Delta oscillations (1-4 Hz) abnormalities are correlated with positive symptoms e.g. psychosis and gamma oscillations (30-80 Hz) are correlated with cognitive symptoms observed in schizophrenia. After measuring power and cross power changes across cortical-striatal regions, we reported PCP decreased gamma power and delta cross power. 94A resulted in antipsychotic activity to PCP challenge by increasing delta cross power and gamma power.

5.7 Integrating dopaminergic dynamics into a PCP drug effect model

As the dopamine hypothesis is a core focus in schizophrenia research and antipsychotic drug targets, we wanted to investigate cortical dopaminergic dynamics. The first reason is due to 94A unique pharmacodynamic profile of acting like a D₂R agonist in the prefrontal cortex. The second reason is to have an in vivo integration of

dopamine signaling directly correlated with neurophysiological changes captured by our dCSFA model. We completed fiber photometry experiments using a dopamine biosensor, GRAB.DA1, in the prefrontal cortex to pilot this experiment before integrating 94A.

To test whether PCP, when administered to drug-naive mice, causes a DA increase in the prefrontal cortex. we recorded the fluorescence changes of an intensity-based genetically encoded DA sensor (GRAB DA1) in freely moving mice with fiber photometry We delivered an adeno associated virus encoding dopamine biosensor (AAV9-CAG- GRABDA1) in the prelimbic cortex, followed by implantation of an optic fiber for recordings. GRABDA1 enables optical readout of changes in DA concentration by coupling the agonist binding-induced conformational changes in human DA receptors to changes in the fluorescence intensity of circularly permuted (cp) GFP derived from GCaMP6(203,204). Although the prefrontal cortex has low dopamine, the GRAB DA has successfully been used in low dopaminergic regions. The GRAB DA1 sensor has a higher affinity for dopamine than the previous dlight1.1 sensor , Kd 130 nM and 330 nM, respectively(204,205). To then test the effects of PCP on prelimbic dopamine levels, animals were habituated to being plugged in their home cage and systemically injected with either saline or PCP (4 mg/kg) on subsequent days. Contrary to many fiber photometry studies, we did not have a specific event or stimulus to time lock with fluorescence changes. We monitored fluorescence over a continuous 40 minute

recording session. While our previous experiments were 160 minutes total (30 minutes habituation, 10 minute inter trial interval between 94A and PCP injection, and 120 minute observation after PCP), we did not want to photo bleach the prelimbic cortex and limited the 40 minutes. We plotted the dF/F over 35 minutes , 5 minutes before PCP injection, to capture the peak effect of PCP. A representative trace from one animal is shown in **Figure 39**. We analyzed our results of 5 mice with a Wilcoxon rank sum test and reported $p = 0.0625$ (**Figure 39D**). Although our results were not significant, it is promising that we can integrate fiber photometry into future studies. We plan to increase our PCP dosage from 4 mg/kg to 10 mg/kg. 10 mg/kg has also been used without inducing aberrant seizure activity which is a concern with increasing dosage of other NMDAR antagonist drugs.

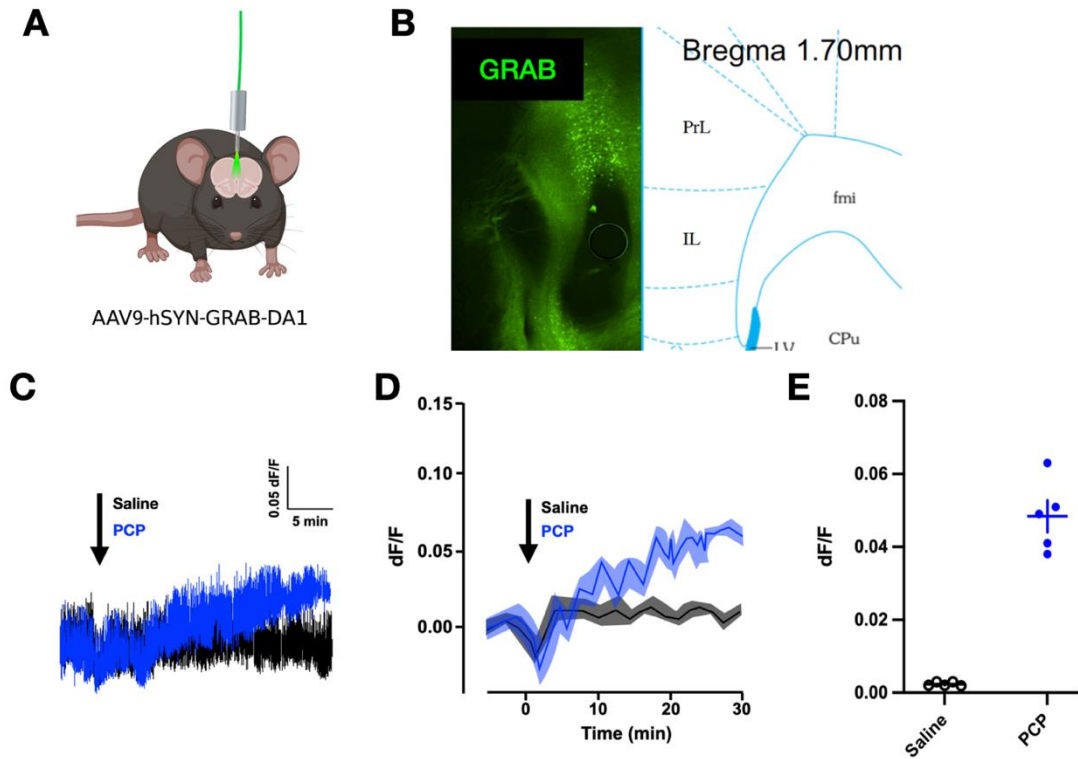


Figure 39 Measuring PCP effects on dopamine with a dopaminergic biosensor.

(A) Dopamine biosensor viral construct: AAV9-CAG-GRAB-DA1. (B) Histological verification of GRAB-DA1 in prefrontal cortex. (C) dF/F trace in one mouse, 30 minutes after PCP (4 mg/kg, i.p.) (D) dF/F average trace 30 min after PCP (4 mg/kg, i.p.) (E) Quantification of D. PCP significantly increased dF/F compared to saline * $p=0.0312$, Wilcoxon rank sum test; $n=5$.

We recently designed a fiberoptic- a multisite electrode that integrates an optic fiber to enable simultaneous neurophysiology and dopaminergic dynamics. We will further profile the antipsychotic effects of 94A by studying the network changes and dopaminergic dynamics in vivo. This will shed light on the beta-arrestin biased D₂R cellular and neurophysiological mechanisms and uncover key pathophysiology contributing to schizophrenia deficits.

6. Conclusions

The experiments outlined in this document sought to investigate the cellular and neurophysiological mechanism that contribute to cognitive and negative deficits in schizophrenia. Previous work in our lab showed therapeutic potential for β arr2 - mediated signaling downstream of the D₂R in the prefrontal cortex and the striatum.

This work presented in this document significantly contributes to the fields of cellular biology, pharmacology, and neuroscience. First, we recapitulated the paradoxical dopaminergic signaling within the corticostriatal circuit using CRISPR/Cas9 as a gene editing tool. Now that we have validated our constructs against *Drd2*, this opens the possibility of creating many cell type specific genetically modified mice to further investigate regional differences or signaling cascades that may underlie schizophrenia abnormalities.

Next, we measured the behavioral effects of two different D₂-like functionally selective ligands against challenge of psychotomimetic drugs – PCP and AMPH. Our work showed β arr2- D₂R signaling generally produced more antipsychotic like effects in both the prefrontal cortex and striatum to inhibit PCP or AMPH effects, excluding loss of inhibition in cortex with AMPH challenge. Our work lays the foundation to follow up with the unique cortical β arr2-D₄R activity exhibited by UCSF.

After, we validated the β arr2-biased DREADD for the first time in vivo. Using DREADDs to create synthetic pharmacology of 94A activity in the prefrontal cortex, we

showed β arr2- signaling is necessary to produce antipsychotic like activity. Stimulating GABAergic interneurons was sufficient to inhibit PCP's response but the effect was completely lost in β arr2-KO mice. This also provides in vivo support that 94A acts as an agonist in the prefrontal cortex and increases excitability of GABAergic interneurons. These findings show 94A may have potential benefits to treating cognitive deficits in schizophrenia.

Finally, using machine learning and in vivo neurophysiology, we identified relevant neurological features that mediate antipsychotic effects. Our preclinical pharmacoeEG experiment identified several neural abnormalities observed in schizophrenia, namely disruptions to cortical gamma oscillations, delta oscillations, and altered synchrony within corticostriatal regions. Importantly, our dCSFA model identified the prelimbic region, the brain region we manipulated in chapter 4 with DREADDs and provide additional support that this region is heavily involved in regulating corticostriatal dynamics and should be considered for therapeutic targets for schizophrenia (**Figure 40**). Furthermore, the development of the fiberoptic to simultaneously measure dopamine transients and neurophysiological circuit changes

can transform the way we understand drug effects and disease modeling in vivo.

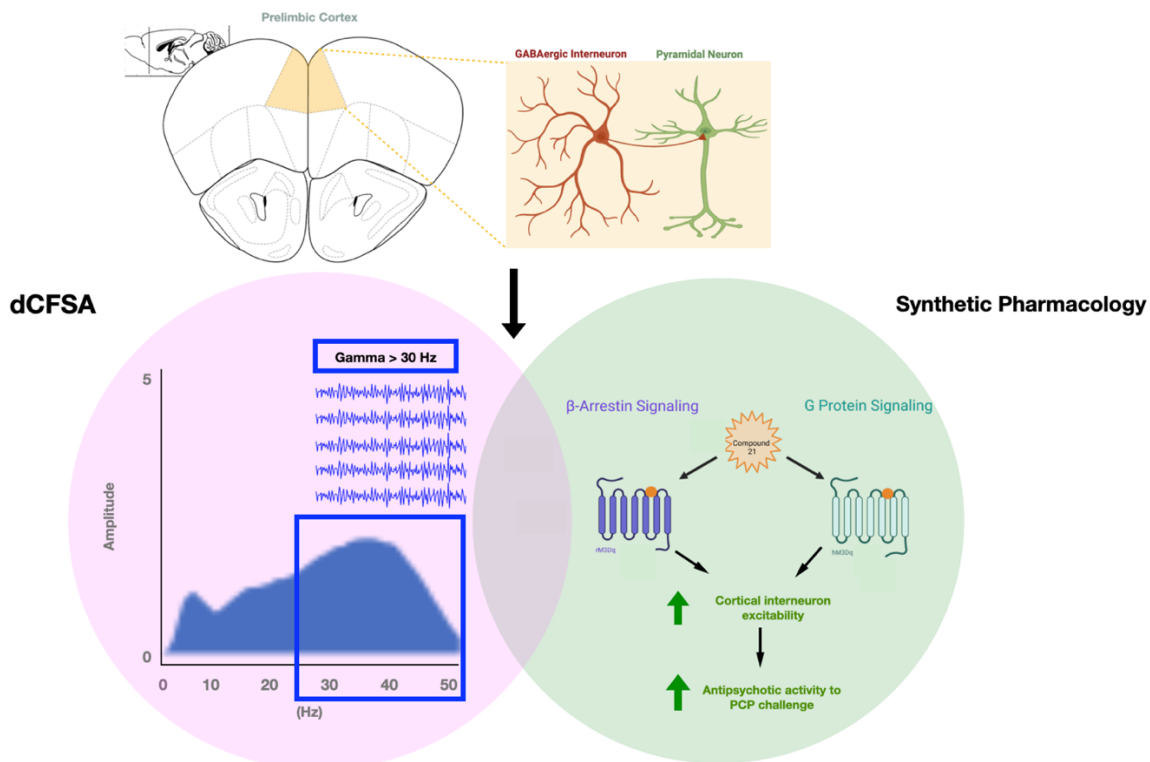


Figure 40 Prelimbic cortex identified as an antipsychotic drug relevant brain region

Venn diagram shows our supervised machine learning tool dCSFA (pink) describing 94A's effect on PCP induced network changes and the synthetic pharmacology using DREADDs (green) to excite cortical interneurons converge on antipsychotic activity in the prelimbic cortex is related to GABAergic interneuron function.

Appendix A : Methods and Materials

Animals

All mouse studies were conducted in accordance with the National Institutes of Health Guidelines for Animal Care and Use of Laboratory Animals and with approved animal protocols from the Duke University Animal Care and Use Committee. Adult male and female C57BL/6J and global β arrestin-2 KO, and their respective WT littermate mice were used in the reported studies. All mice were between 10-24 weeks old, weighing between 18-32 grams, and were age- and sex-matched for individual experiments. All mice were housed in a barrier facility, maintained on a 12:12 hour light:dark cycle in a temperature- and humidity-controlled room and fed a standard laboratory diet, with food and tap water provided ad libitum. All mice were group housed for all experiments (2-5 per cage), the exception being mice used in local (mPFC or dorsal striatum) drug infusion studies. These mice were singly housed and provided additional enrichment following cannula implantation.

Drugs and Chemicals

D-Amphetamine (AMPH), phencyclidine (PCP) HCl, haloperidol and UCSF924 were purchased from MilliporeSigma (Burlington, MA (Henry Schein, Raleigh, NC). UNC9994A (94A) and Compound 38 (Cpd38) were synthesized and provided as a gift from Dr. Jian Jin at Mt. Sinai School of Medicine (New York, NY). D4G180 and UCSF924

were provided by Dr. Brian Shoichet at the University of California – San Francisco (San Francisco, CA) DREADD agonist 21 (Cpd21), Compound 101 (Cpd101), A412997 and PD168,077 were purchased from Tocris Bioscience (Bristol, UK).

Open Field Activity: Systemic (i.p.) Drug Effects

Open field activity was measured using the Accuscan activity monitor (Omnitech Electronics, Inc., Columbus, OH), as previously described. Briefly, to evaluate drug challenges to stimulant induced hyperlocomotion, drug-naïve male and female C57BL6 mice were acclimated to the activity monitors for 30 minutes prior to administration intraperitoneally (i.p.) of vehicle (saline or 5% DMSO, 10% cyclodextrin) or drug (UNC9994A, UCSF924, Cpd21). Mice were then returned to the activity monitors for 10 minutes prior to systemic administration of psychostimulant (AMPH, PCP). Animals were immediately returned to the open field, and locomotor activity was monitored over 120 minutes in 5-minute intervals.

Cannulation: Local Drug Infusion

To locally inject drugs, bilateral guide cannulas (Plastics One) were designed to target either the mPFC (AP: + 2.3, ML: ± 0.5, DV: -1.8) or dorsal striatum (AP: +1.1, ML: ± 1.5, DV: -3.0). Anesthesia was induced using 2% isoflurane and Cannulas were affixed to the skull using dental cement (C&B Metabond® Quick Adhesive Cement System, Parkell, NY) and mice were allowed a minimum recovery period of 1 week prior to experimentation. On the day of experimentation, mice were acclimated to the open field

for 30 minutes prior to local infusion of drug or vehicle using an automated injection system. Exactly 0.5 μ l and 0.75 μ l of drug or vehicle was delivered to each hemisphere in the mPFC and dorsal striatum respectively, at a rate of 0.4 μ l/min. In experiments with the GRK2/3 blocker Cpd101, it was co-injected with UCSF924 or UNC9994A. After local injection, mice were placed in activity monitors for 10 minutes prior to systemic (i.p.) administration of psychostimulant (AMPH or PCP). Mice were immediately returned to the open field, and locomotor activity was monitored over 120 minutes in 5-minute intervals.

A.1 Materials and methods for chapter 2

Adeno-Associated Virus (AAV) production

Following complete sequencing, constructs were packaged into adeno-associated virus (AAV) pseudotype 10 and the XX680 helper plasmid using the triple-transfection technique, as previously described (Xiao, 1998). Titers of each AAV were determined to be between 10^{12} - 10^{13} vg/ml using qPCR.

AAV stereotaxic surgeries

Stereotaxic surgeries were performed as previously described. Briefly, mice were anesthetized under continuous 1-2% isoflurane and injected stereotactically in the mPFC (AP: +2.3, ML: \pm 0.3, DV: -1.8) with 0.5 μ l of AAV at a rate of 0.2 μ l/min. The needle was held in place for an additional 3 minutes prior to its gentle extraction. Mice were allowed a recovery period of 2 weeks prior to experimentation.

FAP

The MarsCy1 sequence is from (70). The MarsCy1-FAP was cloned onto the N-terminus of the mus musculus D2R previously tagged with eYFP on the C-terminus. The MarsCy1-FAP-tagged D2R was completed by standard cloning techniques and verified by sanger sequencing. Stable U2O2 cells expressing the Drd2-Cas9 plasmid were generated as described in(65). U2O2 cells were incubated with 20 nM SCi1 for 5 minutes and then imaged. No washing was performed. Infrared plate imaging of a 12-well plate with FAP-tagged D2R pulsed with SCi1 and a primary HA-epitope antibody at 4 °C and then fixed. The SCi1 dye was synthesized as in (206) and was resuspended in ethanol with 5% acetic acid at 78 uM. Cells were incubated with 20 nM SCi1 for 5 minutes. The 680 nm setting on LI-COR Odyssey infrared Western blot imager was used to image cells. Focal offsets were adjusted accordingly to match the focal plane of the plate.

A.2 Materials and methods for chapter 3

See animals, drug preparation, cannulation, and open field assay in Appendix A.

A.3 Materials and methods for chapter 4

Plasmids DREADDs

The interneuron selective DLX-hM3D(Gq)-mCherry plasmid was engineered through modification of pAAV-CaMKIIa-hM3D(Gq)-mCherry (Addgene #50476; gift from Bryan Roth). The pcDNA3.1 plasmid encoding the β -arrestin biased rM3D DREADD was a kind gift from Jürgen Wess and used to engineer the pAAV-DLX-

rM3D(β arr)-mCherry plasmid. The hM3D-RlucII, rM3D(β arr)-RlucII, β arrestin2-Venus and GRK2-FLAG constructs. The constructs and cell lines used for the TGF α shedding assay were generously provided by Dr. Asuka Inoue (Tohoku University, Sendai, Japan). All plasmids used will be made available on Addgene.

TGF α Shedding Assay

Unless otherwise noted, all GPCRs and G α proteins used in this study were from human origin and, to avoid artifacts, did not contain an epitope tag. GPCR sequences were cloned into mammalian expression vector pCAGGS (gift from J. Miyazaki, Osaka University) or pcDNA3.1 (Invitrogen). G α protein sequences were cloned into pCAGGS. A plasmid encoding AP-TGF α was constructed by S.H. and described previously. Plasmids were purified using NucleoBond PC 20 kit or Xtra Midi Plus kit (Macherey-Nagel). All clones were verified by sequencing (ABI Prism 3700, Applied Biosystems).

TGF α shedding assays were performed as previously described (Pack et al., 2018). Alkaline phosphatase activity was measured using a ClarioStar plate reader equipped with a fluorescent reader. Excitation and emission were set at 360 nm (\pm 10 nm) and 450 nm (\pm 15 nm), respectively. Data were collected over the course of 5 minutes. Shedding activity was calculated by dividing the amount of phosphatase activity present in the conditioned media by the amount present on the cells plus the

conditioned media. These values were standardized to background shedding activity, defined as compound-induced shedding activity in non-NTR1 expressing HEK293T cells, and represented at mean standardized shedding \pm SEM.

Bioluminescence Resonance Energy Transfer (BRET) Assays

BRET assays were performed as described. Day 1, HEK293T cells were seeded at 70% confluence in a 6-well plate and transfected via the calcium phosphate method using 200 ng/well of hM3Dq-RlucII, rM3D(Gq)-RlucII or rM3D(β arr)-RlucII and 2 μ g of β arr2-mVenus. Day 2, cells were transfected with 500 ng GRK2-FLAG. Both days, media was changed 6 hours after transfection. The following day, cells were plated onto poly-D-lysine-coated, clear-bottom, white-walled 96-well plates using clear minimum Eagle's medium supplemented with 10 mM HEPES, 1 \times GlutaMax, 2% fetal bovine serum, and 1 \times Antibiotic-Antimycotic. On Day 4, the media was removed, and cells were incubated with 80 μ l of Hank's Balanced Salt Solution (HBSS) containing calcium and magnesium for 2-3 hours prior to treatment. 10 \times concentrations of DREADD agonist 21 (CPD21) were prepared in distilled water just prior to experimentation.

A white vinyl sticker was placed on the bottom of the plate and 10 μ l of Cpd21 was added 10 minutes prior to reading. 10 μ l of a 10 \times concentration of coelenterazine h (final concentration, \sim 4.7 μ M) was added 5 minutes prior to reading to bring the total volume to 100 μ l. Plates were read on a Berthold Mithras LB 940 plate reader (Bad Wildbad, Germany) set at 35°C. Readings were averaged per plate and the NET BRET

ratio was calculated by subtracting the stimulated CPD21 Venus/RlucII ratios from the unstimulated vehicle Venus/RlucII ratio. The NET BRET ratio presented is a combined average from 3 experiments. Data are presented as Mean NET BRET ratio \pm SEM.

Immunohistochemistry (IHC)

Using a vibratome, formalin-fixed mouse brains were sectioned to obtain 50-micrometer thick sections for IHC analysis, as previously described(106). Sections were washed in TBS and treated with 10% normal goat serum (#31872, Invitrogen) and 0.3% Triton X-100 for 1 h. To confirm localization of DLX promoter driven DREADDs to interneurons, sections were incubated overnight at 4°C in mouse anti-GAD67 (1:500, MAB5406 clone 1G10.2, Millipore Sigma), goat anti-PV (1:500; PVG-213; Swant Inc.), and mouse anti- SST (1:500, H-11 sc-74556, Santa Cruz) were used. As a negative control, mouse anti-CAMKII (1:500, ab22609, Abcam) were used to label CamKIIa + neurons. The following day, sections were rinsed in TBS and incubated in goat anti-mouse IgG (H+L) Cross-Adsorbed Secondary Antibody, Alexa Fluor 568 (Invitrogen A-11004, 1:1000) for 1 hour at room temperature. Sections were then mounted on Superfrost Plus microscope slides (Thermo Fisher Scientific, catalog #12-550-15) and coverslipped. Images were taken using a Zeiss Axiozoom microscope

Analysis of DREADD Interneuron Expression

Images from representative sections of the IHC are at least 3 per group; sections in the prefrontal cortex, striatum, and hippocampus were collected. We analyzed red

(DLX-hM3Dq-mCherry) and orange (interneuron antibody-Alexa Fluor 568) channels separately to minimize channel interference with labeling. To optimize evaluation of marker colocalization after cells were labeled, the red and orange channels were merged and artificially labeled purple and green, respectively. In every instance where a cell body contained markers for the mCherry DREADD construct, we evaluated whether GAD67 was also present. The number of double-labeled cells was compared with the total number of GAD67+ neurons to quantify the mCherry+ cortical interneurons expressing DREADDs.

Curve fitting and statistical analysis

Dose-response curves were fit using GraphPad Prism's log (agonist) vs. response (three parameters) nonlinear fit function in order to calculate logEC50 and max efficacy values.

Statistical analysis was performed in Prism version 9.0 (GraphPad Software Inc., La Jolla, CA) as indicated in the text. Experiments testing the effect of a manipulation at each receptor were considered as one statistical unit. Two-way ANOVA were performed before Bonferroni's corrected t-tests. Each BRET or TGF shedding assay was performed in duplicate with at least 3 independent replicates.

A.4 Materials and methods for chapter 5

Neurophysiological data acquisition

Neuronal activity was sampled at 30kHz using the Cerebus acquisition system (Blackrock Microsystems Inc., UT). Local field potentials (LFPs) were bandpass filtered at 0.5–250Hz and stored at 1000Hz. Neuronal data were referenced online against a wire within the same brain area that did not exhibit a SNR > 3:1. At the end of the recording, cells were sorted again using an offline sorting algorithm (Plexon Inc., TX) to confirm the quality of the recorded cells. Only cellular clusters well-isolated with respect to background noise, defined as a Mahalanobis distance greater than 3 compared to the null point, were used for our unit-Event Factor correlation analysis. Clusters that exhibited more than 99.5% of their inter-spike-interval distribution above 2ms were defined as single units (53% of recorded neurons). Ultimately, we chose to use both single and multi-units for our analysis since our sole objective was to determine whether the Event Factor Activity showed temporal dynamics that reflected cellular activity. Neurophysiological recordings were referenced to a ground wire connected to both ground screws.

Electrode implantation surgery

Mice were anesthetized with 1.5% isoflurane, placed in a stereotaxic device, and metal ground screws were secured above the cerebellum and anterior cranium. The recording bundles designed to target amygdala (AMY), NAc, VTA, PFC, and VHip were centered based on stereotaxic coordinates measured from bregma (AMY: -1.6mm AP, 2.75 mm ML, -3.9 mm DV from the dura; NAc: 1.6mm AP, 1.4mm ML, -3.5 mm DV

from the dura; PFC: 1.7mm AP, 0mm ML, 2.25mm DV from the dura; VTA: -3.3mm AP, 0.5 mm ML, -4.25 mm DV from the dura; (VHip: -3.7mm AP, 3.0mm ML, -3.5mm DV from the dura). We targeted PrL and IL using the PFC bundle by building a 0.5mm DV stagger into our electrode bundle. Histological analysis of implantation sites was performed at the conclusion of experiments to confirm recording sites used for neurophysiological analysis.

Homecage recordings

Mice were connected to a headstage (Blackrock Microsystems, UT, USA) without anesthesia, and placed in a new home cage. Recordings were initiated after a 30-min habituation period.

LFP preprocessing to remove signal artifact

We used a heuristic to remove recording segments with non-physiological signals. First, we estimated the envelope of the signal in each channel using the magnitude of the Hilbert transform. For any 1-second window where the envelope exceeds above a pre-selected low threshold, the entire segment is removed if the envelope exceeds a second, high threshold at any point within that window. The two thresholds were determined independently for each brain region. The high threshold was selected to be 5 times the median absolute deviation of the envelope value for that region. Five median absolute deviations was chosen as the high threshold because it is roughly equivalent to 3 standard deviations from the mean for normally distributed

data, but is robust to outliers in the data. The low threshold was empirically chosen to be 3.33% of the high threshold. If more than half the window was removed for a channel, we removed the rest of that window for that channel as well. In addition, any windows where the standard deviation of the channel is less than 0.01 were also removed.

Determination of LFP oscillatory power and cross power

LFPs were averaged across wires within region to yield a composite LFP measure. Signal processing was performed using Matlab (The MathWorks, Inc., Natick, MA). For LFP power, a sliding Fourier transform with Hamming window was applied to the averaged LFP signal using a 1 second window and a 1 second step. Frequencies were analyzed with a resolution of 1Hz. LFP cross-structural coherence was calculated from the pairs of averaged LFPs using magnitude-squared coherence where coherence is a function of the power spectral densities of A and B, and their cross-spectral densities.

Cross power volumes were calculated using Welch's method with 1024 samples (about 1 second of LFP sampled at 1 kHz) and half overlap, using median averaging over periodograms. For regions comprising multiple channels, the average cross-power over all pairs of channels was taken as the cross power. The LFPs were windowed at 1 minute, resulting in a cross-power volume for each minute of recording.

We applied a Supervised Cross-Spectral Factor Analysis – Nonnegative Matrix Factorization (CSFA-NMF) model, which is fully described elsewhere (Talbot et al., 2020), to these calculated cross-power volumes. Briefly, this method performs logistic

regression to predict label (in our case, baseline recording vs. PCP recording) using the cross-power features. However, this logistic regression task is regularized with the task of reconstructing the features using a nonnegative weighting a small set of nonnegative factors. The logistic regression also passes through this low-dimensional weighting (factor score) bottleneck, thereby associating each class of the prediction task with a nonnegative factor or “network” used to reconstruct the cross-power volume. Therefore, the CSFA-NMF model makes “interpretable” predictions in that its label predictions are associated with the relative strength of different nonnegative cross-power volumes. One notable difference from the CSFA-NMF approach described by Talbot et al. (2020) is that the nonnegative factors in this work, in addition to being linear, are additionally constrained to be rank-1 volumes (tensor products of three vectors). This restricted hypothesis class can help generalization and respects the intrinsic 3-dimensional nature of the cross-power volumes.

Discriminative Cross-Spectral Factor Analysis – Nonnegative Matrix Factorization

To apply our Supervised Cross-Spectral Factor Analysis – Nonnegative Matrix Factorization (CSFA-NMF) model, which fully described elsewhere (Talbot et al., 2020), we consider each window of data to be an independent stationary measurement. This implies that the relevant dynamics happens at the scale of windows, so the extracted electome scores are all that is needed for later analysis. In this work, we choose a 1 second window because this balanced fine-grained behavior with enough length of

signal to estimate the relevant LFP features. Prior work has shown relative robustness to windows between 0.5s to 5s in similar methods (Ulrich et al., 2015), so we expect similar results for similar window lengths; however, 5s here would not be able to capture the short-term scale of behavior necessary for this analysis.

For each window of data, we have the generated features, consisting of spectral power features, coherence features, and exponential granger features, totaling distinct features per window. Using the subscript to denote window and state that there are total windows. We describe the preprocessed data as (the -dimensional non-negative domain) and the observed behavioral label as , where the binary indicates a social or non-social behavioral label. To briefly described this model, we set up an objective function to learn the different electome factors, the electome factor scores are given by the multi-output function , and the relationship between the electome factor scores and the behavioral labels is given by . This equation has a mean squared error loss on the behavior labels. In practice for binary behavioral labels, we instead use a binary cross-entropy loss. The relative importance of reconstructing the observed data and the importance of the predictive task were balanced by choosing the hyperparameter. This represents a novel method to fit an NMF model using supervised autoencoders and requires the user to choose a parametrization for . In our method, this is simply set to an affine function following by a non-linearity, , where the parameters of the function are and the softplus means an element-wise operation of the operation , which maps a real number to the

non-negative space. This function can vary in complexity to allow greater model complexity, but we found that this function was sufficient in practice. Because this objective function follows a supervised autoencoder structure, a common deep learning structure, we can implement this technique in Tensorflow (Abadi et al., 2016) using the ADAM algorithm for learning (Diederik and Ba, 2014).

A benefit of using this structure for learning is that performing statistical inference from new data is fast and straightforward. In factor models, one typically has to set up an optimization algorithm to find the maximum a posteriori estimate. However, in our supervised CSFA-NMF framework, we can calculate the electome scores on new data simply by calling the function, allowing easy portability and facilitating future real time applications.

Fiber Photometry

Wildtype mice were chronically implanted with an optic fiber (MFC_400/430–0.48_4mm_ZF2.5(G)_FLT, Doric Lenses) above prelimbic cortex) and control LED light (405 nm, M405FP1, Thorlabs) was passed through excitation filters and focused onto a patch cord (MFP_400/430/1100–0.48_4 m_FC-ZF2.5, Doric Lenses). The fiber patch cord was connected to the chronically implanted fiber, and emission light (500–550 nm) was collected through the same fiber and passed onto a photoreceiver (Newport 2151, Doric Lenses). Excitation light was sinusoidally modulated at 211 and 531 Hz (470 nm and 405 nm light, respectively) and collected raw signal was demodulated by a real-time signal

processor (RZ5P, Tucker Davis Systems) to determine contributions from 470 nm and 405 nm excitation sources (see Lerner et al., 2015). For recordings of cortical dopamine dynamics using AAV9-CAG-GRABDA1, after habituation to handling, animals were injected intraperitoneally while freely moving in their homecage. In order to assess the effects of phencyclidine. (4 mg/kg), intraperitoneal Injections were performed within subject with a 1 week wash out. To account for fluorescence bleaching effect, the light was turned on 10 minutes prior to recording. During each day, fluorescence was recorded for at least 40 continuous minutes- 5 minute baseline period before injection, and a 35-minute period after injection to capture the peak effect of PCP.

All data analyses were performed offline in Matlab (custom script <https://github.com/tjd2002/tjdshared-code> , Davidson, 2016). To calculate dF/F , a linear fit was applied to the 405 nm signal during the baseline period to align it to the 470 nm signal, producing a fitted 405 nm signal that was used as F_0 to normalize the 470 nm using standard dF/F normalization: $(470 \text{ nm signal} - \text{fitted } 405 \text{ nm signal})/\text{fitted } 405 \text{ nm signal}$. dLight experiments, the average signal in the five minutes preceding IP injection was compared to the average signal between thirty minutes after IP injection.

Mice were euthanized and brains fixed in paraformaldehyde to prepare histological slices for verification of virus expression and optic fiber placement.

References

1. Grace AA, Gomes FV. The circuitry of dopamine system regulation and its disruption in schizophrenia: insights into treatment and prevention. *Schizophr Bull.* 2019 Jan 1;45(1):148–57.
2. Carbon M, Correll CU. Thinking and acting beyond the positive: the role of the cognitive and negative symptoms in schizophrenia. *CNS Spectr.* 2014 Dec;19 Suppl 1:38–52; quiz 35.
3. Nucifora FC, Woznica E, Lee BJ, Cascella N, Sawa A. Treatment resistant schizophrenia: Clinical, biological, and therapeutic perspectives. *Neurobiol Dis.* 2019 Nov;131:104257.
4. Mohebi A, Pettibone JR, Hamid AA, Wong J-MT, Vinson LT, Patriarchi T, et al. Dissociable dopamine dynamics for learning and motivation. *Nature.* 2019 Jun;570(7759):65–70.
5. Holloway ZR, Freels TG, Comstock JF, Nolen HG, Sable HJ, Lester DB. Comparing phasic dopamine dynamics in the striatum, nucleus accumbens, amygdala, and medial prefrontal cortex. *Synapse.* 2018 Oct 13;e22074.
6. Seeman MV. History of the dopamine hypothesis of antipsychotic action. *World J Psychiatry.* 2021 Jul 19;11(7):355–64.
7. van Rossum JM. The significance of dopamine-receptor blockade for the mechanism of action of neuroleptic drugs. *Arch Int Pharmacodyn Ther.* 1966 Apr;160(2):492–4.
8. Snyder SH. Amphetamine psychosis: a “model” schizophrenia mediated by catecholamines. *Am J Psychiatry.* 1973 Jan;130(1):61–7.
9. dela Peña I, Gevorkiana R, Shi W-X. Psychostimulants affect dopamine transmission through both dopamine transporter-dependent and independent mechanisms. *Eur J Pharmacol.* 2015 Oct 5;764:562–70.
10. Koychev I, El-Deredy W, Mukherjee T, Haenschel C, Deakin JFW. Core dysfunction in schizophrenia: electrophysiology trait biomarkers. *Acta Psychiatr Scand.* 2012 Jul;126(1):59–71.

11. Galiñanes GL, Taravini IRE, Murer MG. Dopamine-dependent periadolescent maturation of corticostriatal functional connectivity in mouse. *J Neurosci*. 2009 Feb 25;29(8):2496–509.
12. Quintana C, Beaulieu J-M. A fresh look at cortical dopamine D2 receptor expressing neurons. *Pharmacol Res*. 2019 Jan;139:440–5.
13. Rao N, Northoff G, Tagore A, Rusjan P, Kenk M, Wilson A, et al. Impaired prefrontal cortical dopamine release in schizophrenia during a cognitive task: A [11C]FLB 457 positron emission tomography study. *Schizophr Bull*. 2018 Jun 7;45(3):670–9.
14. Reneaux M, Gupta R. Prefronto-cortical dopamine D1 receptor sensitivity can critically influence working memory maintenance during delayed response tasks. *PLoS One*. 2018 May 29;13(5):e0198136.
15. Adams B, Moghaddam B. Corticolimbic dopamine neurotransmission is temporally dissociated from the cognitive and locomotor effects of phencyclidine. *J Neurosci*. 1998 Jul 15;18(14):5545–54.
16. Urs NM, Peterson SM, Caron MG. New concepts in dopamine D2 receptor biased signaling and implications for schizophrenia therapy. *Biol Psychiatry*. 2017 Jan 1;81(1):78–85.
17. Del Arco A, Mora F. NMDA and AMPA/kainate glutamatergic agonists increase the extracellular concentrations of GABA in the prefrontal cortex of the freely moving rat: modulation by endogenous dopamine. *Brain Res Bull*. 2002 Mar 15;57(5):623–30.
18. Anver H, Ward PD, Magony A, Vreugdenhil M. NMDA receptor hypofunction phase couples independent γ -oscillations in the rat visual cortex. *Neuropsychopharmacology*. 2011 Jan;36(2):519–28.
19. Adell A. Brain NMDA receptors in schizophrenia and depression. *Biomolecules*. 2020 Jun 23;10(6).
20. Zheng P, Zhang XX, Bunney BS, Shi WX. Opposite modulation of cortical N-methyl-D-aspartate receptor-mediated responses by low and high concentrations of dopamine. *Neuroscience*. 1999;91(2):527–35.

21. Borroto-Escuela DO, Pintsuk J, Schäfer T, Friedland K, Ferraro L, Tanganelli S, et al. Multiple D2 heteroreceptor complexes: new targets for treatment of schizophrenia. *Ther Adv Psychopharmacol*. 2016 Apr;6(2):77–94.
22. Javitt DC. Glutamatergic theories of schizophrenia. *Isr J Psychiatry Relat Sci*. 2010;47(1):4–16.
23. Kapur S, Seeman P. NMDA receptor antagonists ketamine and PCP have direct effects on the dopamine D(2) and serotonin 5-HT(2)receptors-implications for models of schizophrenia. *Mol Psychiatry*. 2002;7(8):837–44.
24. Curic S, Leicht G, Thiebes S, Andreou C, Polomac N, Eichler I-C, et al. Reduced auditory evoked gamma-band response and schizophrenia-like clinical symptoms under subanesthetic ketamine. *Neuropsychopharmacology*. 2019 Jun;44(7):1239–46.
25. Volman V, Behrens MM, Sejnowski TJ. Downregulation of parvalbumin at cortical GABA synapses reduces network gamma oscillatory activity. *J Neurosci*. 2011 Dec 7;31(49):18137–48.
26. Tamás G, Buhl EH, Lörincz A, Somogyi P. Proximally targeted GABAergic synapses and gap junctions synchronize cortical interneurons. *Nat Neurosci*. 2000 Apr;3(4):366–71.
27. Tanaka-Koshiyama K, Koshiyama D, Miyakoshi M, Joshi YB, Molina JL, Sprock J, et al. Abnormal spontaneous gamma power is associated with verbal learning and memory dysfunction in schizophrenia. *Front Psychiatry*. 2020 Aug 31;11:832.
28. Wong FK, Bercsenyi K, Sreenivasan V, Portalés A, Fernández-Otero M, Marín O. Pyramidal cell regulation of interneuron survival sculpts cortical networks. *Nature*. 2018 May 30;557(7707):668–73.
29. Yao Y, Wu M, Wang L, Lin L, Xu J. Phase coupled firing of prefrontal parvalbumin interneuron with high frequency oscillations. *Front Cell Neurosci*. 2020 Nov 25;14:610741.
30. Anastasiades PG, Marlin JJ, Carter AG. Cell-Type Specificity of Callosally Evoked Excitation and Feedforward Inhibition in the Prefrontal Cortex. *Cell Rep*. 2018 Jan 16;22(3):679–92.

31. Santana N, Artigas F. Laminar and cellular distribution of monoamine receptors in rat medial prefrontal cortex. *Front Neuroanat.* 2017 Sep 28;11:87.
32. Cho KKA, Hoch R, Lee AT, Patel T, Rubenstein JLR, Sohal VS. Gamma rhythms link prefrontal interneuron dysfunction with cognitive inflexibility in *Dlx5/6(+/-)* mice. *Neuron.* 2015 Mar 18;85(6):1332–43.
33. Javitt DC, Zukin SR, Heresco-Levy U, Umbricht D. Has an angel shown the way? Etiological and therapeutic implications of the PCP/NMDA model of schizophrenia. *Schizophr Bull.* 2012 Sep;38(5):958–66.
34. Piccart E, Tschumi CW, Beckstead MJ. Acute and subchronic PCP attenuate D2 autoreceptor signaling in substantia nigra dopamine neurons. *Eur Neuropsychopharmacol.* 2019 Mar;29(3):444–9.
35. Rampino A, Marakhovskaia A, Soares-Silva T, Torretta S, Veneziani F, Beaulieu JM. Antipsychotic drug responsiveness and dopamine receptor signaling; old players and new prospects. *Front Psychiatry.* 2018;9:702.
36. Schizophrenia Psychiatric Genome-Wide Association Study (GWAS) Consortium. Genome-wide association study identifies five new schizophrenia loci. *Nat Genet.* 2011 Sep 18;43(10):969–76.
37. Shioda N. Dopamine D2L receptor-interacting proteins regulate dopaminergic signaling. *J Pharmacol Sci.* 2017 Oct 14;
38. Martel JC, Gatti McArthur S. Dopamine receptor subtypes, physiology and pharmacology: new ligands and concepts in schizophrenia. *Front Pharmacol.* 2020 Jul 14;11:1003.
39. Condon AF, Robinson BG, Asad N, Dore TM, Tian L, Williams JT. The residence of synaptically released dopamine on D2 autoreceptors. *Cell Rep.* 2021 Aug 3;36(5):109465.
40. Tritsch NX, Sabatini BL. Dopaminergic modulation of synaptic transmission in cortex and striatum. *Neuron.* 2012 Oct 4;76(1):33–50.
41. Inoue A, Raimondi F, Kadji FMN, Singh G, Kishi T, Uwamizu A, et al. Illuminating G-Protein-Coupling Selectivity of GPCRs. *Cell.* 2019 Jun 13;177(7):1933–1947.e25.

42. Onfroy L, Galandrin S, Pontier SM, Seguelas M-H, N'Guyen D, Sénard J-M, et al. G protein stoichiometry dictates biased agonism through distinct receptor-G protein partitioning. *Sci Rep*. 2017 Aug 11;7(1):7885.
43. Gilchrist A, Vanhauwe JF, Li A, Thomas TO, Voyno-Yasenetskaya T, Hamm HE. G alpha minigenes expressing C-terminal peptides serve as specific inhibitors of thrombin-mediated endothelial activation. *J Biol Chem*. 2001 Jul 13;276(28):25672–9.
44. Daigle TL, Ferris MJ, Gainetdinov RR, Sotnikova TD, Urs NM, Jones SR, et al. Selective deletion of GRK2 alters psychostimulant-induced behaviors and dopamine neurotransmission. *Neuropsychopharmacology*. 2014 Sep;39(10):2450–62.
45. Pack TF, Orlen MI, Ray C, Peterson SM, Caron MG. The dopamine D2 receptor can directly recruit and activate GRK2 without G protein activation. *J Biol Chem*. 2018 Apr 20;293(16):6161–71.
46. Peterson SM, Pack TF, Caron MG. Receptor, ligand and transducer contributions to dopamine D2 receptor functional selectivity. *PLoS One*. 2015 Oct 30;10(10):e0141637.
47. Peterson SM, Pack TF, Wilkins AD, Urs NM, Urban DJ, Bass CE, et al. Elucidation of G-protein and β -arrestin functional selectivity at the dopamine D2 receptor. *Proc Natl Acad Sci USA*. 2015 Jun 2;112(22):7097–102.
48. Lee M-H, Appleton KM, Strungs EG, Kwon JY, Morinelli TA, Peterson YK, et al. The conformational signature of β -arrestin2 predicts its trafficking and signalling functions. *Nature*. 2016 Mar 31;531(7596):665–8.
49. Asher WB, Terry DS, Gregorio GGA, Kahsai AW, Borgia A, Xie B, et al. GPCR-mediated β -arrestin activation deconvoluted with single-molecule precision. *Cell*. 2022 May 12;185(10):1661–1675.e16.
50. Beaulieu J-M, Gainetdinov RR, Caron MG. Akt/GSK3 signaling in the action of psychotropic drugs. *Annu Rev Pharmacol Toxicol*. 2009;49:327–47.
51. Beaulieu J-M, Sotnikova TD, Marion S, Lefkowitz RJ, Gainetdinov RR, Caron MG. An Akt/beta-arrestin 2/PP2A signaling complex mediates dopaminergic neurotransmission and behavior. *Cell*. 2005 Jul 29;122(2):261–73.

52. Emamian ES. AKT/GSK3 signaling pathway and schizophrenia. *Front Mol Neurosci.* 2012 Mar 15;5:33.
53. Urs NM, Snyder JC, Jacobsen JPR, Peterson SM, Caron MG. Deletion of GSK3 β in D2R-expressing neurons reveals distinct roles for β -arrestin signaling in antipsychotic and lithium action. *Proc Natl Acad Sci USA.* 2012 Dec 11;109(50):20732–7.
54. Beaulieu J-M, Marion S, Rodriguiz RM, Medvedev IO, Sotnikova TD, Ghisi V, et al. A beta-arrestin 2 signaling complex mediates lithium action on behavior. *Cell.* 2008 Jan 11;132(1):125–36.
55. Puig MV, Antzoulatos EG, Miller EK. Prefrontal dopamine in associative learning and memory. *Neuroscience.* 2014 Dec 12;282:217–29.
56. Arnsten AFT, Wang M, Paspalas CD. Dopamine's actions in primate prefrontal cortex: challenges for treating cognitive disorders. *Pharmacol Rev.* 2015 Jul;67(3):681–96.
57. Mack KJ, O'Malley KL, Todd RD. Differential expression of dopaminergic D2 receptor messenger RNAs during development. *Developmental Brain Research.* 1991 Apr;59(2):249–51.
58. Montgomery D, Campbell A, Sullivan H-J, Wu C. Molecular dynamics simulation of biased agonists at the dopamine D2 receptor suggests the mechanism of receptor functional selectivity. *J Biomol Struct Dyn.* 2018 Aug 19;1–49.
59. Cohen MX, Frank MJ. Neurocomputational models of basal ganglia function in learning, memory and choice. *Behav Brain Res.* 2009 Apr 12;199(1):141–56.
60. Robinson BG, Bunzow JR, Grimm JB, Lavis LD, Dudman JT, Brown J, et al. Desensitized D2 autoreceptors are resistant to trafficking. *Sci Rep.* 2017 Jun 29;7(1):4379.
61. DeBaker MC, Marron Fernandez de Velasco E, McCall NM, Lee AM, Wickman K. Differential Impact of Inhibitory G-Protein Signaling Pathways in Ventral Tegmental Area Dopamine Neurons on Behavioral Sensitivity to Cocaine and Morphine. *eNeuro.* 2021 Apr;8(2).
62. Tycko J, Myer VE, Hsu PD. Methods for Optimizing CRISPR-Cas9 Genome

- Editing Specificity. *Mol Cell*. 2016 Aug 4;63(3):355–70.
63. Savić N, Schwank G. Advances in therapeutic CRISPR/Cas9 genome editing. *Transl Res*. 2016 Feb;168:15–21.
 64. Kato T, Takada S. In vivo and in vitro disease modeling with CRISPR/Cas9. *Brief Funct Genomics*. 2017 Jan;16(1):13–24.
 65. Cong L, Ran FA, Cox D, Lin S, Barretto R, Habib N, et al. Multiplex genome engineering using CRISPR/Cas systems. *Science*. 2013 Feb 15;339(6121):819–23.
 66. Zhang X-H, Tee LY, Wang X-G, Huang Q-S, Yang S-H. Off-target effects in CRISPR/Cas9-mediated genome engineering. *Mol Ther Nucleic Acids*. 2015 Nov 17;4:e264.
 67. Dong F, Xie K, Chen Y, Yang Y, Mao Y. Polycistronic tRNA and CRISPR guide-RNA enables highly efficient multiplexed genome engineering in human cells. *Biochem Biophys Res Commun*. 2017 Jan 22;482(4):889–95.
 68. Riesenberg S, Helmbrecht N, Kanis P, Maricic T, Pääbo S. Improved gRNA secondary structures allow editing of target sites resistant to CRISPR-Cas9 cleavage. *Nat Commun*. 2022 Jan 25;13(1):489.
 69. Perkins LA, Bruchez MP. Fluorogen activating protein toolset for protein trafficking measurements. *Traffic*. 2020 Apr;21(4):333–48.
 70. Zhang M, Chakraborty SK, Sampath P, Rojas JJ, Hou W, Saurabh S, et al. Fluoromodule-based reporter/probes designed for in vivo fluorescence imaging. *J Clin Invest*. 2015 Oct 1;125(10):3915–27.
 71. Gallo E. Fluorogen-Activating Proteins: Next-Generation Fluorescence Probes for Biological Research. *Bioconjug Chem*. 2020 Jan 15;31(1):16–27.
 72. Snyder JC, Pack TF, Rochelle LK, Chakraborty SK, Zhang M, Eaton AW, et al. A rapid and affordable screening platform for membrane protein trafficking. *BMC Biol*. 2015 Dec 17;13:107.
 73. Gompf HS, Budygin EA, Fuller PM, Bass CE. Targeted genetic manipulations of neuronal subtypes using promoter-specific combinatorial AAVs in wild-type animals. *Front Behav Neurosci*. 2015 Jul 2;9:152.

74. Jones SR, Gainetdinov RR, Wightman RM, Caron MG. Mechanisms of amphetamine action revealed in mice lacking the dopamine transporter. *J Neurosci*. 1998 Mar 15;18(6):1979–86.
75. Urs NM, Caron MG. The physiological relevance of functional selectivity in dopamine signalling. *Int J Obes Suppl*. 2014 Jul 8;4(Suppl 1):S5-8.
76. Calipari ES, Ferris MJ. Amphetamine mechanisms and actions at the dopamine terminal revisited. *J Neurosci*. 2013 May 22;33(21):8923–5.
77. Kargieman L, Santana N, Mengod G, Celada P, Artigas F. Antipsychotic drugs reverse the disruption in prefrontal cortex function produced by NMDA receptor blockade with phencyclidine. *Proc Natl Acad Sci USA*. 2007 Sep 11;104(37):14843–8.
78. Nakao K, Jeevakumar V, Jiang SZ, Fujita Y, Diaz NB, Pretell Annan CA, et al. Schizophrenia-Like Dopamine Release Abnormalities in a Mouse Model of NMDA Receptor Hypofunction. *Schizophr Bull*. 2019 Jan 1;45(1):138–47.
79. Inada T, Yagi G. Current topics in neuroleptic-induced extrapyramidal symptoms in Japan. *Keio J Med*. 1996 Jun;45(2):95–9.
80. Sykes DA, Moore H, Stott L, Holliday N, Javitch JA, Lane JR, et al. Extrapyramidal side effects of antipsychotics are linked to their association kinetics at dopamine D2 receptors. *Nat Commun*. 2017 Oct 2;8(1):763.
81. Kapur S, Seeman P. Does fast dissociation from the dopamine d(2) receptor explain the action of atypical antipsychotics?: A new hypothesis. *Am J Psychiatry*. 2001 Mar;158(3):360–9.
82. Nucifora FC, Mihaljevic M, Lee BJ, Sawa A. Clozapine as a model for antipsychotic development. *Neurotherapeutics*. 2017 Jul;14(3):750–61.
83. Van Tol HH, Bunzow JR, Guan HC, Sunahara RK, Seeman P, Niznik HB, et al. Cloning of the gene for a human dopamine D4 receptor with high affinity for the antipsychotic clozapine. *Nature*. 1991 Apr 18;350(6319):610–4.
84. Sharma A, Kramer ML, Wick PF, Liu D, Chari S, Shim S, et al. D4 dopamine receptor-mediated phospholipid methylation and its implications for mental illnesses such as schizophrenia. *Mol Psychiatry*. 1999 May;4(3):235–46.

85. Sánchez-Soto M, Yano H, Cai N-S, Casadó-Anguera V, Moreno E, Casadó V, et al. Revisiting the Functional Role of Dopamine D4 Receptor Gene Polymorphisms: Heteromerization-Dependent Gain of Function of the D4.7 Receptor Variant. *Mol Neurobiol*. 2019 Jul;56(7):4778–85.
86. Wang S, Wacker D, Levit A, Che T, Betz RM, McCorvy JD, et al. D4 dopamine receptor high-resolution structures enable the discovery of selective agonists. *Science*. 2017 Oct 20;358(6361):381–6.
87. Quantitative analysis of the dopamine D4 receptor in the mouse brain [Internet]. [cited 2022 Jun 9]. Available from: <https://onlinelibrary.wiley.com/doi/pdfdirect/10.1002/%28SICI%291097-4547%2820000115%2959%3A2%3C202%3A%3AAID-JNR6%3E3.0.CO%3B2-5>
88. Keck TM, Suchland KL, Jimenez CC, Grandy DK. Dopamine D4 receptor deficiency in mice alters behavioral responses to anxiogenic stimuli and the psychostimulant methylphenidate. *Pharmacol Biochem Behav*. 2013 Feb;103(4):831–41.
89. Kocsis B, Lee P, Deth R. Enhancement of gamma activity after selective activation of dopamine D4 receptors in freely moving rats and in a neurodevelopmental model of schizophrenia. *Brain Struct Funct*. 2014 Nov;219(6):2173–80.
90. Rubinstein M, Cepeda C, Hurst RS, Flores-Hernandez J, Ariano MA, Falzone TL, et al. Dopamine D4 receptor-deficient mice display cortical hyperexcitability. *J Neurosci*. 2001 Jun 1;21(11):3756–63.
91. Meador-Woodruff JH, Damask SP, Wang J, Haroutunian V, Davis KL, Watson SJ. Dopamine receptor mRNA expression in human striatum and neocortex. *Neuropsychopharmacology*. 1996 Jul;15(1):17–29.
92. Defagot MC, Falzone TL, Low MJ, Grandy DK, Rubinstein M, Antonelli MC. Quantitative analysis of the dopamine D4 receptor in the mouse brain. *J Neurosci Res*. 2000 Jan 15;
93. Szűcs E, Ducza E, Büki A, Kekesi G, Benyhe S, Horvath G. Characterization of dopamine D2 receptor binding, expression and signaling in different brain regions of control and schizophrenia-model Wistar rats. *Brain Res*. 2020 Dec 1;1748:147074.

94. Lipska BK, Lerman DN, Khaing ZZ, Weickert CS, Weinberger DR. Gene expression in dopamine and GABA systems in an animal model of schizophrenia: effects of antipsychotic drugs. *Eur J Neurosci*. 2003 Jul;18(2):391–402.
95. Buzsáki G, Wang X-J. Mechanisms of gamma oscillations. *Annu Rev Neurosci*. 2012 Mar 20;35:203–25.
96. Chung DW, Fish KN, Lewis DA. Pathological basis for deficient excitatory drive to cortical parvalbumin interneurons in schizophrenia. *Am J Psychiatry*. 2016 Nov 1;173(11):1131–9.
97. Zhong P, Yan Z. Distinct Physiological Effects of Dopamine D4 Receptors on Prefrontal Cortical Pyramidal Neurons and Fast-Spiking Interneurons. *Cereb Cortex*. 2016 Jan;26(1):180–91.
98. Wang Y-L, Wang J-G, Guo F-L, Gao X-H, Zhao D-D, Zhang L, et al. Selective dopamine receptor 4 activation mediates the hippocampal neuronal calcium response via IP3 and ryanodine receptors. *Brain Res*. 2017 Sep 1;1670:1–5.
99. Jones CA, Watson DJG, Fone KCF. Animal models of schizophrenia. *Br J Pharmacol*. 2011 Oct;164(4):1162–94.
100. Amato D, Canneva F, Cumming P, Maschauer S, Groos D, Dahlmanns JK, et al. A dopaminergic mechanism of antipsychotic drug efficacy, failure, and failure reversal: the role of the dopamine transporter. *Mol Psychiatry*. 2020 Sep;25(9):2101–18.
101. Lladó-Pelfort L, Troyano-Rodriguez E, van den Munkhof HE, Cervera-Ferri A, Jurado N, Núñez-Calvet M, et al. Phencyclidine-induced disruption of oscillatory activity in prefrontal cortex: Effects of antipsychotic drugs and receptor ligands. *Eur Neuropsychopharmacol*. 2016 Mar;26(3):614–25.
102. Morshedi MM, Meredith GE. Differential laminar effects of amphetamine on prefrontal parvalbumin interneurons. *Neuroscience*. 2007 Nov 9;149(3):617–24.
103. Edwards CM, Strother J, Zheng H, Rinaman L. Amphetamine-induced activation of neurons within the rat nucleus of the solitary tract. *Physiol Behav*. 2019 May 15;204:355–63.
104. Segovia KN, Vontell R, López-Cruz L, Salamone JD, Correa M. c-Fos

immunoreactivity in prefrontal, basal ganglia and limbic areas of the rat brain after central and peripheral administration of ethanol and its metabolite acetaldehyde. *Front Behav Neurosci.* 2013 May 24;7:48.

105. de Almeida J, Mengod G. D2 and D4 dopamine receptor mRNA distribution in pyramidal neurons and GABAergic subpopulations in monkey prefrontal cortex: implications for schizophrenia treatment. *Neuroscience.* 2010 Nov 10;170(4):1133–9.
106. Urs NM, Gee SM, Pack TF, McCorvy JD, Evron T, Snyder JC, et al. Distinct cortical and striatal actions of a β -arrestin-biased dopamine D2 receptor ligand reveal unique antipsychotic-like properties. *Proc Natl Acad Sci USA.* 2016 Dec 13;113(50):E8178–86.
107. Rose SJ, Pack TF, Peterson SM, Payne K, Borrelli E, Caron MG. Engineered D2R Variants Reveal the Balanced and Biased Contributions of G-Protein and β -Arrestin to Dopamine-Dependent Functions. *Neuropsychopharmacology.* 2018;43(5):1164–73.
108. Farrell MS, Roth BL. Pharmacosynthetics: Reimagining the pharmacogenetic approach. *Brain Res.* 2013 May 20;1511:6–20.
109. Zhu H, Roth BL. DREADD: a chemogenetic GPCR signaling platform. *Int J Neuropsychopharmacol.* 2014 Oct 31;18(1).
110. Roth BL. DREADDs for neuroscientists. *Neuron.* 2016 Feb 17;89(4):683–94.
111. Farrell MS, Pei Y, Wan Y, Yadav PN, Daigle TL, Urban DJ, et al. A *G α s* DREADD mouse for selective modulation of cAMP production in striatopallidal neurons. *Neuropsychopharmacology.* 2013 Apr 1;38(5):854–62.
112. Wess J, Nakajima K, Jain S. Novel designer receptors to probe GPCR signaling and physiology. *Trends Pharmacol Sci.* 2013 Jul;34(7):385–92.
113. Nakajima K, Wess J. Design and functional characterization of a novel, arrestin-biased designer G protein-coupled receptor. *Mol Pharmacol.* 2012 Oct;82(4):575–82.
114. Thompson KJ, Khajehali E, Bradley SJ, Navarrete JS, Huang XP, Slocum S, et al. DREADD Agonist 21 Is an Effective Agonist for Muscarinic-Based DREADDs in

- Vitro and in Vivo. *ACS Pharmacol Transl Sci*. 2018 Sep 14;1(1):61–72.
115. Inoue A, Ishiguro J, Kitamura H, Arima N, Okutani M, Shuto A, et al. TGF α shedding assay: an accurate and versatile method for detecting GPCR activation. *Nat Methods*. 2012 Oct;9(10):1021–9.
 116. Kamato D, Thach L, Bernard R, Chan V, Zheng W, Kaur H, et al. Structure, function, pharmacology, and therapeutic potential of the G protein, $g\alpha/q,11$. *Front Cardiovasc Med*. 2015 Mar 24;2:14.
 117. Uhlhaas PJ, Haenschel C, Nikolić D, Singer W. The role of oscillations and synchrony in cortical networks and their putative relevance for the pathophysiology of schizophrenia. *Schizophr Bull*. 2008 Sep;34(5):927–43.
 118. Meier MA, Lemercier CE, Kulisch C, Kiss B, Lendvai B, Adham N, et al. The novel antipsychotic cariprazine stabilizes gamma oscillations in rat hippocampal slices. *Br J Pharmacol*. 2020 Apr;177(7):1622–34.
 119. Rapanelli M, Frick LR, Bernardez-Vidal M, Zanutto BS. Different MK-801 administration schedules induce mild to severe learning impairments in an operant conditioning task: role of buspirone and risperidone in ameliorating these cognitive deficits. *Behav Brain Res*. 2013 Nov 15;257:156–65.
 120. Tseng K-Y, O'Donnell P. Dopamine modulation of prefrontal cortical interneurons changes during adolescence. *Cereb Cortex*. 2007 May;17(5):1235–40.
 121. Gao C, Wolf ME. Dopamine receptors regulate NMDA receptor surface expression in prefrontal cortex neurons. *J Neurochem*. 2008 Sep;106(6):2489–501.
 122. Dzirasa K, Ramsey AJ, Takahashi DY, Stapleton J, Potes JM, Williams JK, et al. Hyperdopaminergia and NMDA receptor hypofunction disrupt neural phase signaling. *J Neurosci*. 2009 Jun 24;29(25):8215–24.
 123. Mohn AR, Gainetdinov RR, Caron MG, Koller BH. Mice with reduced NMDA receptor expression display behaviors related to schizophrenia. *Cell*. 1999 Aug 20;98(4):427–36.
 124. Bezu M, Maliković J, Kristofova M, Engidawork E, Höger H, Lubec G, et al. Spatial Working Memory in Male Rats: Pre-Experience and Task Dependent Roles of Dopamine D1- and D2-Like Receptors. *Front Behav Neurosci*. 2017 Oct

13;11:196.

125. Winship IR, Dursun SM, Baker GB, Balista PA, Kandratavicius L, Maia-de-Oliveira JP, et al. An overview of animal models related to schizophrenia. *Can J Psychiatry*. 2019 Jan;64(1):5–17.
126. Matsumoto Y, Niwa M, Mouri A, Noda Y, Fukushima T, Ozaki N, et al. Adolescent stress leads to glutamatergic disturbance through dopaminergic abnormalities in the prefrontal cortex of genetically vulnerable mice. *Psychopharmacology*. 2017 Oct;234(20):3055–74.
127. Benekareddy M, Stachniak TJ, Bruns A, Knoflach F, von Kienlin M, Künnecke B, et al. Identification of a corticohabenular circuit regulating socially directed behavior. *Biol Psychiatry*. 2018 Apr 1;83(7):607–17.
128. Deserno L, Sterzer P, Wüstenberg T, Heinz A, Schlagenhauf F. Reduced prefrontal-parietal effective connectivity and working memory deficits in schizophrenia. *J Neurosci*. 2012 Jan 4;32(1):12–20.
129. Lee HJ, Preda A, Ford JM, Mathalon DH, Keator DB, van Erp TGM, et al. Functional magnetic resonance imaging of motor cortex activation in schizophrenia. *J Korean Med Sci*. 2015 May;30(5):625–31.
130. Dzirasa K, Fuentes R, Kumar S, Potes JM, Nicolelis MAL. Chronic in vivo multi-circuit neurophysiological recordings in mice. *J Neurosci Methods*. 2011 Jan 30;195(1):36–46.
131. Hultman R, Ulrich K, Sachs BD, Blount C, Carlson DE, Ndubuizu N, et al. Brain-wide Electrical Spatiotemporal Dynamics Encode Depression Vulnerability. *Cell*. 2018 Mar 22;173(1):166–180.e14.
132. Mague SD, Talbot A, Blount C, Walder-Christensen KK, Duffney LJ, Adamson E, et al. Brain-wide electrical dynamics encode individual appetitive social behavior. *Neuron*. 2022 May 18;110(10):1728–1741.e7.
133. Shorter E. The history of nosology and the rise of the Diagnostic and Statistical Manual of Mental Disorders. *Dialogues Clin Neurosci*. 2015 Mar;17(1):59–67.
134. Talpalaru A, Bhagwat N, Devenyi GA, Lepage M, Chakravarty MM. Identifying schizophrenia subgroups using clustering and supervised learning. *Schizophr*

- Res. 2019 Dec;214:51–9.
135. Subasi A, Ismail Gursoy M. EEG signal classification using PCA, ICA, LDA and support vector machines. *Expert Syst Appl.* 2010 Dec;37(12):8659–66.
 136. Habtewold TD, Rodijk LH, Liemburg EJ, Sidorenkov G, Boezen HM, Bruggeman R, et al. A systematic review and narrative synthesis of data-driven studies in schizophrenia symptoms and cognitive deficits. *Transl Psychiatry.* 2020 Jul 21;10(1):244.
 137. Brumback AC, Ellwood IT, Kjaerby C, Iafrati J, Robinson S, Lee AT, et al. Identifying specific prefrontal neurons that contribute to autism-associated abnormalities in physiology and social behavior. *Mol Psychiatry.* 2018;23(10):2078–89.
 138. Poot M, van der Smagt JJ, Brilstra EH, Bourgeron T. Disentangling the myriad genomics of complex disorders, specifically focusing on autism, epilepsy, and schizophrenia. *Cytogenet Genome Res.* 2011 Nov 12;135(3–4):228–40.
 139. Ayalew M, Le-Niculescu H, Levey DF, Jain N, Changala B, Patel SD, et al. Convergent functional genomics of schizophrenia: from comprehensive understanding to genetic risk prediction. *Mol Psychiatry.* 2012 Sep;17(9):887–905.
 140. Soni S, Muthukrishnan SP, Samanchi R, Sood M, Kaur S, Sharma R. Pre-trial and pre-response EEG microstates in schizophrenia: An endophenotypic marker. *Behav Brain Res.* 2019 Oct 3;371:111964.
 141. Cea-Cañas B, Gomez-Pilar J, Núñez P, Rodríguez-Vázquez E, de Uribe N, Díez Á, et al. Connectivity strength of the EEG functional network in schizophrenia and bipolar disorder. *Prog Neuropsychopharmacol Biol Psychiatry.* 2020 Mar 2;98:109801.
 142. Gallagher N, Ulrich K, Talbot A, Dzirasa K, Carin L, Carlson D. Cross Spectral Frequency Analysis. *Adv Neural Inf Process Syst.* 2017 Nov;
 143. Perez-Costas E, Melendez-Ferro M, Roberts RC. Basal ganglia pathology in schizophrenia: dopamine connections and anomalies. *J Neurochem.* 2010 Apr;113(2):287–302.
 144. Wang J, Li J, Yang Q, Xie Y-K, Wen Y-L, Xu Z-Z, et al. Basal forebrain mediates

- prosocial behavior via disinhibition of midbrain dopamine neurons. *Proc Natl Acad Sci USA*. 2021 Feb 16;118(7).
145. Buchsbaum MS. The frontal lobes, basal ganglia, and temporal lobes as sites for schizophrenia. *Schizophr Bull*. 1990;16(3):379–89.
 146. Hultman R, Mague SD, Li Q, Katz BM, Michel N, Lin L, et al. Dysregulation of Prefrontal Cortex-Mediated Slow-Evolving Limbic Dynamics Drives Stress-Induced Emotional Pathology. *Neuron*. 2016 Jul 20;91(2):439–52.
 147. Berquist MD, Hyatt WS, Bauer-Erickson J, Gannon BM, Norwood AP, Fantegrossi WE. Phencyclidine-like in vivo effects of methoxetamine in mice and rats. *Neuropharmacology*. 2018 May 15;134(Pt A):158–66.
 148. Sams-Dodd F. Effects of dopamine agonists and antagonists on PCP-induced stereotyped behaviour and social isolation in the rat social interaction test. *Psychopharmacology*. 1998 Jan;135(2):182–93.
 149. Green JT, Bouton ME. New functions of the rodent prelimbic and infralimbic cortex in instrumental behavior. *Neurobiol Learn Mem*. 2021 Nov;185:107533.
 150. Balleine BW, O'Doherty JP. Human and rodent homologues in action control: corticostriatal determinants of goal-directed and habitual action. *Neuropsychopharmacology*. 2010 Jan;35(1):48–69.
 151. Xu H, Liu L, Tian Y, Wang J, Li J, Zheng J, et al. A disinhibitory microcircuit mediates conditioned social fear in the prefrontal cortex. *Neuron*. 2019 May 8;102(3):668–682.e5.
 152. Sharpe MJ, Killcross S. The prelimbic cortex uses higher-order cues to modulate both the acquisition and expression of conditioned fear. *Front Syst Neurosci*. 2014;8:235.
 153. Rossignoli MT, Lopes-Aguiar C, Ruggiero RN, Do Val da Silva RA, Bueno-Junior LS, Kandratavicius L, et al. Selective post-training time window for memory consolidation interference of cannabidiol into the prefrontal cortex: Reduced dopaminergic modulation and immediate gene expression in limbic circuits. *Neuroscience*. 2017 May 14;350:85–93.
 154. Chow JJ, Reiner DJ. From head to tail (of the VTA): role of projections from

- prelimbic cortex to rostromedial tegmental nucleus in cocaine reinstatement. *Neuropsychopharmacology*. 2021 Jan 15;
155. Bastos AM, Loonis R, Kornblith S, Lundqvist M, Miller EK. Laminar recordings in frontal cortex suggest distinct layers for maintenance and control of working memory. *Proc Natl Acad Sci USA*. 2018 Jan 30;115(5):1117–22.
 156. Song C, Moyer JR. Layer- and subregion-specific differences in the neurophysiological properties of rat medial prefrontal cortex pyramidal neurons. *J Neurophysiol*. 2018 Jan 1;119(1):177–91.
 157. Kosmal A, Stepniewska I, Markow G. Laminar organization of efferent connections of the prefrontal cortex in the dog. *Acta Neurobiol Exp (Wars)*. 1983;43(2):115–27.
 158. The Role of Molecular Layer Interneurons in Motor Learning within the Cerebellar Microcircuit.
 159. van Aerde KI, Heistek TS, Mansvelder HD. Prelimbic and infralimbic prefrontal cortex interact during fast network oscillations. *PLoS One*. 2008 Jul 16;3(7):e2725.
 160. Bitzenhofer SH, Sieben K, Siebert KD, Spehr M, Hanganu-Opatz IL. Oscillatory activity in developing prefrontal networks results from theta-gamma-modulated synaptic inputs. *Cell Rep*. 2015 Apr 21;11(3):486–97.
 161. Leyrer-Jackson JM, Thomas MP. Layer-specific effects of dopaminergic D1 receptor activation on excitatory synaptic trains in layer V mouse prefrontal cortical pyramidal cells. *Physiol Rep*. 2018 Aug;6(15):e13806.
 162. Jia L, Sun Z, Shi D, Wang M, Jia J, He Y, et al. Effects of different patterns of electric stimulation of the ventromedial prefrontal cortex on hippocampal-prefrontal coherence in a rat model of depression. *Behav Brain Res*. 2019 Jan 1;356:179–88.
 163. Finn ES, Huber L, Jangraw DC, Molfese PJ, Bandettini PA. Layer-dependent activity in human prefrontal cortex during working memory. *Nat Neurosci*. 2019 Oct;22(10):1687–95.
 164. Bitzenhofer SH, Ahlbeck J, Wolff A, Wiegert JS, Gee CE, Oertner TG, et al. Layer-specific optogenetic activation of pyramidal neurons causes beta-gamma

- entrainment of neonatal networks. *Nat Commun.* 2017 Feb 20;8:14563.
165. Tomasella E, Bechelli L, Ogando MB, Mininni C, Di Guilmi MN, De Fino F, et al. Deletion of dopamine D2 receptors from parvalbumin interneurons in mouse causes schizophrenia-like phenotypes. *Proc Natl Acad Sci USA.* 2018 Mar 27;115(13):3476–81.
 166. Inan M, Zhao M, Manuszak M, Karakaya C, Rajadhyaksha AM, Pickel VM, et al. Energy deficit in parvalbumin neurons leads to circuit dysfunction, impaired sensory gating and social disability. *Neurobiol Dis.* 2016 Sep;93:35–46.
 167. Gullledge AT, Jaffe DB. Multiple effects of dopamine on layer V pyramidal cell excitability in rat prefrontal cortex. *J Neurophysiol.* 2001 Aug;86(2):586–95.
 168. Gabbott PLA, Warner TA, Jays PRL, Salway P, Busby SJ. Prefrontal cortex in the rat: projections to subcortical autonomic, motor, and limbic centers. *J Comp Neurol.* 2005 Nov 14;492(2):145–77.
 169. Aghajanian GK, Marek GJ. Serotonin, via 5-HT_{2A} receptors, increases EPSCs in layer V pyramidal cells of prefrontal cortex by an asynchronous mode of glutamate release. *Brain Res.* 1999 Apr 17;825(1–2):161–71.
 170. Ninan I, Jardemark KE, Wang RY. Differential effects of atypical and typical antipsychotic drugs on N-methyl-D-aspartate- and electrically evoked responses in the pyramidal cells of the rat medial prefrontal cortex. *Synapse.* 2003 May;48(2):66–79.
 171. Sorg BA, Berretta S, Blacktop JM, Fawcett JW, Kitagawa H, Kwok JCF, et al. Casting a wide net: role of perineuronal nets in neural plasticity. *J Neurosci.* 2016 Nov 9;36(45):11459–68.
 172. Klimczak P, Rizzo A, Castillo-Gómez E, Perez-Rando M, Gramuntell Y, Beltran M, et al. Parvalbumin interneurons and perineuronal nets in the hippocampus and retrosplenial cortex of adult male mice after early social isolation stress and perinatal NMDA receptor antagonist treatment. *Front Synaptic Neurosci.* 2021 Sep 22;13:733989.
 173. Yu Z, Chen N, Hu D, Chen W, Yuan Y, Meng S, et al. Decreased Density of Perineuronal Net in Prelimbic Cortex Is Linked to Depressive-Like Behavior in Young-Aged Rats. *Front Mol Neurosci.* 2020 Jan 28;13:4.

174. Alcaide J, Guirado R, Crespo C, Blasco-Ibáñez JM, Varea E, Sanjuan J, et al. Alterations of perineuronal nets in the dorsolateral prefrontal cortex of neuropsychiatric patients. *Int J Bipolar Disord*. 2019 Nov 15;7(1):24.
175. Jorgensen ET, Gonzalez AE, Harkness JH, Hegarty DM, Thakar A, Burchi DJ, et al. Cocaine memory reactivation induces functional adaptations within parvalbumin interneurons in the rat medial prefrontal cortex. *Addict Biol*. 2021 May;26(3):e12947.
176. Garcia-Mompo C, Curto Y, Carceller H, Gilabert-Juan J, Rodriguez-Flores E, Guirado R, et al. Δ -9-Tetrahydrocannabinol treatment during adolescence and alterations in the inhibitory networks of the adult prefrontal cortex in mice subjected to perinatal NMDA receptor antagonist injection and to postweaning social isolation. *Transl Psychiatry*. 2020 Jun 1;10(1):177.
177. Venturino A, Schulz R, De Jesús-Cortés H, Maes ME, Nagy B, Reilly-Andújar F, et al. Microglia enable mature perineuronal nets disassembly upon anesthetic ketamine exposure or 60-Hz light entrainment in the healthy brain. *Cell Rep*. 2021 Jul 6;36(1):109313.
178. Dzyubenko E, Juckel G, Faissner A. The antipsychotic drugs olanzapine and haloperidol modify network connectivity and spontaneous activity of neural networks in vitro. *Sci Rep*. 2017 Sep 14;7(1):11609.
179. Roberts AC, Clarke HF. Why we need nonhuman primates to study the role of ventromedial prefrontal cortex in the regulation of threat- and reward-elicited responses. *Proc Natl Acad Sci USA*. 2019 Dec 23;
180. Schneiderman JS, Hazlett EA, Chu K-W, Zhang J, Goodman CR, Newmark RE, et al. Brodmann area analysis of white matter anisotropy and age in schizophrenia. *Schizophr Res*. 2011 Aug;130(1–3):57–67.
181. Zalesky A, Pantelis C, Cropley V, Fornito A, Cocchi L, McAdams H, et al. Delayed development of brain connectivity in adolescents with schizophrenia and their unaffected siblings. *JAMA Psychiatry*. 2015 Sep;72(9):900–8.
182. Bohlken MM, Brouwer RM, Mandl RCW, Van den Heuvel MP, Hedman AM, De Hert M, et al. Structural brain connectivity as a genetic marker for schizophrenia. *JAMA Psychiatry*. 2016 Jan;73(1):11–9.

183. Sugihara G, Oishi N, Son S, Kubota M, Takahashi H, Murai T. Distinct Patterns of Cerebral Cortical Thinning in Schizophrenia: A Neuroimaging Data-Driven Approach. *Schizophr Bull.* 2017 Jul 1;43(4):900–6.
184. Benes FM, Vincent SL, Todtenkopf M. The density of pyramidal and nonpyramidal neurons in anterior cingulate cortex of schizophrenic and bipolar subjects. *Biol Psychiatry.* 2001 Sep 15;50(6):395–406.
185. Hu Y, Wu J, Cao Y, Tang X, Wu G, Guo Q, et al. Abnormal neural oscillations in clinical high risk for psychosis: a magnetoencephalography method study. *Gen Psych.* 2022 Apr 28;35(2):e100712.
186. Olejarczyk E, Jernajczyk W. Graph-based analysis of brain connectivity in schizophrenia. *PLoS One.* 2017 Nov 30;12(11):e0188629.
187. Saletu B, Anderer P, Saletu-Zyhlarz GM, Pascual-Marqui RD. EEG mapping and low-resolution brain electromagnetic tomography (LORETA) in diagnosis and therapy of psychiatric disorders: evidence for a key-lock principle. *Clin EEG Neurosci.* 2005 Apr;36(2):108–15.
188. Delgado-Sallent C, Nebot P, Gener T, Fath AB, Timplallexi M, Puig MV. Atypical, but Not Typical, Antipsychotic Drugs Reduce Hypersynchronized Prefrontal-Hippocampal Circuits during Psychosis-Like States in Mice: Contribution of 5-HT_{2A} and 5-HT_{1A} Receptors. *Cereb Cortex.* 2021 Dec 7;
189. Kang SS, MacDonald AW, Chafee MV, Im C-H, Bernat EM, Davenport ND, et al. Abnormal cortical neural synchrony during working memory in schizophrenia. *Clin Neurophysiol.* 2018;129(1):210–21.
190. Shahbazi Avarvand F, Bartz S, Andreou C, Samek W, Leicht G, Mulert C, et al. Localizing bicoherence from EEG and MEG. *Neuroimage.* 2018 Jul 1;174:352–63.
191. Racz FS, Farkas K, Stylianou O, Kaposzta Z, Czoch A, Mukli P, et al. Separating scale-free and oscillatory components of neural activity in schizophrenia. *Brain Behav.* 2021 May;11(5):e02047.
192. Uhlhaas PJ, Singer W. High-frequency oscillations and the neurobiology of schizophrenia. *Dialogues Clin Neurosci.* 2013 Sep;15(3):301–13.
193. Morris BJ, Cochran SM, Pratt JA. PCP: from pharmacology to modelling

- schizophrenia. *Curr Opin Pharmacol*. 2005 Feb;5(1):101–6.
194. Hasegawa E, Miyasaka A, Sakurai K, Cherasse Y, Li Y, Sakurai T. Rapid eye movement sleep is initiated by basolateral amygdala dopamine signaling in mice. *Science*. 2022 Mar 4;375(6584):994–1000.
 195. Fultz NE, Bonmassar G, Setsompop K, Stickgold RA, Rosen BR, Polimeni JR, et al. Coupled electrophysiological, hemodynamic, and cerebrospinal fluid oscillations in human sleep. *Science*. 2019 Nov 1;366(6465):628–31.
 196. Howells FM, Temmingh HS, Hsieh JH, van Dijen AV, Baldwin DS, Stein DJ. Electroencephalographic delta/alpha frequency activity differentiates psychotic disorders: a study of schizophrenia, bipolar disorder and methamphetamine-induced psychotic disorder. *Transl Psychiatry*. 2018 Apr 12;8(1):75.
 197. Puvvada KC, Summerfelt A, Du X, Krishna N, Kochunov P, Rowland LM, et al. Delta vs gamma auditory steady state synchrony in schizophrenia. *Schizophr Bull*. 2018 Feb 15;44(2):378–87.
 198. Mäki-Marttunen T, Krull F, Bettella F, Hagen E, Næss S, Ness TV, et al. Alterations in Schizophrenia-Associated Genes Can Lead to Increased Power in Delta Oscillations. *Cereb Cortex*. 2018 Nov 22;29(2):875–91.
 199. Neske GT. The Slow Oscillation in Cortical and Thalamic Networks: Mechanisms and Functions. *Front Neural Circuits*. 2015;9:88.
 200. Metzner C, Mäki-Marttunen T, Karni G, McMahon-Cole H, Steuber V. The effect of alterations of schizophrenia-associated genes on gamma band oscillations. *Schizophr*. 2022 Dec;8(1):46.
 201. Polter AM, Barcomb K, Tsuda AC, Kauer JA. Synaptic function and plasticity in identified inhibitory inputs onto VTA dopamine neurons. *Eur J Neurosci*. 2018 May;47(10):1208–18.
 202. Beier KT, Steinberg EE, DeLoach KE, Xie S, Miyamichi K, Schwarz L, et al. Circuit Architecture of VTA Dopamine Neurons Revealed by Systematic Input-Output Mapping. *Cell*. 2015 Jul 30;162(3):622–34.
 203. Sun F, Zhou J, Dai B, Qian T, Zeng J, Li X, et al. New and improved GRAB fluorescent sensors for monitoring dopaminergic activity *in vivo*. *BioRxiv*. 2020

Mar 28;

204. Labouesse MA, Cola RB, Patriarchi T. GPCR-Based Dopamine Sensors-A Detailed Guide to Inform Sensor Choice for In vivo Imaging. *Int J Mol Sci.* 2020 Oct 28;21(21).
205. Patriarchi T, Cho JR, Merten K, Howe MW, Marley A, Xiong W-H, et al. Ultrafast neuronal imaging of dopamine dynamics with designed genetically encoded sensors. *Science.* 2018 Jun 29;360(6396).
206. Munoz IM, Szyniarowski P, Toth R, Rouse J, Lachaud C. Improved genome editing in human cell lines using the CRISPR method. *PLoS One.* 2014 Oct 10;9(10):e109752.

Biography

Gwenaëlle E. Thomas was born July 15, 1994 to Mona L. Thomas and Louis A. Thomas. After graduating high school in 2012, she was awarded the prestigious Meyerhoff Scholarship and became a National Institute of Drug Abuse scholar. She graduated in 2016 with a dual degree B.S.in Biochemistry and Molecular Biology and Psychology from the honors university, University of Maryland Baltimore County. During her time as an undergraduate researcher she studied bioinformatics at the Jackson Laboratory with Janan Eppig, PhD, behavioral neuroscience at the University of Chicago with Stephanie Dulawa, PhD, and neuroengineering at Duke University with Kafui Dzirasa, MD, PhD. Gwenaëlle joined the Department of Neurobiology in 2016 for her PhD training. She completed her dissertation on “Characterizing antipsychotic drug behavioral and neurophysiological responses to psychotomimetic challenge” under the joint mentorship of Marc Caron. PhD and Kafui Dzirasa, MD, PhD.. During this time, Gwenaëlle completed the Certificate for College Teaching and earned the Borden Scholarship as a Duke Scholar in Molecular Medicine. During her graduate career, Gwenaëlle earned the National Science Foundation Graduate Research Fellowship (2018), was admitted to the Society for Neuroscience -Neuroscience Scholars Programs, and was awarded the Dean’s Award for Excellence in Teaching (2020).